A NEW METHOD TO SYNTHESIZE A SHOCK RESPONSE SPECTRUM COMPATIBLE BASE ACCELERATION TO IMPROVE MULTI-DEGREE OF FREEDOM SYSTEM RESPONSE

A DISSERTATION
SUBMITTED TO THE FACULTY OF THE
UNIVERSITY OF MINNESOTA
BY

J. EDWARD ALEXANDER

IN PARTIAL FULFILLMENT OF THE REQUIREMENTS
FOR THE DEGREE OF
DOCTOR OF PHILOSOPHY

PROFESSOR SUSAN C. MANTELL

NOVEMBER 2015

Acknowledgements

I would like to acknowledge my advisor, Dr. Susan C. Mantell, for accepting me back as a PhD student after a long haitus in my program due to personal reasons. Her interest, advice, guidance and friendship have been much appreciated. I also would like to thank the other members of my dissertation committee, Dr. William Durfee, Dr. Rajesh Rajamani and Dr. Henryk Stolarski for their interest, questions, suggestions and insightful comments.

Dedication

This document is dedicated to Dr. Rudolph Scavuzzo, Dr. Howard Gaberson and Mr. Henry Pusey. These three individuals all played key roles in the field of shock and vibration over the course of their lives and are universally recognized as subject matter experts in their respective areas of research and leadership.

Dr. Rudolph (Rudy) J. Scavuzzo is a consultant, ASME Fellow and Professor Emeritis, Department of Polymer Engineering, University of Akron. Rudy was one of the original developers of the Practical Naval Shock Analysis and Design short course. Rudy and I both worked at Bettis Atomic Power Laboratory in Pittsburgh, however not at the same time. Rudy handed the torch to me to continue teaching his material for the naval shock course when he was physically no longer able to travel.

Dr. Howard (Howie) A. Gaberson (1931-2013) was the Division Director of the U. S. Naval Civil Engineering Laboratory which later became the Facilities Engineering Service Center. After retirement from government service, Howie continued research on the pseudo-velocity shock spectrum. During his long career, Howie was an enthusiac advocate for the pseudo-velocity shock spectrum as the best indicator of system damage. Howie preeched the pseudo-velocity shock spectrum gospel for decades. Howie asked me to continue his life-long mission for advocating the merits of the pseudo-velocity shock spectrum.

Mr. Henry C. Pusey (1927 – 2014) is frequently referred to as the "Godfather" of shock and vibration. Henry was the fourth and final Director of the Shock and Vibration Information Center, Naval Reseach Laboratory. Henry was my friend and mentor for more than three decades, and was instrumental in including me as an instructor in the Practical Naval Shock Analysis and Design course, as well as numerous panels and meetings. Henry was a true southern gentleman.

These three gentlemen provided not only guidance to me, but also to hundreds of other engineers in the field of shock and vibration. They were my inspiration, mentors and role models. I owe a debt of gratitude to all, and miss Howie and Henry greatly.

Abstract

A new method has been developed to synthesize a shock response spectrum (*SRS*) compatible base acceleration with additional parameters in the synthesis process beyond current practices. Current base acceleration synthesis methods address only *SRS* compatibility. However, additional information is available to synthesize a base acceleration to improve multi-degree of freedom (*MDOF*) system response accuracy. Expanding the synthesis procedure to include energy input and temporal information provides more constraints on the development of the synthesized acceleration. Similar to the *SRS*, an energy input spectrum (*EIS*) is a frequency based relationship for the peak energy input per unit mass to a series of single-degree of freedom (*SDOF*) oscillators from a base acceleration. The *EIS* represents total input energy contributions (kinetic, damped and absorbed energy). Temporal information includes overall shape of the transient shock pulse envelope $E(t)$ (rise, plateau, decay) and a T_E duration where strong shock occurs. When *EIS*, $E(t)$ and T_E compatibility are added to the synthesis procedure, an improved base acceleration results. To quantify the significance of these quantities, a regression analysis was performed based on linear and nonlinear *3DOF* model responses. The regression analysis confirmed that compatibility with *SRS*, *EIS* and T_E were significant factors for accurate *MDOF* model response. To test this finding, a base acceleration was synthesized with the expanded procedure. Four other accelerations were synthesized with current state of the art methods which match the *SRS* only. The five synthesized accelerations were applied to a *3DOF* model based on a US naval medium weight shock machine (*MWSM*). *MWSM* model results confirmed that the *SRS*, *EIS*, T_E compatible acceleration resulted in improved accuracy of peak mass accelerations and

displacements in the majority of the cases, and consistently gave more accurate peak energy input to the *MWSM* model. Energy input to a structure is a significant factor for damage potential. The total kinetic, damped and absorbed energy input represents a system damage potential which the structure as a whole must dissipate.

Table of Contents

List of Tables

List of Figures

Nomenclature

3DOF	Three degree of freedom
a_D	Design acceleration
a_S	Synthesized acceleration
a_{S2}	Final synthesized acceleration from updated merit function
A_n	Amplitude of n^{th} sinusoid
EI	Energy input
EIS	Energy input spectrum
EIS_D	Energy input spectrum for a_D
EIS_S	Energy input spectrum for a_S
EIS_{S2}	Energy input spectrum for a_{S2}
$EIS_{\%}$	*EIS* percent error of a_S relative to a_D averaged over frequency bandwidth
En	Total peak energy input to *MDOF* model
EOM	Equation of motion
$E(t)$	Envelope function for synthesized acceleration
f	Frequency, H_z
f_n	Natural frequency of n^{th} *SDOF* oscillator, *Hz*
g	Acceleration due to gravity
H_0	Null hypothesis in regression analysis
H_1	Alternative hypothesis in regression analysis
H_V	Velocity transfer function
Hz	Hertz (cycles/second)
i	Iteration index for a_S synthesis iteration process
ITOP	International test operations procedure
j	Index for j^{th} m, c and k in *MDOF* model
k	Index for time step increment
k_j	j^{th} spring stiffness in *MDOF* model
KPH	Kilometers per hour
M	Merit function
m	Mass
m_j	j^{th} mass in *MDOF* model
MDOF	Multi-degree of freedom
MOD	Ministry of Defense
MWSM	Medium weight shock machine
N_n	Number of half sines in n^{th} wavelet
n	Frequency index
P_n	Participation factor for n^{th} mode of vibration
PSD	Power spectral density
R^2	Percent that regression model explains the variation in response

SDOF	Single degree of freedom
SRS	Shock response spectrum
SRS_D	Shock response spectrum for a_D
SRS_S	Shock response spectrum for a_S
SRS_{S2}	Shock response spectrum for a_{S2}
SRS_{vel}	Velocity *SRS*
$SRS_{\%}$	*SRS* percent error of a_S relative to a_D averaged over frequency bandwidth
t_{dn}	Wavelet time delay
T_E	Temporal duration of acceleration time-history defined in Chapter 3.2
T_{ED}	Temporal duration T_E for a_D
T_{ES}	Temporal duration T_E for a_S
$T_{E\%}$	T_E percent error of a_S relative to a_D
$u(t)$	Absolute acceleration
$\dot{u}(t)$	Absolute velocity
$\ddot{u}(t)$	Absolute acceleration
$\ddot{u}_b(t)$	Base acceleration
UK	United Kingdom
W_{EIS}	$EIS_{\%}$ weighting in merit function (*M*) equation
W_{SRS}	$SRS_{\%}$ weighting in merit function (*M*) equation
W_{TE}	$T_{E\%}$ weighting in merit function (*M*) equation
x	Modal coordinate
$\dot{x}(t)$	Modal coordinate velocity
$\ddot{x}(t)$	Modal coordinate acceleration
$z(t)$	Relative displacement
$\dot{z}(t)$	Relative velocity
$\ddot{z}(t)$	Relative acceleration

Greek Alphabet Nomenclature:

α	Mass matrix coefficient for Raleigh damping
β	Stiffness matrix coefficient for Raleigh damping
Δ	Elastic limit for nonlinear-elastic springs in *3DOF* models
ζ	Percent of critical damping
φ_n	Phase angle for n^{th} sinusoid
ω_i	Circular frequency for i^{th} mode of vibration, radians/second
ω_n	Natural frequency of n^{th} *SDOF* oscillator, radians/second

Matrix Nomenclature:

$[C]$	Damping matrix
$[C_L]$	Linear part of damping matrix

$[C_{NL}]$	Nonlinear part of damping matrix which is function of velocity
$[K]$	Stiffness matrix
$[K_L]$	Linear part of stiffness matrix
$[K_{NL}]$	Nonlinear part of stiffness matrix which is function of displacement
$[M]$	Mass matrix
$\{x_i\}$	Modal coordinate vector for mode i
$\{u\}$	Absolute displacement vector
$\{z\}$	Relative displacement vector
$\{\ddot{z}\}$	Relative acceleration vector
$\{\varphi\}_n$	Mode shape vector for mode n
$[\Phi]$	Mode transformation matrix

1 Spectral Methods to Characterize Shock and Energy

1.1 Overview

The shock response spectrum (*SRS*), conceived by Maurice Biot (1932), has been used as a structural dynamic method to characterize the seismic and mechanical shock environment for more than eight decades. The *SRS*, by definition, is the peak acceleration response of a series of single-degree of freedom (*SDOF*) mechanical oscillators of different frequencies, all with same the percent of critical damping, subjected to the same transient base input acceleration. The *SRS* is most frequently presented as a log-log graph of the peak *SDOF* acceleration responses as a function of the frequency bandwidth of interest. Early research and application of the *SRS* was conducted in the 1950's by the seismic community (Hudson, 1956), (Housner, 1959) to characterize the earthquake seismic shock environment. After the 1950's the use of the *SRS* expanded significantly for the seismic, aerospace and defense communities. The *SRS* is frequently employed to specify the design requirement for the structural dynamic shock environment that a physical system must survive (Bureau of Ships, 1961), (Department of Defense, 2008), (NASA, 1999), (NASA, 2001).

When structural dynamic requirements are specified in terms of a design shock response spectrum, termed SRS_D, the evaluation of a structure to meet this requirement can be demonstrated by either analysis or test. If it can be demonstrated the structure will survive the input shock specified by SRS_D and continue to meet operational requirements,

it is considered to be shock qualified. When the system to be shock qualified can be modelled as a linear structure (i.e., linear equations of motion), a mode superposition analysis procedure can be performed directly, using SRS_D, to estimate the peak dynamic response (accelerations, displacements) of a multi-degree of freedom (*MDOF*) system.

However, if the structure is to be shock qualified by electro-dynamic shaker testing, or if the structure to be analyzed is nonlinear (i.e., nonlinear equations of motion), the SRS_D cannot be used directly. In these instances an SRS_D compatible acceleration time-history, a_S, must be synthesized. The synthesized a_S can be input directly as a transient base acceleration for transient analysis of the nonlinear *MDOF* model, or to drive the armature of an electro-dynamic shock test machine.

Synthesis of an SRS_D compatible base acceleration time-history is not difficult to execute and numerous procedures have been documented for this purpose. However, past research has demonstrated that synthesis of an SRS_D compatible acceleration time-history a_S does not, by itself, guarantee that the peak dynamic structure responses will be accurate. Accurate, in the context of this document, is defined as system response from a synthesized base acceleration that matches the corresponding system response from a design acceleration with good accuracy, for example within 10%. Current SRS_D compatible synthesis methods do not consider compatibility with the energy input spectrum (*EIS*) nor the temporal shape of a_S. Motivation for the research documented herein is to augment existing SRS_D compatible transient acceleration a_S synthesis processes to improve the accuracy of peak *MDOF* system response. Additional constraints beyond only SRS_D compatibility are:

- Matching the energy input to the structure based on the synthesized acceleration's compatibility with the energy input spectrum (*EIS*) and,
- Constraining the synthesized acceleration to match predefined temporal requirements including the overall shape envelope of the transient acceleration and the duration T_E of strong shock as defined by Military Standard 801G (Department of Defense, 2008).

1.2 Shock Response Spectrum Definition

Shock is a major structural design consideration for a wide variety of systems and their components. Shock is a sudden, sometimes violent, change in velocity (rapid acceleration) of a physical system due to the transient application of an external force or acceleration. The shock response spectrum is a way to characterize the frequency response of a series of single degree-of-freedom (*SDOF*) systems all subjected to the same transient base input shock acceleration. The *SRS* has been used for more than 80 years to characterize the frequency response from transient shock acceleration. The *SRS* is defined simply as the peak acceleration response (either positive or negative) of a series of base excited linear *SDOF* oscillators of different frequencies subjected to the same transient base acceleration input.

Figure (1-1) is a graphical representation of how an *SRS* is determined. Consider a base transient shock input acceleration time-history where the entire base experiences this acceleration. A series of *SDOF* linear oscillators of different frequencies mounted on the rigid base will also experience this transient shock input. To illustrate the *SRS*, the response of six *SDOF* oscillators is examined in this example. These *SDOF* oscillators

are tuned to frequencies of 30 Hz, 60 Hz, 200 Hz, 500 Hz, 1000Hz and 1300 Hz. The transient mass acceleration response of each is plotted above the corresponding *SDOF* oscillator and the peak value is indicated on each plot. For example, the peak acceleration response of the 30 Hz *SDOF* oscillator is -10.46g as indicated on the plot, which is the lowest magnitude of the six *SDOF* oscillators. The peak amplitude of the 60 Hz *SDOF* oscillator is 22.7g. The *SDOF* peak amplitudes continue to increase to 151.2g for the 1300 Hz oscillator. Had higher frequency oscillators been included in this example, at some *SDOF* frequency, the peak *SDOF* acceleration response value would reach a maximum. For *SDOF* oscillators with frequencies above this limiting frequency, the peak acceleration response would begin to decrease. In the limit, at the extreme high frequency end of the spectrum, the peak amplitude of the highest frequency oscillator would asymptotically converge to 47.5g, which is the peak amplitude of the input base acceleration. This is because, at the high frequency end of the spectrum, the *SDOF* oscillator is so stiff that it acts like a rigid (infinitely stiff) element attached to the base, and as such experiences acceleration identical to that of the base input acceleration. The *SRS* approaching the high frequency asymptote is demonstrated by the *SRS* of Figure (2-3) in Chapter 2.

The peak acceleration response of each of the six *SDOF* oscillators is plotted as a function of frequency at the top of Figure (1-1). These six points are indicated on the *SRS* plot at the corresponding frequencies of each oscillator. It is noted that the peak acceleration of each *SDOF* oscillator do not occur at the same point in time during the transient. The *SRS* gives the peak response of each *SDOF*, but does not retain temporal information as to when the peak occurs. The complete *SRS* is developed for *SDOF*

oscillators covering the frequency band width of interest, 10 Hz to 3000 Hz in this case. A good overview of the early historical development of the *SRS* is given by Trifunace (2008)

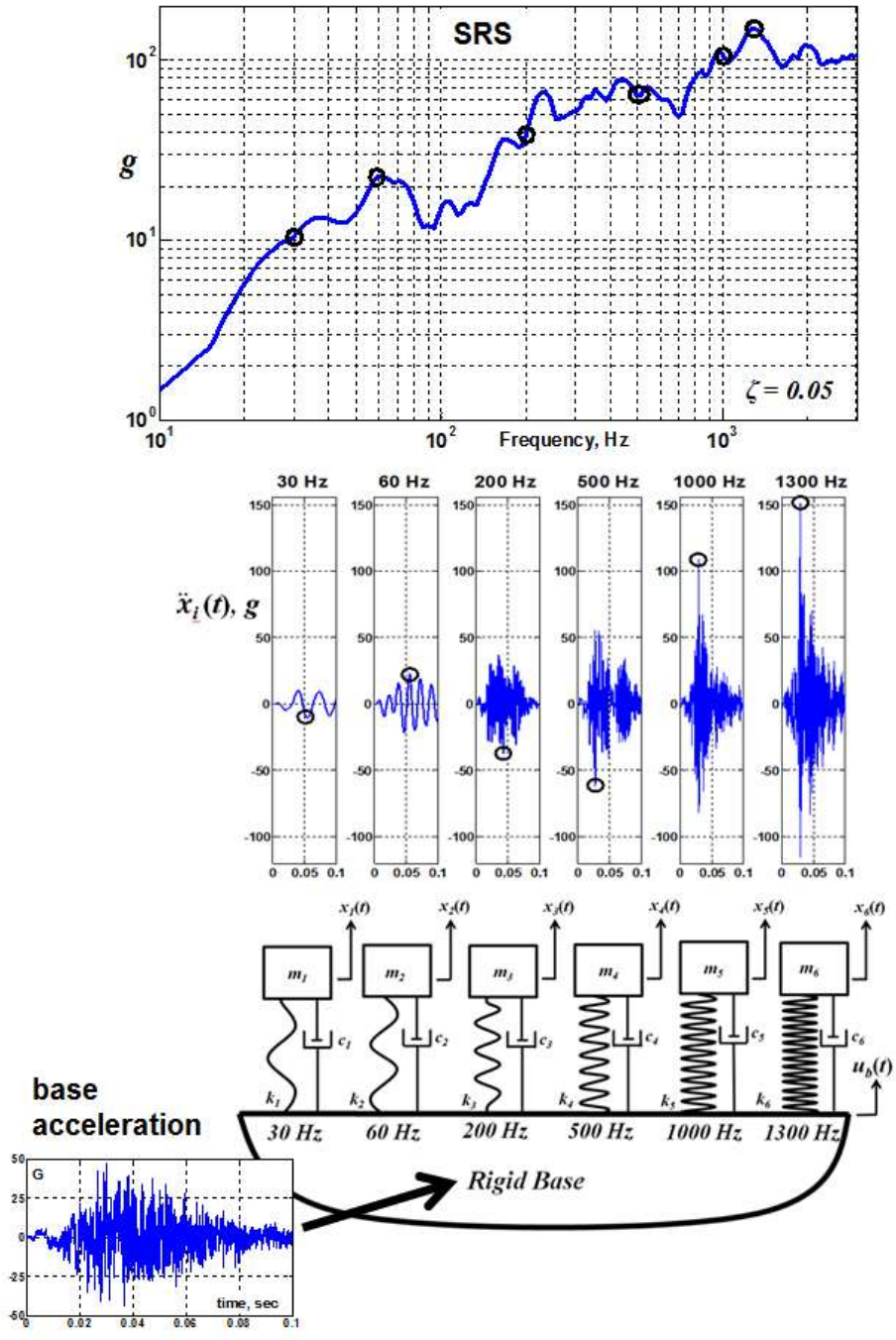

Figure (1-1) Graphical Representation of the Shock Response Spectrum

1.3 Shock Response Spectrum SRS_D as a Shock Design Specification

The *SRS* is used widely in the defense, aerospace and seismic communities. The *SRS* is often prescribed as a structural design shock design specification, termed SRS_D herein, to characterize the requirement for the structural shock design environment. A design shock response spectrum SRS_D is frequently determined from platform (i.e., ship, ground vehicle, etc.) field testing. In these cases, numerous transient accelerations data records are recorded during testing. Figure (1-2) is an illustrative example of multiple acceleration-time histories from field tests. The test acceleration signals also provide typical shock pulse temporal parameters (rise time, decay time, strong shock duration, overall shock pulse envelope) for a particular shock event (underwater explosions, earthquakes, pyrotechnics, ballistic impact, etc.). The acceleration-time histories from platform field tests can be transformed to an ensemble of shock response spectra as illustrated in Figure (1-2). The transformation to an *SRS* gives the *SDOF* response maxima for all frequencies. However, as demonstrated by the transient plots of Figure (1-1), the peak mass accelerations do not occur at the same time. As such, the *SRS* does not retain the timing of when the transient acceleration peaks occurs. In order to develop a single design SRS_D, a maximum envelope of all spectra is constructed. A single design SRS_D which envelopes all SRS_i is illustrated by the graph on the right side of the Figure (1-2).

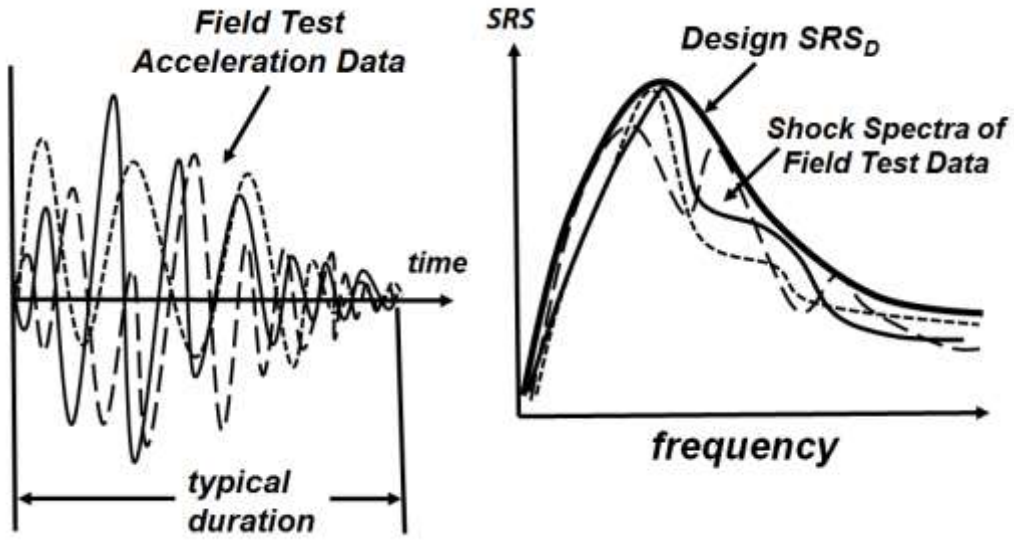

Figure (1-2) Development of a Design SRS_D from Field Test Data

There are numerous examples where structural dynamic environment requirements for a shock event are specified by a design SRS_D. The seismic environment for ground structures was the first case of this approach for design. Housner (1959) published both velocity and acceleration spectra based on enveloping the four strongest earthquake ground motions recorded at the time (El Centro-1934, El Centro-1940, Olympia-1949, Tehachapi-1952). Subsequently, Newmark, et al, (Newmark, Blume, & Kapur, 1973) published a recommended design shock response spectrum SRS_D for nuclear power plants based on the evaluation of seventeen recorded earthquake horizontal and vertical accelerations. The Newmark horizontal design SRS_D, Figure (1-3), has survived for more than 40 years and remains the U. S. Nuclear Regulatory Commission's SRS_D requirement for nuclear power plants as specified in Regulatory Guide 1.60 (U. S. Nuclear Regulatory Commission, Office of Nuclear Regulatory Research, 2014).

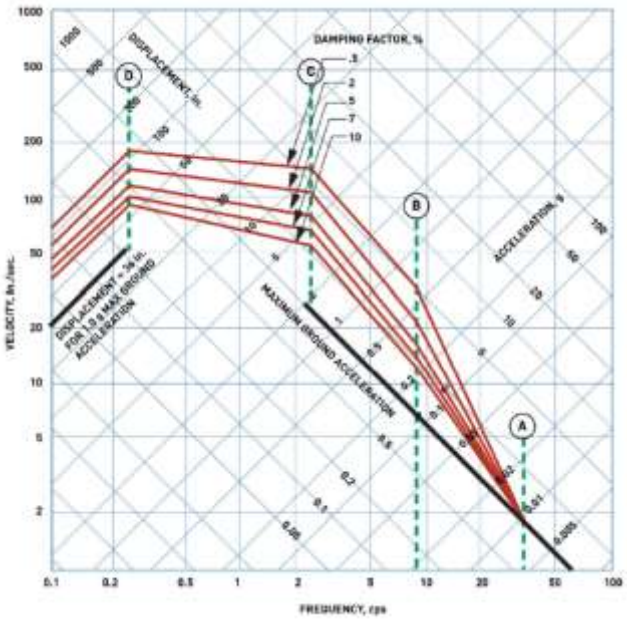

Figure (1-3) U.S. NRC Horizontal SRS_D for Nuclear Power Plants

Similar shock response spectrum requirements for equipment aboard US naval ships were first published by the Naval Research Laboratory in 1963. In the case of shipboard equipment, the design spectra is specified based on the type of ship (surface ship or submarine) and the mounting location of the equipment in the ship, (hull, deck or shell mounted). Interim unclassified design SRS_D values were first published by Naval Research Lab engineers O'Hara and Belsheim (Feb, 1963). Subsequently a classified SRS_D requirements document was issued by the US Navy (Department of the Navy, Naval Sea Systems Command, 1972). This document remains the US Navy's SRS_D requirement for shock qualification of naval equipment by analysis.

For other military equipment, MIL-STD-810G, Method 516, Shock (Department of Defense, 2008) specifies requirements for a several shock qualification SRS_D. If field test data are available, the general 810G guidance is to determine SRS_D with the

maximum envelope approach illustrated in Figure (1-2). Further, it is possible to determine a temporal duration T_E, defined in Section 3.2, if recorded time history test data are available from field testing. If measured test data are not available, the guidance for functional and crash hazard shock is to use prescribed SRS_D published in MIL-STD-810G, Method 516, Figure (1-4).

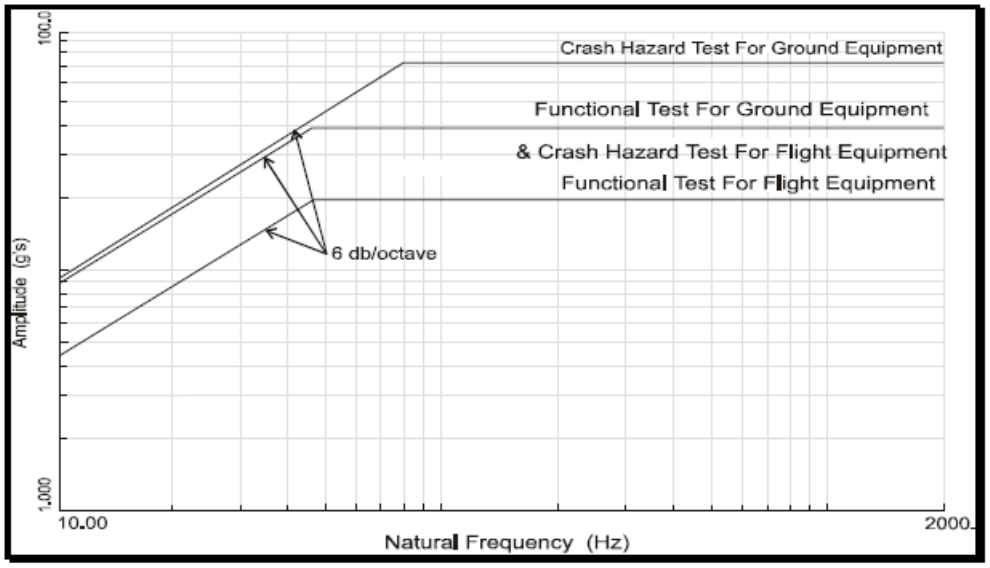

Figure (1-4) MIL-STD-810G, Method 516, Functional and Crash Hazard Shock SRS_D

Similarly, the default SRS_D requirement for a ballistic shock environment resulting from a direct hit to a ground combat vehicle, Figure (1-5), is given by MIL-STD-810G, Method 522, Ballistic Shock (Department of Defense, 2008). This document describes the ballistic shock produced in armored vehicles for hostile attack from mines, explosives, detonation of reactive armor and projectiles. The NATO International Test Operations Procedure (ITOP) representing France, Germany, United Kingdom and the United States (International Test and Evaluation Steering Committee, 2000) has the identical SRS_D requirement for ballistic shock.

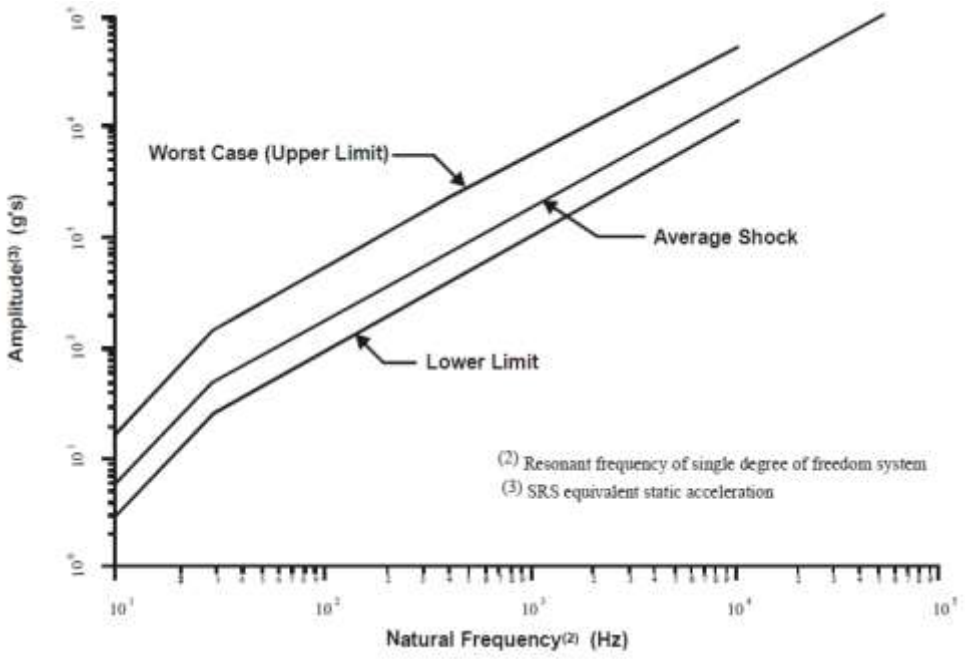

Figure (1-5) MIL-STD-810G, Method 522, Ballistic Shock SRS_D

Pyrotechnic shock, commonly referred to as pyroshock, is the shock resulting from pyrotechnic devices which are typically an explosive or propellant activated event. A pyroshock pulse is highly localized with high acceleration and high frequency content, which can range from 300-300,000 *g*'s at frequencies of 100-1,000,000 *Hz*, and as such excite very high frequency material responses. Pyroshock sources include explosive bolts, separation nuts, pin puller, and pyro-activated operational hardware. For pyroshock, as with functional and ballistic shock, if measured data are not available, MIL-STD-810G, Method 517, Pyroshock (Department of Defense, 2008) specifies a default SRS_D for design purposes, shown in Figure (1-6). NASA also references the SRS_D of Figure (1-6) (NASA, 2001) for pyroshock.

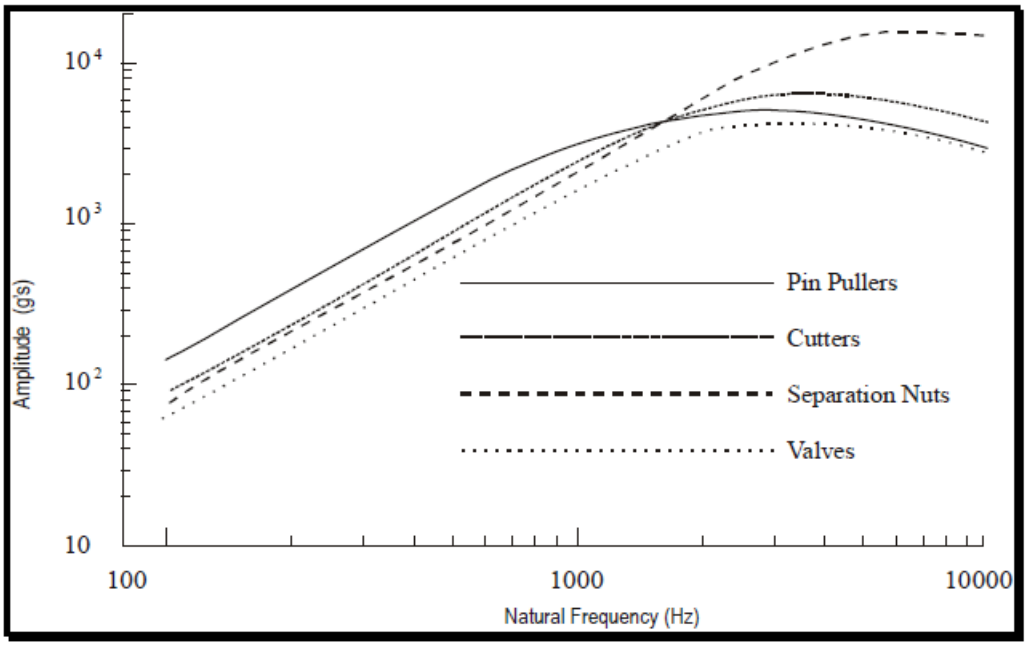

Figure (1-6) MIL-STD-810G, Method 517, Pyrotechnic Devices SRS_D

1.4 Role of a Synthesized Acceleration

As indicated in Section 1.3, the required shock design environment is frequently specified in terms of a design SRS_D. If a linear structural dynamic system is to be analyzed to SRS_D requirements, the analysis can be done directly with the mode superposition process described in Appendix A. Mode superposition is a linear process based on an Eigen value extraction from the linear equations of motion for a linear system. However, if the system has nonlinear elements such as nonlinear springs, dampers or nonlinear material properties, the resulting equations of motion are nonlinear and mode superposition is not possible because the system normal modes of vibration are not stationary.

Similarly, if a physical system is to be shock tested to SRS_D requirements, the SRS_D cannot be used directly to control the test machine. Much of the motivation to

determine a synthesized a_S compatible with a design SRS_D is for shock testing with electro-dynamic shakers (Smallwood & Nord, 1974) (Smallwood, 1986) (Nelson, 1989). These types of test machines have physical limitations in terms of how much force they can deliver to the test article and maximum displacement limitations of the shaker armature. The peak shaker force is based on the peak acceleration of the transient acceleration time-history and the weight of the equipment being tested (max force = mass*peak acceleration). The peak displacement limitation can also be problematic for low frequencies where the acceleration is generally low but the peak displacement is high.

In both cases of analysis or test, a synthesized SRS_D compatible shock acceleration time-history, a_S, is necessary. It is not difficult to synthesize a transient a_S with a corresponding SRS_S that matches a prescribed SRS_D within a specified tolerance envelope requirement. Many techniques exist to synthesize a shock acceleration, described in Section 2.3, based solely on matching the SRS_D with no consideration of other constraints. The assumption has been that if SRS_S from a_S matches SRS_D within prescribed tolerances, when a_S is applied to a system model or test article by analysis or test, respectively, the system response should be accurate. However, past studies have demonstrated that system responses to a synthesized base acceleration a_S can, and frequently do, vary significantly from responses to the design acceleration a_D. Additional useful information is available to mitigate this problem. This information includes the energy input to the structure from the shock acceleration and, if field test data are available, temporal information for the overall shape envelope and temporal duration T_E of the shock acceleration. However, based on published literature, others have not

included this additional information in the a_S synthesis process. The energy input to the system, based on the energy input spectrum *EIS*, provides additional information beyond the SRS_D which can be considered in the synthesis of a_S. Further, while a temporal duration requirement T_E is sometimes required by specification, others have not included strong shock duration T_E or overall temporal shape as a part of the a_S synthesis process. In addition, there is a paucity of published literature where authors have verified the accuracy of the synthesized a_S based on *MDOF* system responses relative to the corresponding responses from a known design acceleration, a_D.

1.5 Research Objectives

The objectives of the research documented herein are to determine a systematic method to:

- Expand the *SRS* compatible base acceleration synthesis process to include energy input and temporal information,
- Demonstrate improved system response from the expanded process, and
- Identify types of systems that are appropriate to this synthesis procedure.

1.6 Thesis Outline

To address these objectives, an expanded approach has been developed for the synthesis of a_S. This approach broadened the current synthesis process (Chapter 2) to include not only SRS_D compatibility, but also compatibility with a design energy input spectrum, EIS_D, and a design temporal duration, T_{ED}. These quantities are determined from a known design acceleration, a_D. An optimization algorithm was developed

(Chapter 3) to return a_S which minimizes the following three factors with a merit function *M*,

$SRS_{\%}$ (average % error of SRS_S:SRS_D),

$EIS_{\%}$ **(**average % error of EIS_S:EIS_D) and

$T_{E\%}$ (average % error of T_{ES}:T_{ED}).

A regression analysis was performed based on eight accelerations synthesized with the merit function and the corresponding eight sets of *3DOF* system responses. Based on regression analysis, an updated merit function was formulated that included the above three factors and also the products (or cross terms) of the factors. An optimized acceleration a_{S2} was synthesized with the updated merit function.

The optimized a_{S2} was compared with four a_S synthesized using common industry practices (classical pulse, damped sines, wavelets, enveloped sines), (Chapter 4). To evaluate the accuracy of the five a_S, a second *3DOF* model was developed based on the U. S. Navy's medium weight shock machine (*MWSM*). Representative linear and nonlinear variants of the *MWSM* model were developed. *MWSM* model responses were determined from the five a_S. Responses evaluated were peak mass accelerations, peak displacements and peak system energy input per unit mass. The peak model responses from synthesized a_S were compared with the corresponding *MWSM* model peak responses from a prescribed design acceleration a_D. The accuracy of each a_S was evaluated based on the *MWSM* model responses.

1.7 Overview of Findings

Evaluation of all a_S was based on the peak responses of the *MWSM 3DOF* models compared to the corresponding response from the design acceleration, a_D. Three *MWSM* model responses evaluated were;

- Average % error of peak mass accelerations,
- Average % error of peak mass displacements, and
- % error of *3DOF* peak energy input.

For the *MWSM* model linear variant, the optimized a_{S2} resulted in the lowest percent errors for all three responses. For the two nonlinear *MWSM* variants, optimized a_{S2} had lower percentage errors relative to the other four synthesized a_S, for peak mass accelerations and displacements in the majority of the cases. For all *MWSM* model variants (linear and nonlinear), the optimized a_{S2} resulted in the lowest peak energy input percent error. The optimized a_{S2} was the only synthesized shock acceleration that included matching the energy input spectrum from the design acceleration, EIS_D, as a part of the optimization process.

Energy input to a system from shock acceleration represents integrating the energy equation over the entire structure, and as such is a comprehensive measure of total system damage potential. On the other hand, local displacements and accelerations cannot represent the damage potential for the entire structure and do not have general significance for the entire structure.

2 Background

2.1 Overview

Numerous methods exist to synthesize a base acceleration a_S to be compatible with a design SRS_D. Current practices focus on the singular goal of achieving the best match of SRS_S with SRS_D. However, additional information is available to augment the synthesis of a_S including the energy input per unit mass, which can be derived from the SRS_D, and temporal information that can be extracted from available test data. An overview of the common a_S synthesis methods is described herein. Derivations of the *SRS* and the energy input equations are presented. Temporal information is defined including shock pulse durations and overall envelope.

2.2 Derivation of the Shock Response Spectrum

The *SRS* was defined and illustrated in Section 1.2 as the maximum response acceleration from a series of linear *SDOF* oscillators covering a frequency range when subjected to a common input base acceleration-time history. In this section the maximum response of each *SDOF* oscillator of circular frequency ω_n is derived. Consider a series of linear damped *SDOF* oscillators with *N* different natural frequencies, all mounted on a common fixed base, shown in Figure (2-1).

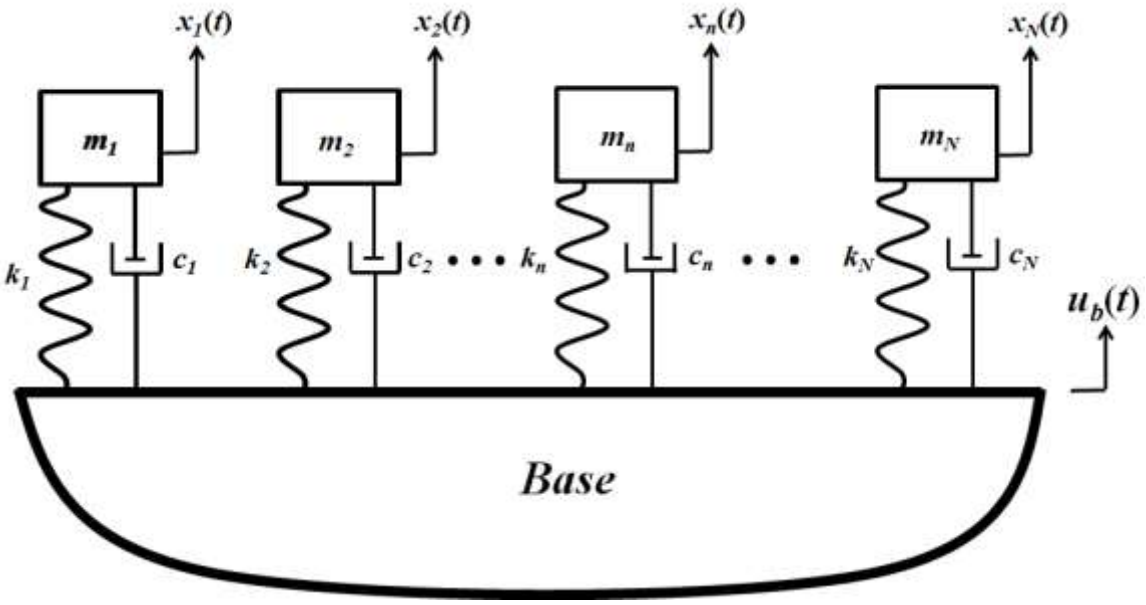

Figure (2-1) Series of SDOF Oscillators on a Common Base

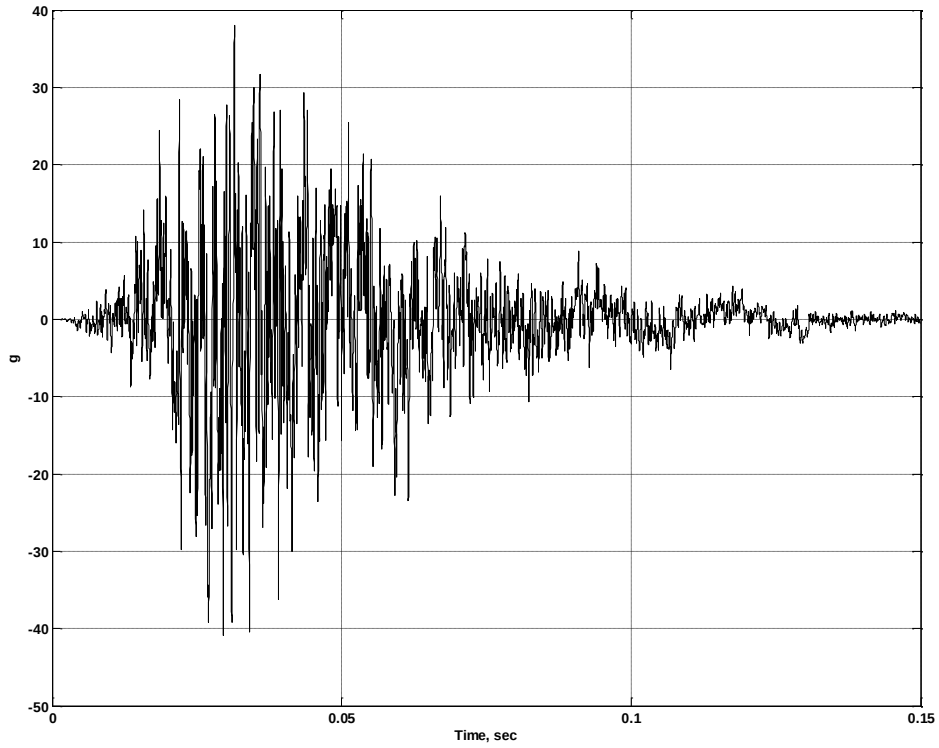

Figure (2-2) Typical Base Acceleration $\ddot{u}_b(t)$

Each oscillator has an independent absolute coordinate, $x_n(t)$. The base coordinate is $u_b(t)$. If the base is subjected to transient shock acceleration $\ddot{u}_b(t)$ such as the one shown in Figure (2-2), this will induce an independent response in each oscillator. The governing equation of motion for the n^{th} oscillator, developed by putting m_n in dynamic force equilibrium from d'Alembert's principle, is

$$m_n\ddot{x}_n(t)+c_n\left(\dot{x}_n(t)-\dot{u}_b(t)\right)+k_n\left(x_n(t)-u_b(t)\right)=0, \tag{2-1}$$

where $x_n(t)$ is an absolute coordinate for the displacement of the n^{th} mass m_n. A relative coordinate for the displacement of the mass relative to the base is defined for each oscillator as,

$$z_n(t)\equiv x_n(t)-u_b(t). \tag{2-2}$$

Substituting (2-2) into (2-1) yields,

$$m_n\left(\ddot{z}_n(t)+\ddot{u}_b(t)\right)+c_n\dot{z}_n(t)+k_nz_n(t)=0. \tag{2-3}$$

Dividing by m_n and moving the base acceleration base acceleration term to the right hand side of the equation gives,

$$\ddot{z}_n(t)+\frac{c_n}{m_n}\dot{z}_n(t)+\frac{k_n}{m_n}z_n(t)=-\ddot{u}_b(t). \tag{2-4}$$

It is recognized that $\frac{k_n}{m_n}=\omega_n^2$ is the squared natural frequency of the n^{th} oscillator and that $\frac{c_n}{m_n}=2\zeta_n\omega_n$ is the damping term where ζ_n is the percent of critical damping. Making these substitutions gives a *SDOF* equation of motion (2-5) in relative coordinates z_n as,

$$\ddot{z}_n(t) + 2\zeta_n\omega_n\dot{z}_n(t) + \omega_n^2 z_n(t) = -\ddot{u}_b(t)\,. \tag{2-5}$$

From (2-1), (2-2) and (2-4), the absolute acceleration of mass m_n is determined from the relative velocity and relative displacement given by equation (2-6),

$$\ddot{x}_n(t) = -2\zeta_n\omega_n\dot{z}_n(t) - \omega_n^2 z_n(t)\,. \tag{2-6}$$

The damping term is frequently ignored on the basis that the damping force contributes little to the equilibrium relationship (Clough & Penzien, 1975), resulting in a relationship between the absolute acceleration and the relative displacement,

$$\ddot{x}_n(t) \cong -\omega_n^2 z_n(t)\,. \tag{2-7}$$

Equation (2-7) indicates that the absolute acceleration of the n^{th} mass is proportional to the relative displacement between the mass and the base, with the proportionality being the squared circular frequency. The solution to equation (2-5) is given by Duhamel's Integral,

$$z_n(t) = -\frac{1}{\omega_n\sqrt{1-\zeta^2}}\int_0^t \ddot{u}_b(\tau)e^{-\zeta_n\omega_n(t-\tau)}\sin\omega_n\sqrt{1-\zeta^2}\,(t-\tau)d\tau\,. \tag{2-8}$$

Substituting (2-8) into (2-7) gives the absolute acceleration of mass m_n, equation (2-9),

$$\ddot{x}_n(t) = \frac{\omega_n}{\sqrt{1-\zeta^2}}\int_0^t \ddot{u}_b(\tau)e^{-\zeta_n\omega_n(t-\tau)}\sin\omega_n\sqrt{1-\zeta^2}\,(t-\tau)d\tau\,. \tag{2-9}$$

The *SRS* defined as the absolute value of the peak mass accelerations over all frequencies ω_n. For the n^{th} frequency this is given by,

$$SRS_n \equiv \left|\ddot{x}_n(t)\right|_{\max}\,. \tag{2-10}$$

Substitution of equation (2-9) into (2-10) gives the SRS_n value for the n^{th} frequency *SDOF* oscillator,

$$SRS_n = \left| \frac{\omega_n}{\sqrt{1-\zeta^2}} \int_0^t \ddot{u}_b(\tau) e^{-\zeta_n \omega_n (t-\tau)} \sin \omega_n \sqrt{1-\zeta^2}\,(t-\tau) d\tau \right|_{\max} . \qquad (2\text{-}11)$$

A graph of a shock response spectrum is developed by plotting SRS_n as a function of ω_n, or more commonly $f_n = \omega_n / 2\pi$ in hertz, for all frequencies. A plot of the *SRS* for the base acceleration of Figure (2-2) is shown in Figure (2-3). Note that at the high frequency end of the plot, the *SRS* is approaching the 40g asymptote which corresponds to the peak amplitude of the base acceleration in Figure (2-2).

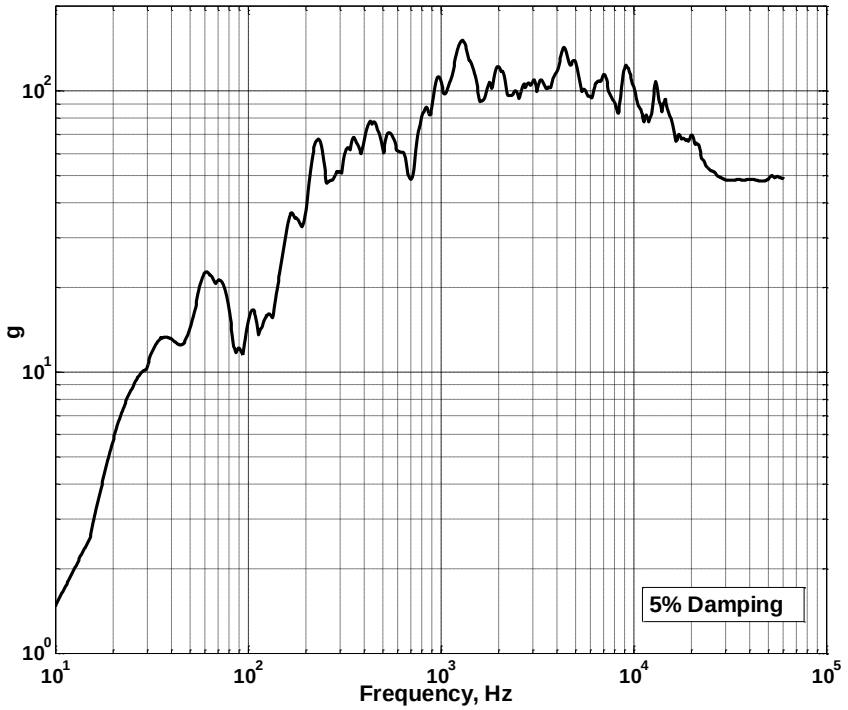

Figure (2-3) Typical Shock Response Spectrum for Mechanical Shock

2.3 Methods to Synthesize *SRS* Compatible Acceleration

Early methods to synthesize spectrum compatible ground accelerations were done in the study of earthquakes by the seismic community. As early as the 1940's, Housner

(1947) modeled an earthquake as a random process with a series of pulses of different magnitudes that occurred randomly in time. Subsequently, Housner (1955) used a technique of modeling an earthquake as the sum of sine wave pulses occurring randomly in time, with frequency and amplitude determined from a probability distribution.

Additional research to synthesize an *SRS* compatible acceleration time-history was continued in the 1960's by the seismic community. Civil engineers recognized the need to model ground structures analytically to determine the survivability to withstand strong earthquakes. Early methods to synthesize base accelerations compatible with a prescribed design SRS_D were approached by modifications of earthquake acceleration records. These approaches were to use either stationary random processes (Housner & Jennings, 1964) (Jennings, Housner, & Tsai, 1968) (Shinozuka, 1973) (Rizzo, Shaw, & Jarecki, 1973) (Preumont, 1980) or non-stationary random processes (Iyengar & Iyengar, 1969) (Saragoni & Hart, 1974) (Iyengar & Rao, 1979) to guide the modification of earthquakes acceleration data for the synthesis of an artificial earthquake. The approach was to choose a starting set of coefficients for each frequency of SRS_D and modify the set iteratively to improve the agreement between the SRS_S of the artificial earthquake and the SRS_D of the real earthquake (Preumont, 1984). Several starting procedures were explored including.

- Selection of an existing earthquake acceleration record which had an *SRS* that was close to the target SRS_D,
- Selection of an initial set of coefficient by modification of the amplitude of the Fourier transform of the existing earthquake and

- Modification of the power spectral density (*PSD*) of the real earthquake for the set of coefficients for each frequency.

During the 1970's, procedures to synthesize SRS_D compatible acceleration time-histories emerged which did not rely on existing earthquake acceleration data records. These methods employed the summation of sinusoids using a temporal envelope function to control the rise and decay of the synthesized acceleration (Scanlan & Sachs, 1974) (Gasparini & Vanmarcke, Jan 1976) (Levy & Wilkinson, 1976) (Kost, Tellkamp, Gantayat, & Weber, 1978) (Ghosh, 1991) (Alexander J. E., 1995).

The introduction of neural networks in the 1990's provided seismic engineers other methods to synthesize spectrum compatible ground accelerations. One such method was to train a two stage neural network from 30 earthquake ground acceleration records (Ghaboussi & Lin, 1998). Another approach employed a five neural network model to synthesize an SRS_D compatible ground acceleration (Lee & Han, 2010). This approach used basic earthquake information such as magnitude, epicenter distance, site conditions and focal depth to train the neural networks. While neural network based processes did result in a synthesized earthquake acceleration, limitations existed based on departure of the earthquake of interest compared to those that trained the neural networks. In general the match of the synthesized SRS_S was not particularly accurate to the target SRS_D.

Soize (2010) published a unique method to synthesize a_S to be compatible with SRS_D using the maximum entropy principal. This principle was used to construct the

probability distribution of a non-stationary stochastic process. The resulting a_S waveform appeared credible and the agreement between SRS_S and SRS_D was reasonable.

Brake (2011) published an interesting approach of combining different basis functions to synthesize an *SRS* compatible base acceleration. These functions were impulses, sines, damped sines and wavelets. With various combinations of these functions and optimizing the coefficients of each with a genetic algorithm, Brake was able to obtain a reasonable match of SRS_S and SRS_D. The resulting transient a_S wave form, however, was obviously a "manufactured" time-history with little temporal relation to real test data.

Others in the seismic community continued to explore the synthesis of *SRS* compatible ground acceleration time-histories using the stationary and non-stationary features of earthquakes to include the power spectral density function (Gupta & Trifunac, 1998) (Zhang, Chen, & Li, 2007).

Presently for mechanical shock, the most common techniques to synthesize an *SRS* compatible acceleration a_S are:

- classical pulse (e.g., half-sine, terminal peak saw-tooth, trapezoid),
- damped sinusoids,
- wavelets and
- enveloped sinusoids.

MIL-STD-810G, Method 516 (Department of Defense, 2008) specifies that if test data are not available, the use of damped or amplitude modulated sinusoids is permissible provided that the SRS_S exceeds a prescribed SRS_D over a frequency range of 5-2000 Hz.

The use of a classical pulse (either terminal peak saw-tooth or trapezoid), while the least desirable approach, is permitted if no test data are available. The UK MOD (Ministry of Defense, 2006) also imposes requirements and tolerances on pulses (half sine, terminal peak saw-tooth, and trapezoidal) and damped sinusoids in terms of peak amplitude and number of shocks pulses.

Beyond classical shock pulses to synthesize an SRS_D compatible a_S, some variant of the summation of sinusoids is the most frequently used method for mechanical shock. One method, especially relevant for control an electro-dynamics shaker test machine, is wavelets (Irvine, 2015). Multiple discrete wavelets, when summed, will result in a synthesized a_S wave form. A discrete wavelet has a sinusoidal motion with a finite and specific number of half sine oscillations with unique parameters for frequency, amplitude and time delay. Iterations for the parameters of each wavelet yield a synthesized a_S with a resulting SRS_S that matches SRS_D within acceptable tolerances. The equation for an individual wavelet, $W_n(t)$, is given by,

$$W_n(t) = 0 \quad t < t_{dn} \tag{2-12}$$

$$W_n(t) = A_n \sin\left\{\frac{\omega_n}{N_n}(t - t_{dn})\right\} \sin\{\omega_n(t - t_{dn})\} \qquad t_{dn} \le t \le \left(t_{dn} + \frac{N_n \pi}{\omega_n}\right) \tag{2-13}$$

$$W_n(t) = 0 \quad t > \left(t_{dn} + \frac{N_n \pi}{\omega_n}\right) \tag{2-14}$$

$$a_S(t) = \sum_{n=1}^{N_n} W_n(t) \tag{2-15}$$

where,

- $W_n(t)$ is the acceleration of wavelet *n* at time *t*,
- A_n is the wavelet amplitude,
- N_n is the number of half-sines in the wavelet (odd integer ≥ 3),
- ω_n is the wavelet frequency and
- t_{dn} is the wavelet time delay.

The complete synthesized a_S is obtained from the summation of all wavelets. An individual wavelet example is shown in Figure (2-4) where A_n = 1.34, f_n = 100 *Hz*, N_n = 19 half-sines and t_{dn} = 0.

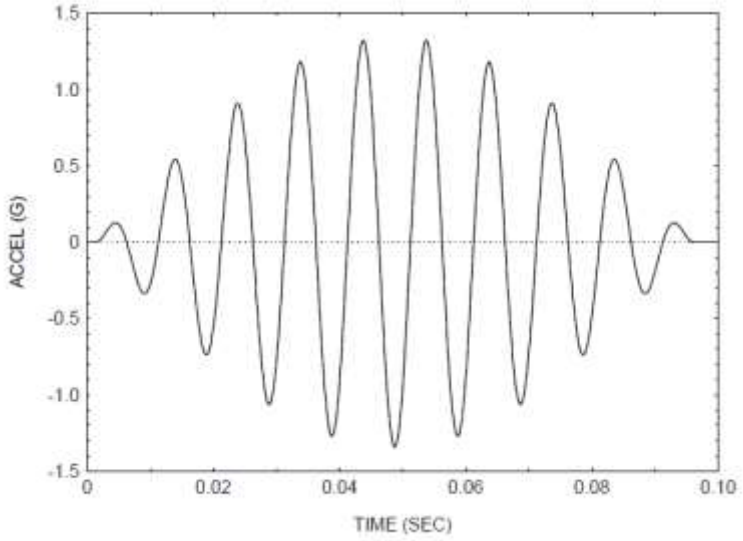

Figure (2-4) Individual Wavelet Example

Other methods to synthesize a_S are with damped and enveloped sinusoids. These approaches are similar to that of wavelets. The primary difference is the way in which the rise, peak and decay of the overall waveform is controlled. In the case of damped sinusoids, as with wavelets, individual sinusoidal pulses are summed. Each individual

damped sine pulse has a unique time delay t_{dn}, damping ζ_n, amplitude A_n, and frequency ω_n defined by,

$$W_n(t) = 0, \quad t < t_{dn} \ , \tag{2-16}$$

$$W_n(t) = A_n e^{-\zeta_n \omega_n (t - t_{dn})} \sin\{\omega_n (t - t_{dn})\} \quad t \geq t_{dn} \quad \textit{and} \tag{2-17}$$

$$a_S(t) = \sum_{n=1}^{N} W_n(t) \ . \tag{2-18}$$

An example of an individual damped sine pulse is shown in Figure (2-5) where A_n = 1.34g, f_n = 100 *Hz*, ζ=0.05 and t_{dn} = .01 seconds.

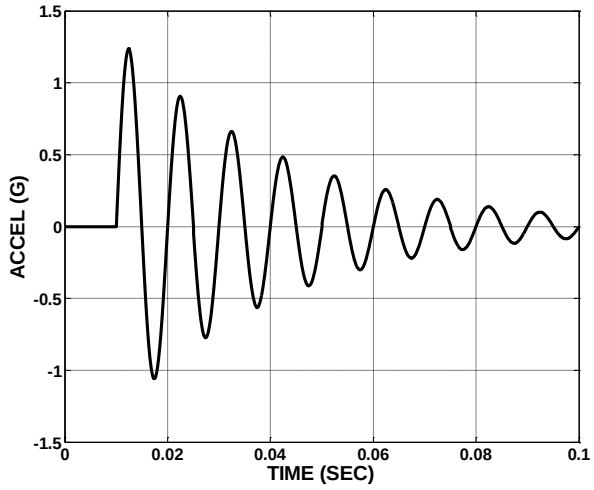

Figure (2-5) Individual Damped Sine Example

The enveloped sinusoids with random phase angles approach is similar to damped sinusoids. The equation for enveloped sinusoids is given by,

$$a_S(t) = E(t) \sum_{n=1}^{N} A_n \sin(\omega_n t + \phi_n) \ , \tag{2-19}$$

where A_n are the amplitude coefficients, ω_n are the frequencies of the sinusoids and φ_n are random phase angles for each frequency *n*. The rise, plateau and decay of a_S is controlled by an envelope function $E(t)$ rather than damping. Since $E(t)$ can be sized to any

temporal shape needed, the synthesized pulse shape of a_S can be closely controlled to match that of available test or design data. Figure (2-6) is a plot of $E(t)$ superimposed on the enveloped sinusoids synthesized acceleration time-history a_S. Inasmuch as $E(t)$ is sized to control the relative rise, plateau and decay of a_S, the value of the plateau is commonly set to unity. However, $E(t)$ was increased by a factor of 40 in Figure (2-6) to better illustrate the relationship of $E(t)$ to the corresponding shape of a_S. The transient pulse is developed as the summation of sinusoids of amplitude A_n over n frequencies needed to span the frequency bandwidth of interest. During each iteration i of the synthesis process, the amplitude coefficients A_n are adjusted to improve the agreement of SRS_S with SRS_D. The updated A_n coefficients are adjust during each iteration for each frequency n from, $A_n^{i+1} = \frac{SRS_D^n}{\left(SRS_S^n\right)^i} A_n^i$.

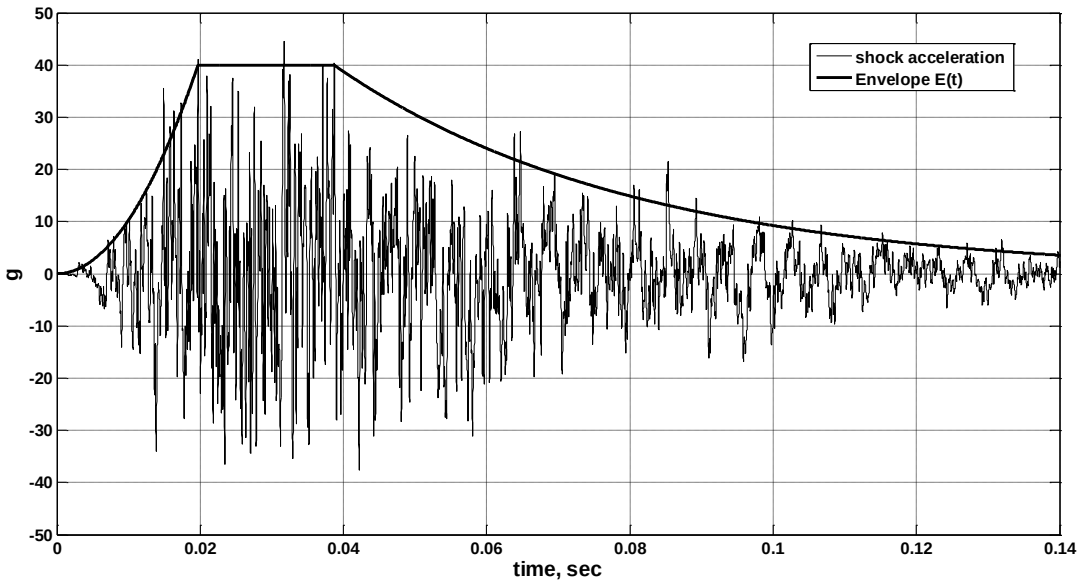

Figure (2-6) Envelope $E(t)$ Superimposed on Corresponding Enveloped Sinusoids a_S

Figure (2-7) is a plot of the design acceleration a_D and four accelerations (half sine, damped sines, wavelets and enveloped sines) synthesized to match SRS_D. No attempt was made to match the energy input spectrum or duration of a_D, *EIS* and T_E, respectively. The time scale of the half sine pulse was expanded by a factor of ten relative to the others in Figure (2-7), to better show the shape of the synthesized waveform. The SRS_S of the synthesized accelerations, with the exception of the half sine, matched SRS_D with good agreement. Figure (2-8) shows SRS_D and SRS_S for the four synthesized a_S. Table (2-1) is the percentage errors for the SRS_S of the synthesized accelerations relative to SRS_D. The percentage error for each is the percent difference between SRS_S and SRS_D averaged over all the frequencies. The error was least for enveloped sines at 4.88% .

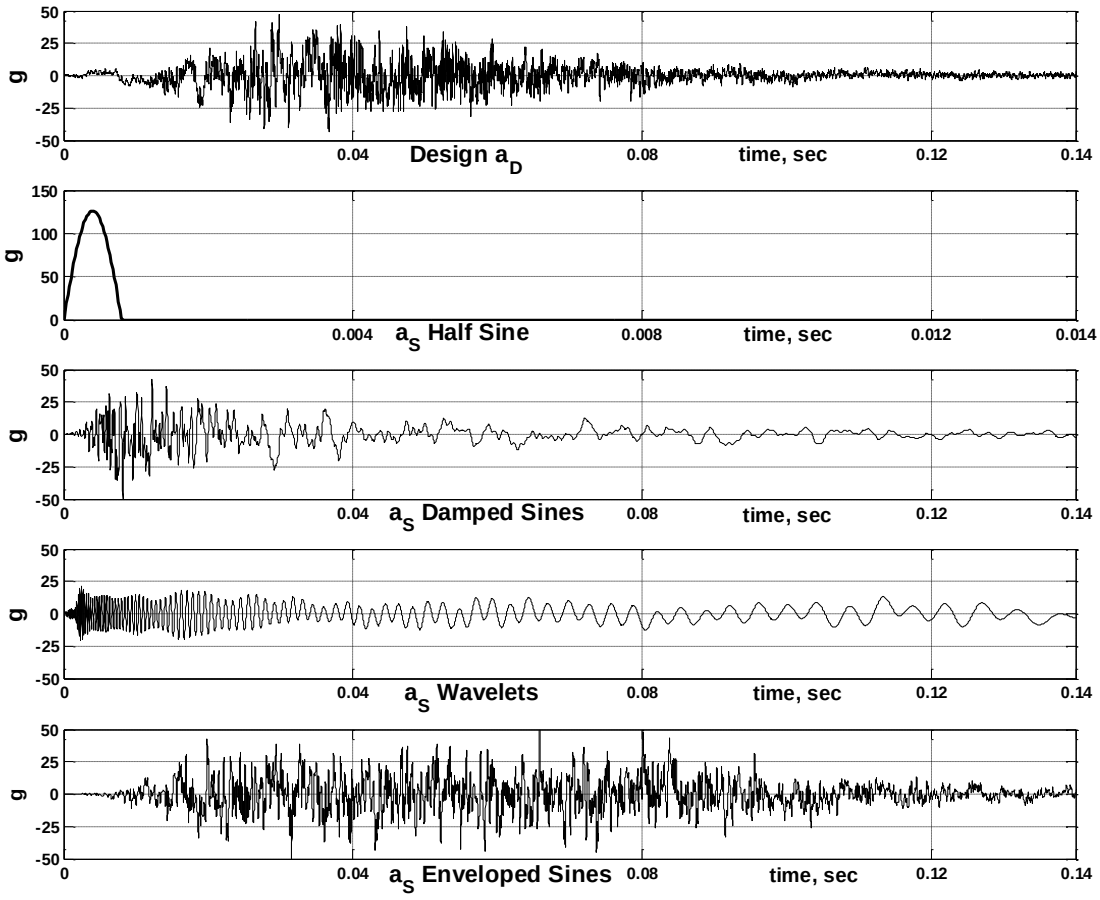

Figure (2-7) Design a_D and Synthesized Accelerations

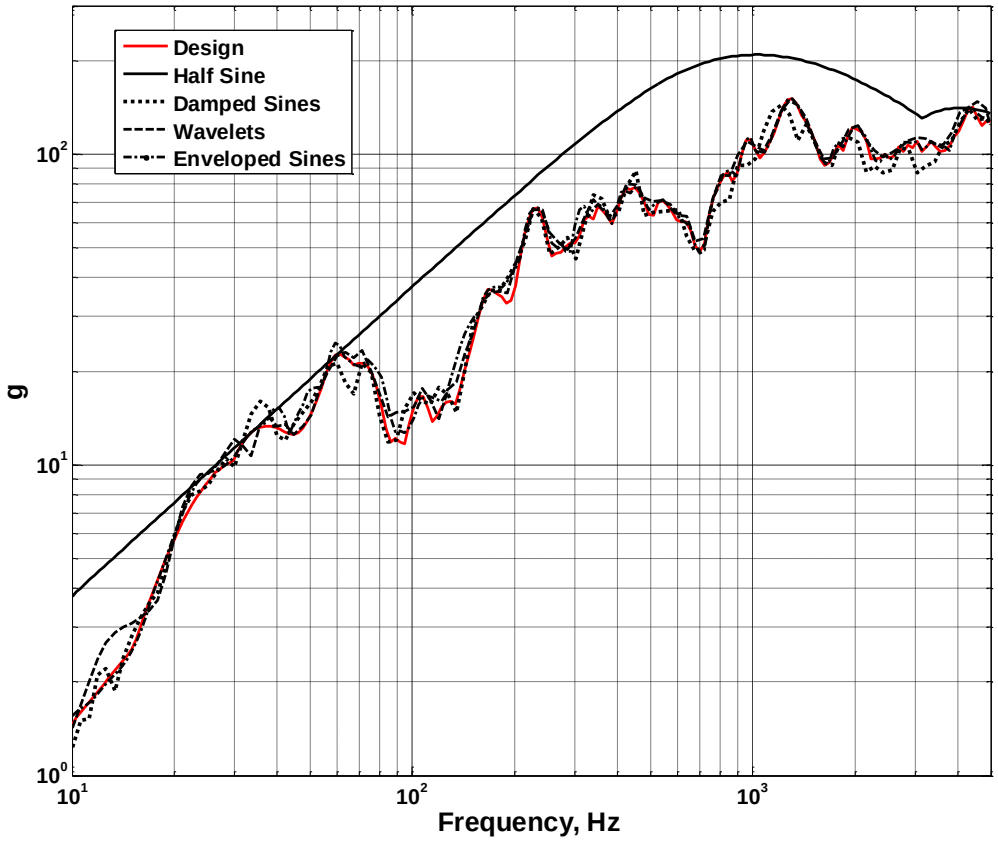

Figure (2-8) Design SRS_D and SRS_S of Synthesized Accelerations

Table (2-1) Synthesized Accelerations SRS_S % Error

	Average $SRS_{\%}$ Error
Half Sine	83.3%
Damped Sines	8.67%
Wavelets	6.97%
Enveloped Sines	4.88%

As demonstrated in Figure (2-8), it is not difficult to synthesize a base acceleration a_S that matches a prescribed design SRS_D within specified tolerance limits, such as ≤ 10% error. However, past research by Alexander (1998) has indicated that to

obtain an accurate response from a structural dynamic model, matching only the SRS_D is not sufficient. While a specific base acceleration transient will result in a unique shock response spectrum, the inverse is not true. There are theoretically an infinite number of base accelerations that will yield the same *SRS*. The phasing of the modes of a structural dynamic model relative to the timing of the synthesized acceleration peaks can significantly affect peak *MDOF* response magnitudes. The goal of the research herein is to determine a process, with additional guidelines beyond common practices, that will yield not only a spectrum compatible synthesized base acceleration, but also will yield improved results when applied to linear and nonlinear physical system models, especially for energy input. To improve the accuracy of a physical system model response to a_s, additional constraints are explored for the acceleration synthesis process. One such constraint is temporal (time) duration of the synthesized transient acceleration pulse. If test data have been acquired, temporal information can be determined from the data set to guide the synthesis of a_S. For example MIL-STD-810G, Method 516 (Department of Defense, 2008) imposes temporal durations termed T_E and T_e on the synthesized acceleration a_s. Additionally, an average or maximum *EIS* can be determined from the test data set.

2.4 Evolution of Energy Methods for Shock and Vibration

Research of energy methods for transient shock response modeling provides another constraint to be applied in the synthesis of a_S. This involves compatibility with not only the SRS_D, but also with the EIS_D. Synthesis of a_S to be compatible with SRS_D, EIS_D and temporal duration T_{ED} offer additional constraints to be considered for the objective of improving *MDOF* system response accuracy.

The seismic community did much of the early research to examine the utility of base acceleration energy input. The use of energy to characterize base excited structural dynamic response dates back to Hudson (1956) and Housner (1959). Hudson documented the maximum energy per unit mass for a *SDOF* oscillator is given by relationship to the velocity shock response spectrum,

$$\frac{\max\ energy}{unit\ mass} = \frac{1}{2} SRS_{vel}^2 \quad . \tag{2-20}$$

Hudson further developed a relationship between the velocity spectrum and the total energy from a series of pulses similar to that of earthquake excitation. Housner derived a relationship for the average energy in a *MDOF* structure based on the superposition of the total modal energies for each of the normal modes of the structure. The average energy in the structure for a transient shock is given as a function of the total mass of the structure and the average of the squared velocity spectral value of all *N* normal modes of the structure,

$$Energy_{ave} = \frac{1}{2} M \left(SRS_{vel_n}^2 \right)_{ave} \quad . \tag{2-21}$$

Other authors who have documented the relationship between energy and the square of the velocity spectrum include (Zahrah & Hall, 1984) (Uang & Berto, 1990) (Edwards, 2007).

Shock motion can be characterized by energy delivered to a structure. It is possible to determine energy input from a base acceleration-time history, and from the conservation of energy, the input energy will balance the energy from system response. The *EIS* is similar to an *SRS* inasmuch as it is a frequency based measure of the response of a series of *SDOF* oscillators subjected to a common base acceleration. However, in the case of an *EIS*, the measure is peak energy input per unit mass to the *SDOF* oscillator

from the base acceleration, instead of peak mass acceleration response as in the case of the *SRS*. As with the *SRS*, peak energy input is determined for a series of *SDOF* oscillators covering the frequency bandwidth of interest. Derivation of the *EIS* is in developed Section 2.5.

As was the case for the *SRS*, much of the ground work to study base excitation of a structure in terms of energy, in general, and the development of the *EIS*, in particular, was done by the seismic community from the mid-1980's to the present. Zahrah and Hall (1984) investigated the response of simple *SDOF* structures from strong earthquake excitations. Eight earthquakes records of magnitudes 4.7 to 7.7 were selected for representative strong ground input motions. The objective of the study was to better quantify factors that influence structural deformation and damage. The approach of the study was to compare the input energy to the dissipated energy by inelastic deformations and damping, to establish an improved damage criteria than peak ground acceleration or the shock response spectrum. The conclusion of the study was that a better damage potential might be defined in terms of the energy input to the structure.

Two formulation of the energy input equation are possible, based on absolute and relative coordinates for the *SDOF* equation of motion. The relative energy equation is given by (2-28). The absolute energy equation is based on derivation of the energy terms from the *SDOF* equation of motion prior to making the substitution for the relative coordinate ($z=u-u_b$). The absolute formulation leads to the energy input term ($EI_{abs} = \int m\ddot{u}\, du_b$). Uang and Bertero (1990) used the absolute energy formulation to compare the results of the input energy per unit mass from the *SDOF EIS* with that of a linear multi-story building. The result was the energy input of the *SDOF* model, on a per unit

mass basis, provided a very good estimate of the input energy of the multi-story building for the dominant frequency.

Manfredi (2001) noted that the input energy *EI* is an effective tool in seismic design and represents a "very stable parameter." For the response of a nonlinear *SDOF* system, Manfredi proposed a modification to Housner's input energy per unit mass assumption for an undamped system given by ½ of the pseudo-velocity squared,

$$\left(\frac{EI}{M}\right)_{\max} = \frac{1}{2}\left(\frac{SRS(\omega)}{\omega}\right)^2_{\max} \quad . \tag{2-22}$$

Manfredi's modification to Housner's equation included the addition of a second term with a dimensionless index I_D to account for the influence of the duration of the ground acceleration,

$$\left(\frac{EI}{M}\right)_{\max} = 0.45\left(\frac{SRS(\omega)}{\omega}\right)^2_{\max} + 0.10 I_D\left(\frac{SRS(\omega)}{\omega}\right)^2_{\max} \quad . \tag{2-23}$$

Ordaz, et al (Ordaz, Huerta, & Reinoso, 2003) derived another method to determine the relative input energy per unit mass using the Fourier amplitude spectrum and the real part of the relative velocity transfer function. The relative input energy per unit mass of an *SDOF* oscillator, derived in Section 2.5, is given by,

$$\frac{EI}{m} = -\int \ddot{u}_b(t)\dot{z}(t)dt \quad . \tag{2-24}$$

The transfer function of the base acceleration to relative velocity $\dot{z}(t)$in the frequency domain is given by,

$$H_v(\omega, \omega_n, \zeta) = -\frac{i\omega}{\omega_n^2 - \omega^2 + 2i\zeta\omega\omega_n} \quad . \tag{2-25}$$

The Fourier spectrum of the base acceleration is given by $\ddot{u}_b(\omega)$. The resulting expression for the energy input per unit mass is given by,

$$\frac{EI}{m} = -\frac{1}{\pi}\int_0^\infty \left|\ddot{u}_b(\omega)\right|^2 \mathrm{Re}\left|H_v(\omega, \omega_n, \zeta)\right| d\omega \quad . \tag{2-26}$$

Initial research and development for the use of energy methods was done almost exclusively by the seismic community to characterize shock damage from earthquakes. More recently other authors have published research in the application of energy methods to characterize mechanical shock as an alternative to the *SRS*. Authors who have considered energy methods for damage potential to mechanical systems include Gaberson (1995), Edwards (2007) (2009) , Iwasa and Shi (2008), and Alexander (2011).

Gaberson (1995) was a passionate advocate for the velocity shock response spectrum, SRS_{vel}, as a measure of damage potential. One of Gaberson's arguments for the use of the SRS_{vel} was the relationship to energy ($\frac{1}{2}\, mSRS^2_{vel}$), first noted by Hudson (1956).

Iwasa and Shi (2008) advocated the maximum total energy spectrum as the best measure of damage potential in the context of pyroshock, and noted that past studies indicated that maximum acceleration does not consistently represent the most accurate measure of damage potential. Their conclusion was that the maximum energy per unit mass of an *SDOF* system is a suitable indicator of pyroshock damage potential. This was confirmed by two mechanical tests, one from impact and one from electro-dynamic shaker input.

Based on a numerical simulation, Edwards (2007) demonstrated that the maximum energy input per unit mass input to a *MDOF* structure can be estimated by the energy input per unit mass of an *SDOF* system (i.e., the *EIS*) with the same frequency of the lowest (dominant) frequency of the *MDOF* structure. Uang and Berto (1990) demonstrated a similar finding. Edward's simulation consisted of five nonlinear *4DOF*

systems with the pre-yield fundamental frequencies of 10 *Hz*, 285 *Hz*, 1716 *Hz*, 7,357 *Hz* and 19,739 *Hz*. In all five cases, the energy input per unit mass of the *4DOF* structure matched the *EIS* at those same frequencies with good agreement.

Alexander (2011) published a study comparing the *EIS* from two base accelerations with the maximum energy per unit mass from the response of a *6DOF* ABAQUS (Dassault Systemes Simulia Corp, 2008) model, for both linear and nonlinear versions of model. The maximum energy per unit mass comparison from the model had good agreement with the *EIS* for the linear model. The same comparison for the nonlinear version of the model, while not unreasonable, had mixed results depending on the frequency.

Honeywell (Hartwig, 2013) was able to successfully use the *EIS* to quantify the total damage potential from packaging, handling and vibration from two different Honeywell operations. The *EIS* was developed for each of the two sites from data collected for each packaging configuration and each mode of transportation. Hartwig noted that the benefit of the *EIS* was that it accounts for the duration of the events and repeated exposures, where the power spectral density (*PSD*) does not. The same issue exists with the *SRS*.

2.5 Derivation of the Energy Input Equations

As with the *SRS*, it is possible to determine an Energy Input Spectrum (*EIS*), from a base acceleration from the peak energy inputs to a series of *SDOF* oscillators of different frequencies. A series of linear damped *SDOF* oscillators mounted to a common base, Figure (2-1), is also applicable for development of an *EIS*. Equation (2-3) is the

equation of motion of the n^{th} *SDOF* oscillator mounted to the base, formulated in terms of the relative coordinates z_n. Moving the inertial force term $m_n \ddot{u}_b(t)$ to the right hand side gives the equation of motion (2-27) for the n^{th} mass,

$$m_n \ddot{\boldsymbol{z}}_n(t) + c_n \dot{\boldsymbol{z}}_n(t) + k_n z_n(t) = - m_n \ddot{\boldsymbol{u}}_b(t) . \qquad (2\text{-}27)$$

Each term of equation (2-27) has units of force. To convert this equation from a force balance to an energy balance, each term is multiplied by in incremental displacement *dz* and integrated with respect to *z*, leading to the energy balance equation (2-28) in relative *z* coordinates,

$$\int m_n \ddot{z}_n(t)dz + \int c_n \dot{z}_n(t)dz + \int k_n z_n(t)dz = -\int m_n \ddot{u}_b(t)dz \; . \qquad (2\text{-}28)$$

The individual terms of on the left hand side of equation (2-28) describe the different forms of energy that are present in the *SDOF* oscillator. The right hand side of (2-28) is the input energy to the *SDOF* oscillator from the base acceleration. The terms on the left had side of (2-28) are kinetic, damped and absorbed energy, respectively. These terms are further expanded as follows.

Kinetic Energy: $$\int m\ddot{z}dz = \int m\frac{d\dot{z}}{dt}dz\frac{dt}{dt} = \int m\dot{z}d\dot{z} = \frac{1}{2}m\dot{z}^2 \,, \qquad (2\text{-}29)$$

Damped Energy: $$\int c\dot{z}dz = \int c\dot{z}\frac{dz}{dt}dt = c\int \dot{z}^2 dt \,, \qquad (2\text{-}30)$$

Absorbed Energy: $$\int kzdz = \frac{kz^2}{2} \text{, and} \qquad (2\text{-}31)$$

Input Energy: $$-\int m\ddot{u}_b\, dz = -\int m\ddot{u}_b dz\frac{dt}{dt} = -m\int \ddot{u}_b\, \dot{z}dt \; . \qquad (2\text{-}32)$$

The kinetic energy term gives the instantaneous kinetic energy of the $SDOF_n$ at the current time *t* from ½ the product of mass and velocity squared. The damped energy term is cumulative and builds during the shock transient. The absorbed energy term for a linear spring (*k* = constant) becomes the instantaneous energy of $\frac{1}{2}kz^2$. In the general

case where there is inelastic behavior of the spring (e.g., elasto-plastic) the absorbed energy would be cumulative during the transient due to plastic strain. Equation (2-32) gives the input energy to the $SDOF_n$ from the base acceleration and relative velocity. The input energy is cumulative for the duration of the shock transient. For any instance in time, the input energy is equal to the sum of the response energy terms on the left hand side of equation (2-28). An updated energy equation for the motion of a linear $SDOF_n$ oscillator is given by equation (2-33),

$$\frac{1}{2}m_n\dot{z}_n(t)^2 + c_n\int \dot{z}_n(t)^2 dt + \frac{1}{2}k_n z_n(t)^2 = -m_n\int \ddot{u}_b(t)\dot{z}_n(t)dt\,. \qquad (2\text{-}33)$$

Figure (2-9) is an example of the individual transient energies and the total transient input energy for a 10 Hz *SDOF* oscillator from a base acceleration. It is apparent from observation of the figure that the sum of the individual energy terms on the left hand side of equation (2-33) are equal to the input energy on the right hand side of equation (2-33) at every instance in time.

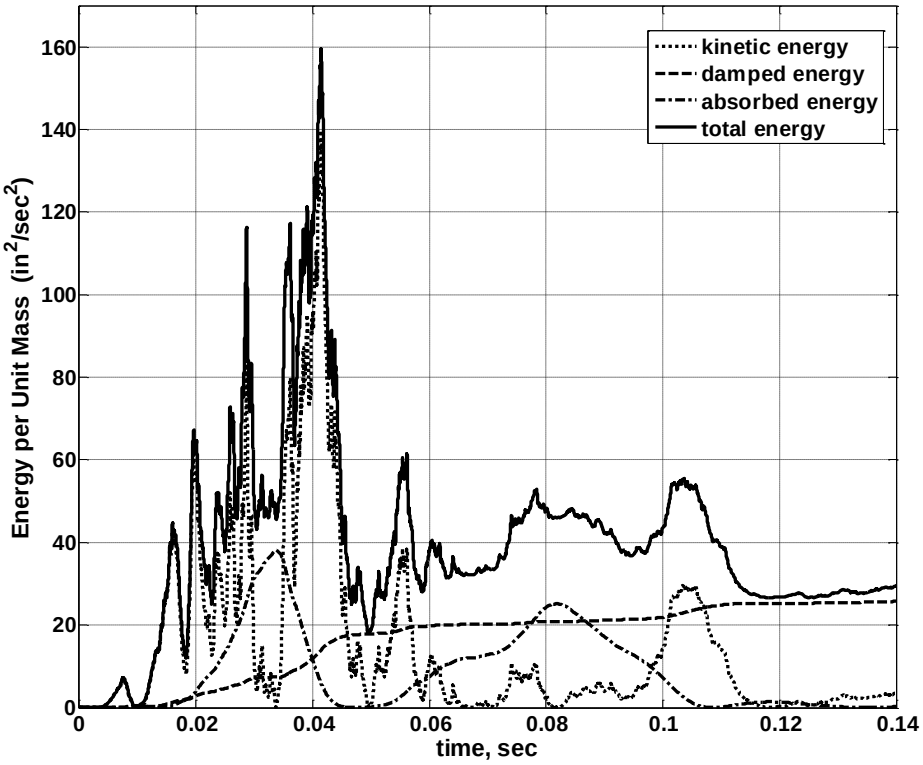

Figure (2-9) Transient Energy Input for 10 Hz *SDOF*

If the peak values of the input energy term, right hand side of equation (2-33), are plotted as a function of frequency for all *N SDOF* systems, an energy input spectrum is determined. Figure (2-10) shows the energy input from transient design base acceleration $\ddot{u_b}(t)$ for three *SDOF* oscillators tuned to frequencies of 10 Hz, 100 Hz and 1,000 Hz. The corresponding peak input energy per unit mass values are 159.6 in^2/sec^2, 74.5 in^2/sec^2 and 67.6 in^2/sec^2, respectively. These points are indicated by a square, an ellipse and a circle, respectively, in Figure (2-10). These peak energy input amplitudes are the magnitudes of the *EIS* for transient base acceleration at the corresponding frequencies, also indicated by a square, an ellipse and a circle, respectively, in Figure (2-11). The

complete *EIS* for the base acceleration $\ddot{u}_b(t)$ covering frequency bandwidth of 10 Hz to 5,000 Hz is plotted in Figure (2-11).

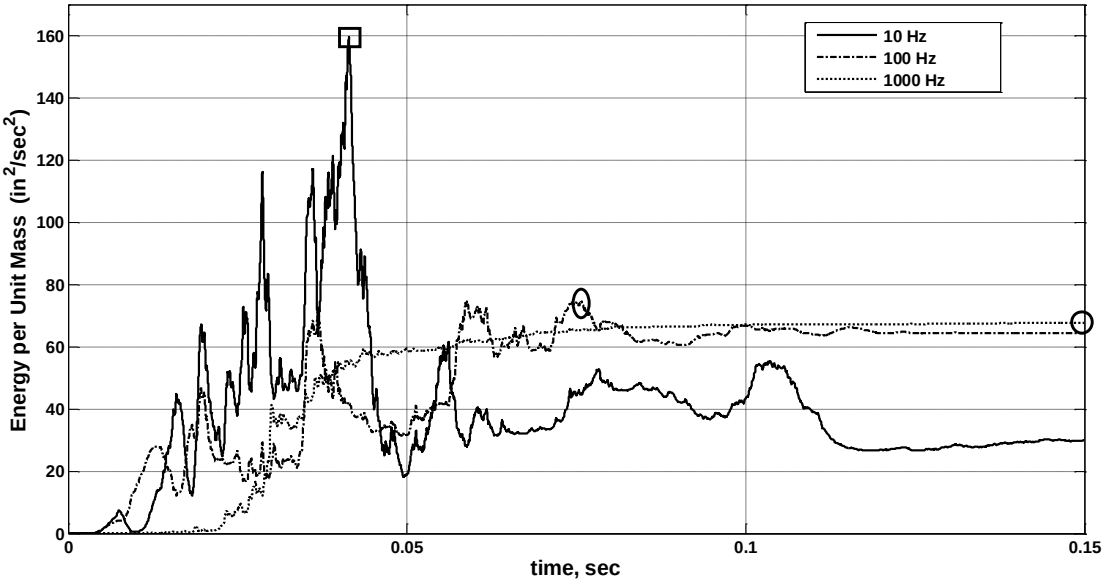

Figure (2-10) Base Acceleration $\ddot{u}_b(t)$ Transient Energy Input for Three *SDOF* Oscillators

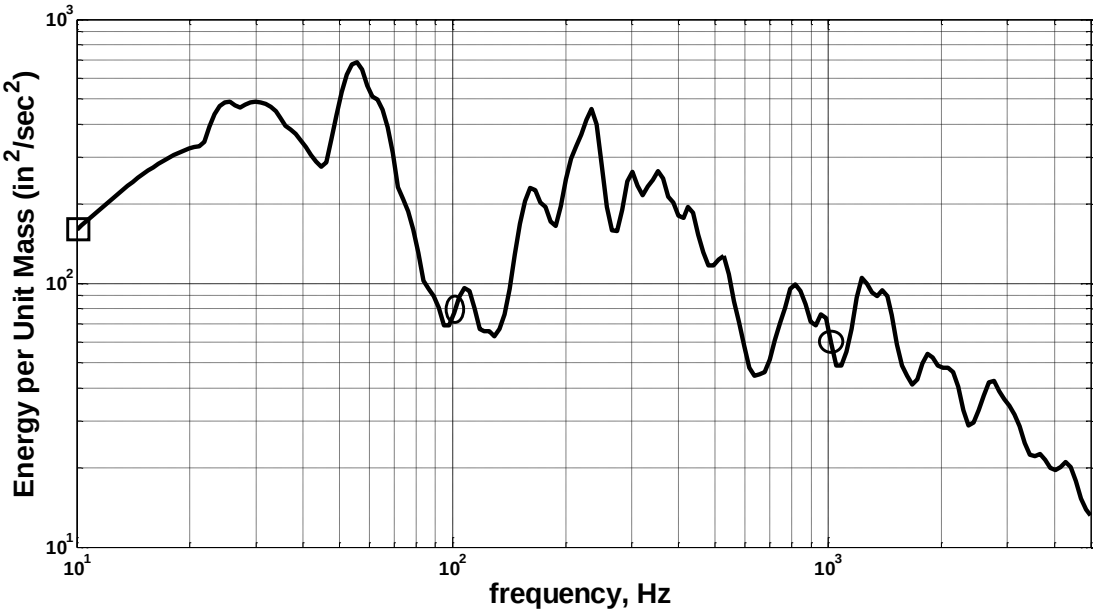

Figure (2-11) Base Acceleration $\ddot{u}_b(t)$ Energy Input Spectrum (*EIS*)

Derivation of an the energy equation for a *MDOF* structure is similar to that of a *SDOF* oscillator, and modifications to the *MDOF* matrix equation of motion are also similar to that of the *SDOF* scalar equation of motion. For a linear *MDOF* system in relative coordinates, the matrix equation of motion is given by equation (2-34),

$$[M]\{\ddot{z}\}+[C]\{\dot{z}\}+[K]\{z\}=-[M]\{1\}\ddot{u}_b \quad . \tag{2-34}$$

To convert equation (2-34) to from a force balance to an energy balance, we again multiply each term by $\{dz\}^T$ and integrate with respect to *z*, leading to the *MDOF* energy equation (2-35),

$$\int \{dz\}^T[M]\{\ddot{z}\}+\int \{dz\}^T[C]\{\dot{z}\}+\int \{dz\}^T[K]\{z\}=-\int \{dz\}^T[M]\{1\}\ddot{u}_b \; . \tag{2-35}$$

Noting that $\{dz\}$ can be rewritten as $\left\{\frac{dz}{dt}\right\}dt$, this substitution in (2-35) for all terms, except the absorbed energy term results in,

$$\int \{\dot{z}\}^T[M]\{\ddot{z}\}dt+\int \{\dot{z}\}^T[C]\{\dot{z}\}dt+\int \{dz\}^T[K]\{z\}=-\int \{\dot{z}\}^T[M]\{1\}\ddot{u}_b\, dt. \tag{2-36}$$

If similar transformations are executed for (2-36) as was done for the *SDOF* energy terms, equation (2-29) through equation (2-32) , the same energy terms occur for the *MDOF* system, given by,

Kinetic Energy: $\frac{1}{2}\{\dot{z}\}^T[M]\{\dot{z}\}$, (2-37)

Damped Energy: $\int \{\dot{z}\}^T[C]\{\dot{z}\}\, dt$, (2-38)

Absorbed Energy: $\frac{1}{2}\{z\}^T[K]\{z\}$ and (2-39)

Input Energy: $-\int \{\dot{z}\}^T[M]\{1\}\, \ddot{u}_b dt.$ (2-40)

For the *3DOF* system models described in Chapters 3 and 4, the input energy was computed from equation (2-40). The time integration was performed using the central

difference numerical integration time stepping routine, where the dynamic analysis is executed by stepping through the transient with equal Δt time increments. The integration procedure evaluates the incremental $\Delta E^k{}_n$ input energy for current time step increment *k*, and adds $\Delta E^k{}_n$ to the cumulative sum of all prior time steps, $E_n{}^{k-1}$. The *3DOF* energy input time stepping procedure is,

$$E_n^k = E_n^{k-1} + \Delta E_n^k \ , \tag{2-41}$$

$$E_n^k = E_n^{k-1} - \begin{bmatrix} \dot{z}_1 & \dot{z}_2 & \dot{z}_3 \end{bmatrix}^k \begin{bmatrix} m_1 & 0 & 0 \\ 0 & m_2 & 0 \\ 0 & 0 & m_3 \end{bmatrix} \begin{Bmatrix} 1 \\ 1 \\ 1 \end{Bmatrix} \ddot{u}_b^k \Delta t \quad \textit{and} \tag{2-42}$$

$$E_n^k = E_n^{k-1} - \left(m_1\dot{z}_1 + m_2\dot{z}_2 + m_3\dot{z}_3\right)\ddot{u}_b^k \Delta t \ . \tag{2-43}$$

2.6 Temporal Information from a Shock Acceleration

In addition to the *SRS* and *EIS*, if temporal information is available from shock test data it offers additional information for the synthesis of a_S. Two characteristics of a typical shock acceleration time-history are the overall envelope shape and a strong shock duration.

The envelope $E(t)$ is the relative temporal shape of the overall rise, plateau and decay of the shock acceleration time-history. Since $E(t)$ is a relative shape of the shock acceleration, the plateau is typically set to 1.0. For a family of test data, $E(t)$ can be determined based on a best fit of the data. Although various shapes are possible, mechanical shock acceleration is frequently characterized by a rapid exponential rise, a relative short plateau region, followed by a more gradual exponential decay. $E(t)$ has the same characteristics.

Another shock acceleration temporal parameter is the strong shock duration T_E, specified by MIL-STD-810G, Method 516 - Shock (2008). The T_E duration is based on the peak magnitude of the shock acceleration, a_{peak}, which can be either a positive or negative peak. T_E is defined as follows for a shock acceleration $a(t)$, where,

$$a_{peak} \equiv |a(t)|_{\max \text{ on } t} \ , \tag{2-44}$$

$$T_{Emin} \equiv \text{first time } |a(t)| \geq 1/3 \ a_{peak} \ , \tag{2-45}$$

$$T_{Emax} \equiv \text{last time } |a(t)| \geq 1/3 \ a_{peak} \text{ and} \tag{2-46}$$

$$T_E \equiv T_{Emax} - T_{Emin} \ . \tag{2-47}$$

Figure (2-12) illustrates $E(t)$ and T_E for a typical shock acceleration time-history. In this case the peak amplitude a_{peak} is -67.2 g with the first crossing of *1/3* a_{peak} at 0.0167 sec and the last 1/3 a_{peak} crossing at 0.0629 sec, resulting in a T_E of 0.0462 sec. The plateau value of $E(t)$ was set to 1.0, however in Figure (2-12) was amplified by a factor of 40 to better illustrate the overall envelope fit relative to the acceleration wave form.

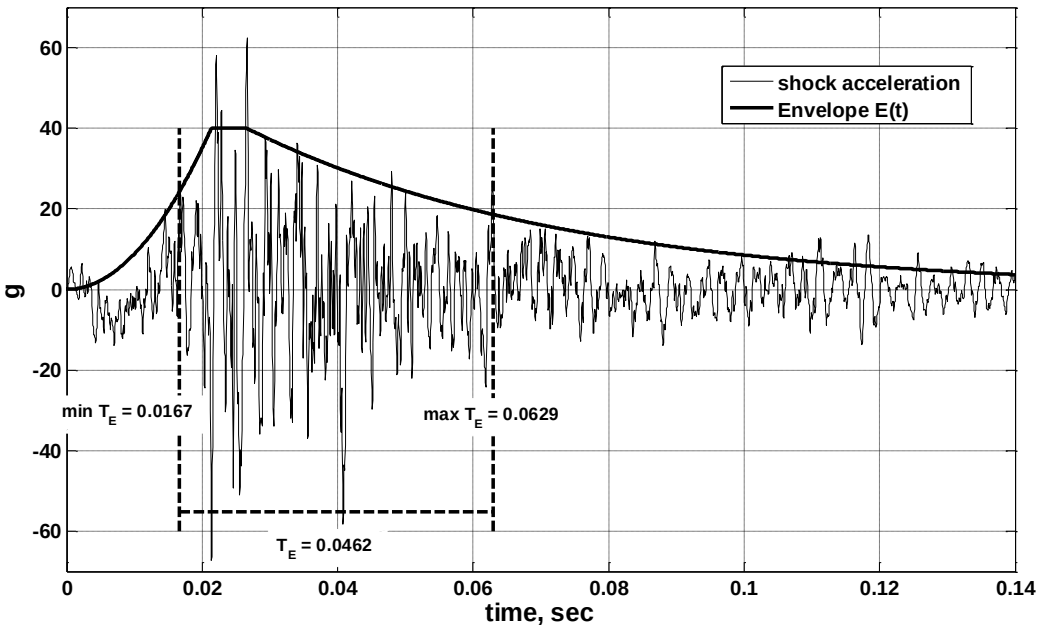

Figure (2-12) Shock Acceleration Envelope *E*(*t*) and Duration T_E

2.7 Define Baseline a_D, SRS_D, EIS_D and T_{ED} for Present Study

Previously in this document, references have been made to a design acceleration a_D and the corresponding design shock response spectrum SRS_D. For the present study, a design acceleration time-history signal a_D was chosen from a typical set of mechanical shock test data. The a_D chosen had an envelope shape and peak amplitude representative of a mechanical shock pulse. The corresponding design shock response spectrum SRS_D, energy input spectrum EIS_D, temporal duration T_{ED} and envelope $E(t)$ were determined from a_D. Figure (2-13) is a plot of a_D with the corresponding T_{ED} and $E(t)$ indicated on the plot. The peak value of the envelope $E(t)$ was 1.0, but was expanded by a factor of 47 in the plot to illustrate the fit with a_D. Figure (2-14) is a plot of SRS_D and EIS_D.

For the present study, these design quantities were needed as a basis of comparison to evaluate the accuracy of synthesized accelerations a_S. These evaluations are the degree to which,

- SRS_S, EIS_S and T_{ES} match the corresponding quantities from a_D, and
- The accuracy of response of *MDOF* models from a_S compared to the corresponding response from a_D.

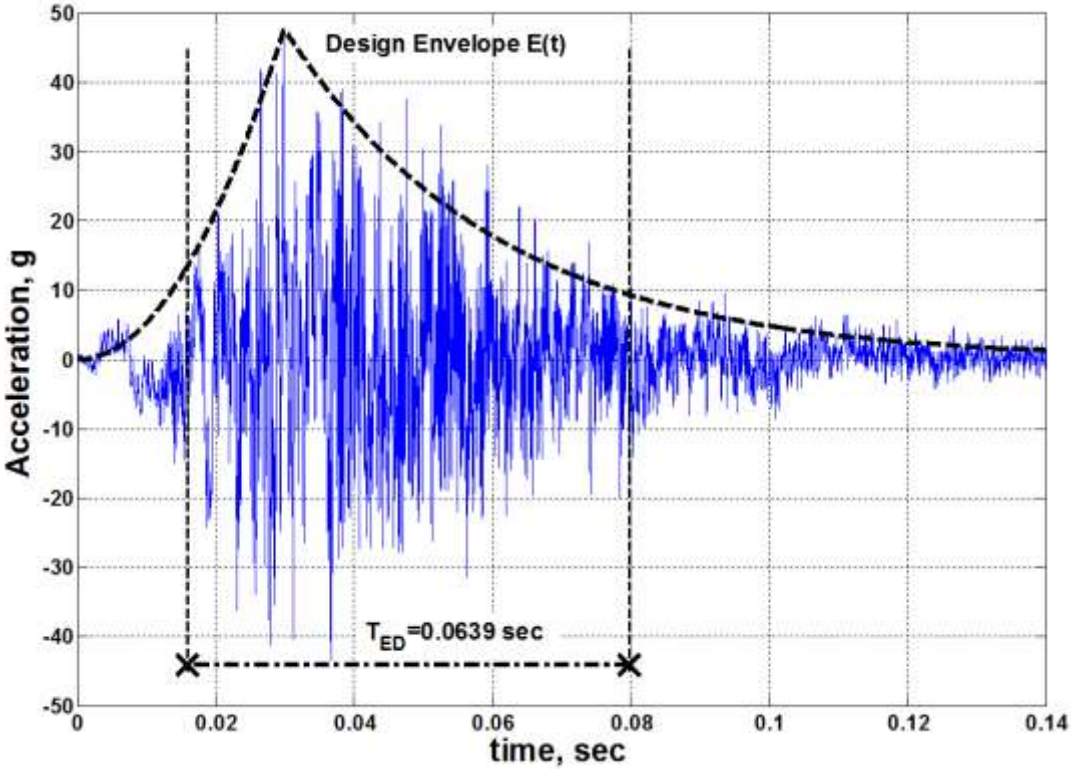

Figure (2-13) Design Acceleration a_D, Duration T_{ED} and Envelope $E(t)$

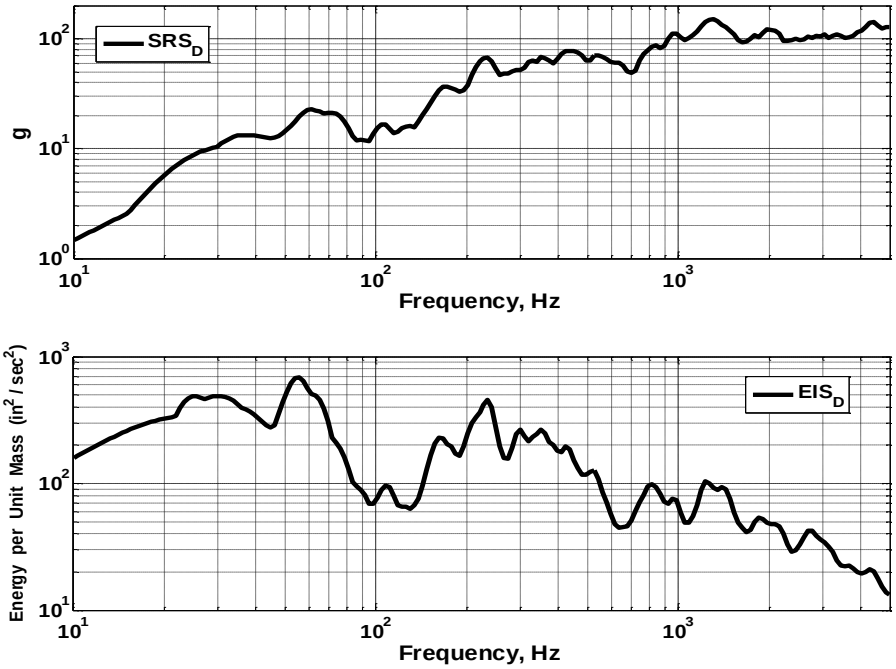

Figure (2-14) Design SRS_D and EIS_D

3 New Approach to Synthesize *SRS* Compatible Acceleration

3.1 Overview

A new approach is described for the synthesis of an *SRS* compatible base acceleration beyond what has been proposed and implemented in the past. This includes the introduction of additional constraints beyond only SRS_D compatibility of the synthesized acceleration, a_S. These additional constraints for a_S are the design energy input spectrum (EIS_D) and a design temporal duration T_{ED}. Given the objective to match multiple constraints, a comprehensive synthesis procedure was required. Two essential differences between how others have determined a_S and the proposed approach are specifically,

- a_S compatibility with EIS_D and T_{ED}, in addition to SRS_D, and
- Quality of a_S evaluated based on the accuracy of *MDOF* model response.

3.2 Traditional Synthesize Methods of SRS_D Compatible Base Acceleration

As described in Chapter 2, past authors have documented numerous methods to synthesize an SRS_D compatible base acceleration. Common synthesis methods include standard wave forms, typically comprised of a classical pulse or some variant of a summation of sinusoids. These methods include:

- Classical acceleration pulse (half sine, trapezoid, triangle, others),
- Damped sinusoids,
- Wavelets and

- Enveloped sinusoids with random phase angles.

Less commonly used methods include trained neural networks, inverse Fourier transforms, and maximum entropy.

Regardless of the method, authors have primarily addressed a single objective to synthesize a base acceleration, a_S, that returns a shock response spectrum, SRS_S, which matches the design shock response spectrum, SRS_D, within prescribed limits. For example, MIL-STD-810G, Method 516.6 (2008) prescribes a tolerance envelope of +3.0 dB/-1.5 dB around SRS_D which SRS_S is to meet. This single objective obviates the motivation to make use of other significant information including input energy and temporal data of the input shock acceleration transient. Specifically:

- Input energy per unit mass of a_S, characterized by an energy input spectrum EIS_S. The *EIS* of a general base acceleration $\ddot{u}_b(t)$ is given by the right hand side of equation (2-33) and as plotted in Figure (2-11).
- Temporal duration T_E for the shock acceleration time duration. T_E is used as a constraint on the duration of the strong shock region of the synthesized acceleration a_S. T_E is based on the peak amplitude of a shock acceleration time-history as defined in Chapter 2, equations (2-44) through (2-47).
- Transient shock shape envelope $E(t)$.

3.3 Synthesis of Base Acceleration a_S

The objective of the synthesis procedure is to determine a_S which is compatible with the corresponding design acceleration quantities of SRS_D, EIS_D, T_{ED} and $E(t)$. To achieve this, the differences between synthesis based quantities SRS_S, EIS_S, and T_{ES} and

the corresponding design quantities are minimized. The percent error factors for these synthesized quantities SRS_S, EIS_S and T_{ES} relative to the corresponding design quantities are given by equations (3-1), (3-2) and (3-3), respectively. The envelope function $E(t)$ is imposed on the overall shape of a_S.

A synthesis optimization flow chart, Figure (3-1), illustrates this process. The approach is to minimize a merit function, M, that is a function of the percentage errors factors $SRS_{\%}$, $EIS_{\%}$ and $T_{E\%}$.

$$SRS_{\%} \equiv \frac{100}{N}\sum_{n=1}^{N}\left|\frac{SRS_S^n - SRS_D^n}{SRS_D^n}\right| \tag{3-1}$$

$$EIS_{\%} \equiv \frac{100}{N}\sum_{n=1}^{N}\left|\frac{EIS_S^n - EIS_D^n}{EIS_D^n}\right| \tag{3-2}$$

$$T_{E\%} \equiv 100\left(\frac{T_{ES} - T_{ED}}{T_{ED}}\right) \tag{3-3}$$

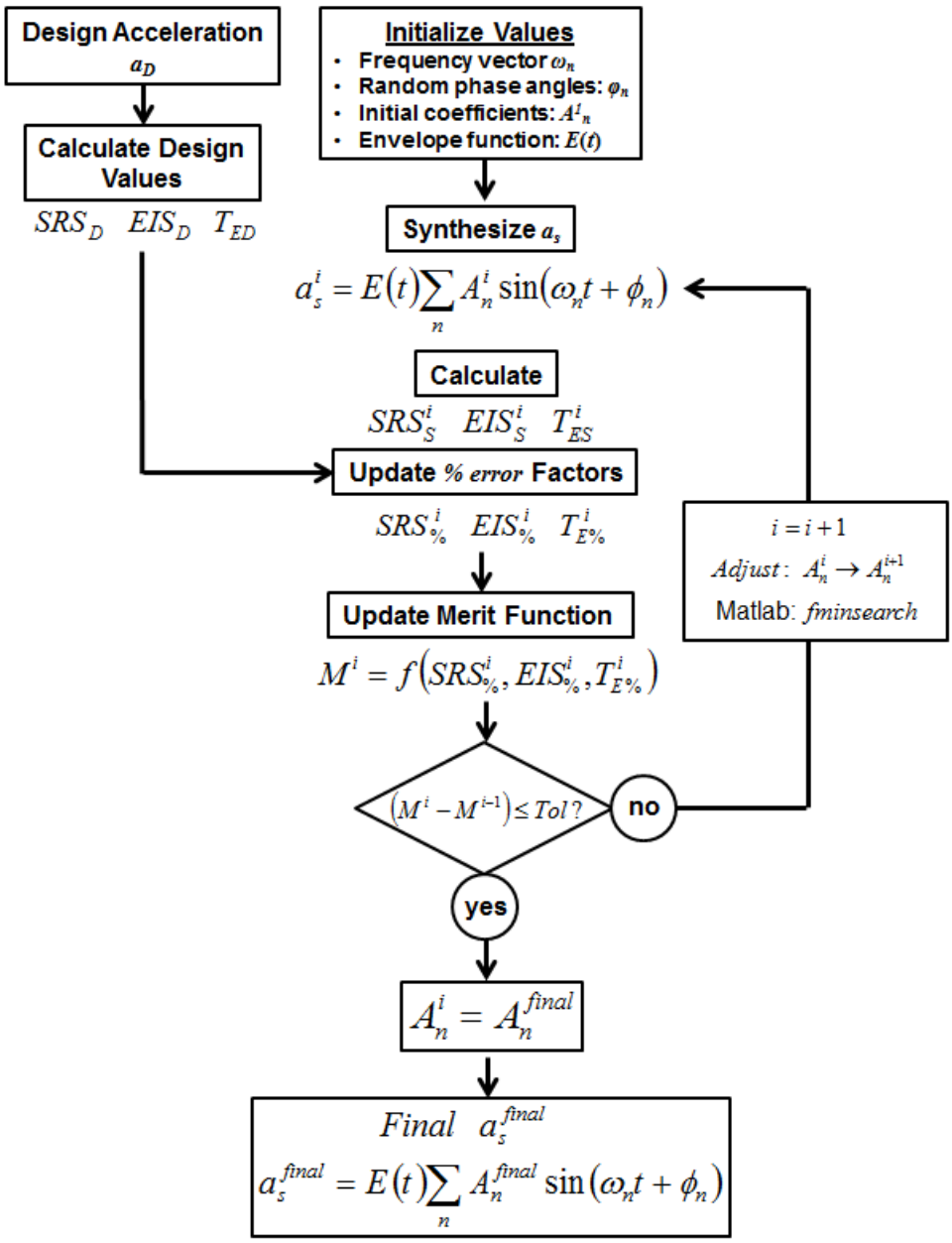

Figure (3-1) a_S Synthesis Optimization Process

The synthesis of a_S is given by equation (3-4). The synthesis method selected for the optimization of a_S was enveloped sinusoids with random phase angles. The envelope function $E(t)$ determines the temporal shape of a_S, giving complete control of the rise, plateau and decay of the synthesized wave form, rather than to rely on time delays and

damping of individual sinusoids. Based on examination of mechanical shock acceleration data, a typical shock pulse has a rapid rise, a brief (if any) plateau, and a gradual decay. The correct choice of $E(t)$ assures this shape for a_S. It has proven to be effective in matching the temporal profile of a_D, or the combined envelope in the case of a family of field data.

$$a_S(t) = E(t)\sum_{n=1}^{N} A_n \sin(\omega_n t + \phi_n). \tag{3-4}$$

The synthesis procedure is iterative as shown in Figure (3-1). The summation in equation (3-4) is over the index n corresponding to all SRS_D N ω_n frequencies. The amplitude coefficients A_n for each sinusoid are independently updated in each iteration to minimization the merit function M. To start the procedure, the following initial quantities are set.

- Temporal envelope function $E(t)$.
- Frequency vector ω_n to span the frequency bandwidth N of SRS_D.
- Vector of N random phase angles φ_n for each frequency ω_n.
- Initial seed of N coefficients A_n, based on a percentage of SRS_D over the frequency range.

$E(t)$, ω_n ,and φ_n remain stationary during the optimization process. The optimization is executed over an iteration loop index i until the change to the merit function ΔM^i meets a predefined tolerance.

The synthesis process is started (i=1) by forming a_s using the initial values of A_n^1. Initial values of A_n (i=1) were chosen to be 3% of SRS_D based on observations of prior results. Initial values of SRS_S^1, EIS_S^1 and T_{ES}^1 are calculated from a_s^1. As the process

proceeds, the percentage errors $SRS_{\%}^{\,i}$, $EIS_{\%}^{\,i}$ and $T_{E\%}^{\,i}$, given by equations (3-1) through (3-3), respectively, are calculated for each iteration *i*.

The merit function $M^{\,i}$, equation (3-5) is evaluated for each iteration *i*. A convergence criterion is given by equation (3-6).

$$M^{\,i} = f\left(SRS_{\%}^{\,i}, EIS_{\%}^{\,i}, T_{E\%}^{\,i}\right) \text{ and} \tag{3-5}$$

$$\Delta M^{\,i} = \left(M^{\,i} - M^{\,i-1}\right) \leq \text{Tol} \,. \tag{3-6}$$

This optimization process was executed with the Matlab optimization tool kit using the *fminsearch* routine (The Mathworks, Inc.). If $\Delta M^{\,i}$ does not meet the predefined tolerance of equation (3-6), the *fminsearch* optimization routine continues to adjust the set of $A_n^{\,i}$ to further reduce $M^{\,i}$. When equation (3-6) is satisfied, a final set of amplitude coefficients, $A_n^{\,final}$, are used to compute the final synthesized acceleration $a_s^{\,final}$ from

$$a_S^{final}(t) = E(t)\sum_{n=1}^{N} A_n^{final} \sin\left(\omega_n t + \phi_n\right) \,. \tag{3-7}$$

3.4 Evaluate a_S from *MDOF* Model Response

Regardless of how well the synthesized a_S meets the spectral and temporal factors of equations (3-1) through (3-3), there is no guarantee that when a_S is applied to a *MDOF* model, the response of the model will agree with the corresponding response from the design acceleration, a_D . To evaluate a_S when applied to a physical model, the process of Figure (3-2) was developed. Both the design and synthesized accelerations were applied to a general *MDOF* model. The model responses from a_S were compared to the corresponding responses from $a_{D.}$

Average percentage errors were calculated for peak mass accelerations, peak relative displacements and peak energy input to the model. These responses were chosen

based on their ability to damage a physical system. Peak accelerations and displacements produce peak forces at discrete locations in the system at discrete points in time. Heavy elements subjected to a high acceleration can result in high inertial forces, from the product of mass and acceleration ($F=ma$). Structural elements connecting discrete components can generate large forces from large relative displacement ($F=kz$). The total energy input (EI) to a system is a cumulative measure of the damage potential for the entire system. A physical system subjected to a peak energy input must distribute and dissipate the energy based on the characteristics of system including system dynamics, damping and deformations.

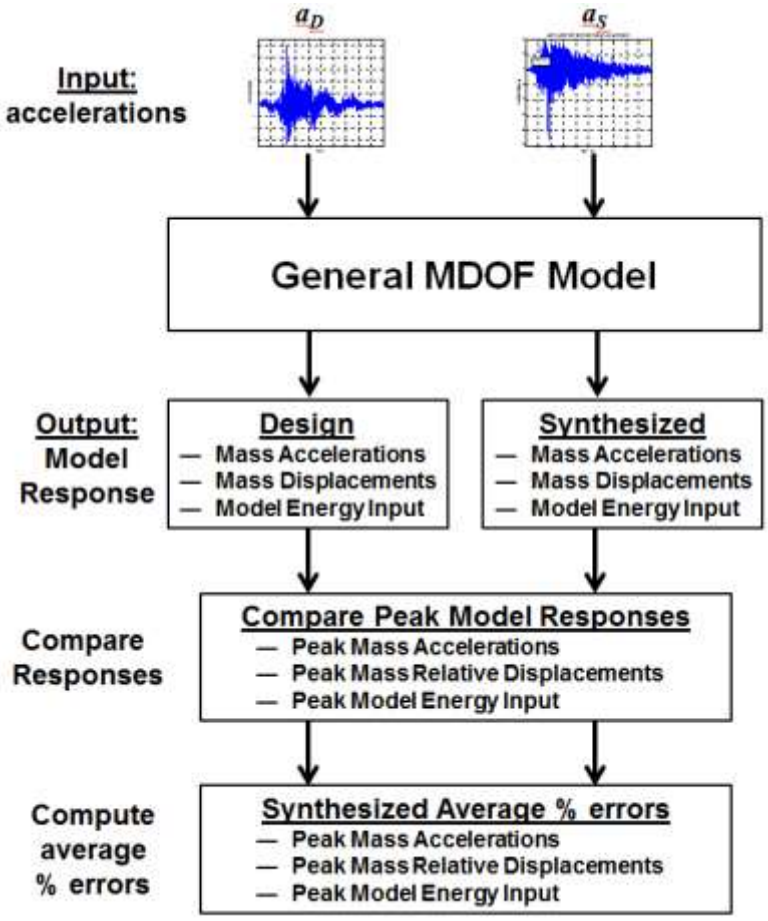

Figure (3-2) Process to Evaluate a_S Accuracy

A general *3DOF* model, Figure (3-3), was developed to evaluate the response of the synthesized base accelerations relative to that of the design acceleration. This *3DOF* model represents a general system where masses and spring rates were sized to result in natural frequencies in the range of interest relative to the magnitudes of SRS_D and EIS_D over the frequency bandwidth. The absolute displacements of masses m_1, m_2 and m_3 are given by u_1, u_2 and u_3, respectively. Since the excitation of interest is a base acceleration, a base coordinate u_b is defined. A relative coordinates is defined for each mass m_i, given by $(u_i - u_b)$. Three springs of stiffness k_1, k_2 and k_3 connect the mass elements, and k_1 connects mass m_1 to the base. The model excitation is a base acceleration, which is the second time derivative of the base coordinate u_b. Damping of $\zeta = 5\%$ of critical damping was prescribed for the entire model.

Three variants of the general *3DOF* model were developed based on three sets of spring force-displacement relationships given by,

- Linear: linear force-displacement relationship for all springs,
- Nonlinear-Stiffening: nonlinear elastic springs where each spring rate increases when the displacement exceeds a predefined value and
- Nonlinear-Softening: nonlinear elastic springs where each spring rate decreases when the displacement exceeds a predefined value.

Details of the general *3DOF* model parameters are given in Appendix B.

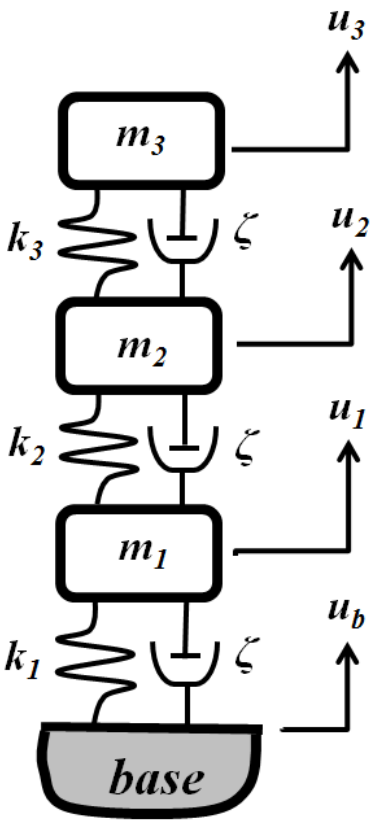

Figure (3-3) General *3DOF* Model

As shown on Figure (3-2), average percentage errors were calculated based on the *3DOF* model response from a_S compare to the corresponding responses from a_D. These percent errors are,

- average percentage error of the peak mass accelerations,
- average percentage error of the peak relative displacements and
- percentage error of the *3DOF* model peak input energy.

These *3DOF* model response percentage errors are defined by equations (3-8), (3-9) and (3-10), respectively, where the superscript "*s*" is the *3DOF* response from the synthesized acceleration and superscript "*D*" is the *3DOF* response from the design acceleration. The *3DOF* model percentage errors are,

$$\ddot{u}_{\max}^{ave\%} \equiv \frac{100}{3}\sum_{i=1}^{3}\left|\frac{\left|\ddot{u}_i\right|_{\max}^{s} - \left|\ddot{u}_i\right|_{\max}^{D}}{\left|\ddot{u}_i\right|_{\max}^{D}}\right| , \tag{3-8}$$

$$z_{\max}^{ave\%} \equiv \frac{100}{3}\sum_{i=1}^{3}\left|\frac{\left|z_i\right|_{\max}^{s} - \left|z_i\right|_{\max}^{D}}{\left|z_i\right|_{\max}^{D}}\right| \quad and \tag{3-9}$$

$$En_{\max}^{\%} \equiv 100\left(\frac{En_{\max}^{s} - En_{\max}^{D}}{En_{\max}^{D}}\right) . \tag{3-10}$$

The relative displacement for each mass m_i is defined by,

$$z_i \equiv u_i - u_b \tag{3-11}$$

3.5 Determine Significant Factors and Merit Function from Regression Analysis

The merit function, *M*, was generally defined in equation (3-5) as a function of the factors $SRS_{\%}$, $EIS_{\%}$ and $T_{E\%}$ given by equations (3-1) through (3-3), respectively. It was not immediately obvious, however, which of these factors should be included in the merit function or what form the merit function should take. To address this, a regression analysis was completed to determined significant factors, equations (3-1) through (3-3), to guide the specific form of the final merit function *M*.

To initiate the regression analysis process, an initial merit function, equation (3-12), was developed as a linear combination of factor percentage errors,

$$M = W_{SRS}SRS_{\%} + W_{EIS}EIS_{\%} + W_{T_E}T_{E\%} \tag{3-12}$$

where each factor, $SRS_{\%}$, $EIS_{\%}$ and $T_{E\%}$ had weighting coefficients W_{SRS}, W_{EIS} and W_{TE}, respectively. For the regression model, each weighting *W* was set to either 0 or 1, to control if the corresponding factor was present, or not, in the merit function.

Accordingly, equation (3-12) has three W coefficients and each had two values, resulting in 2^3=8 total combinations. Each combination of weightings yields a unique a_S. With all combinations of W, eight unique a_S base accelerations were synthesized. Table (3-1) gives the nomenclature for each synthesized acceleration based on W_i values (0 or 1). The eight synthesized accelerations are plotted in Figure (3-4). The percent error factors ($SRS_{\%}$, $EIS_{\%}$, $T_{E\%}$) in the merit equation (3-12) were determined for each a_S and were the inputs factors for the regression analysis.

Table (3-1) Synthesized Acceleration Nomenclature base on *M* Weighting

synthesized accelerations	W_{SRS}	W_{EIS}	W_{TE}
a_s^{000}	0	0	0
a_s^{010}	0	1	0
a_s^{001}	0	0	1
a_s^{011}	0	1	1
a_s^{100}	1	0	0
a_s^{110}	1	1	0
a_s^{101}	1	0	1
a_s^{111}	1	1	1

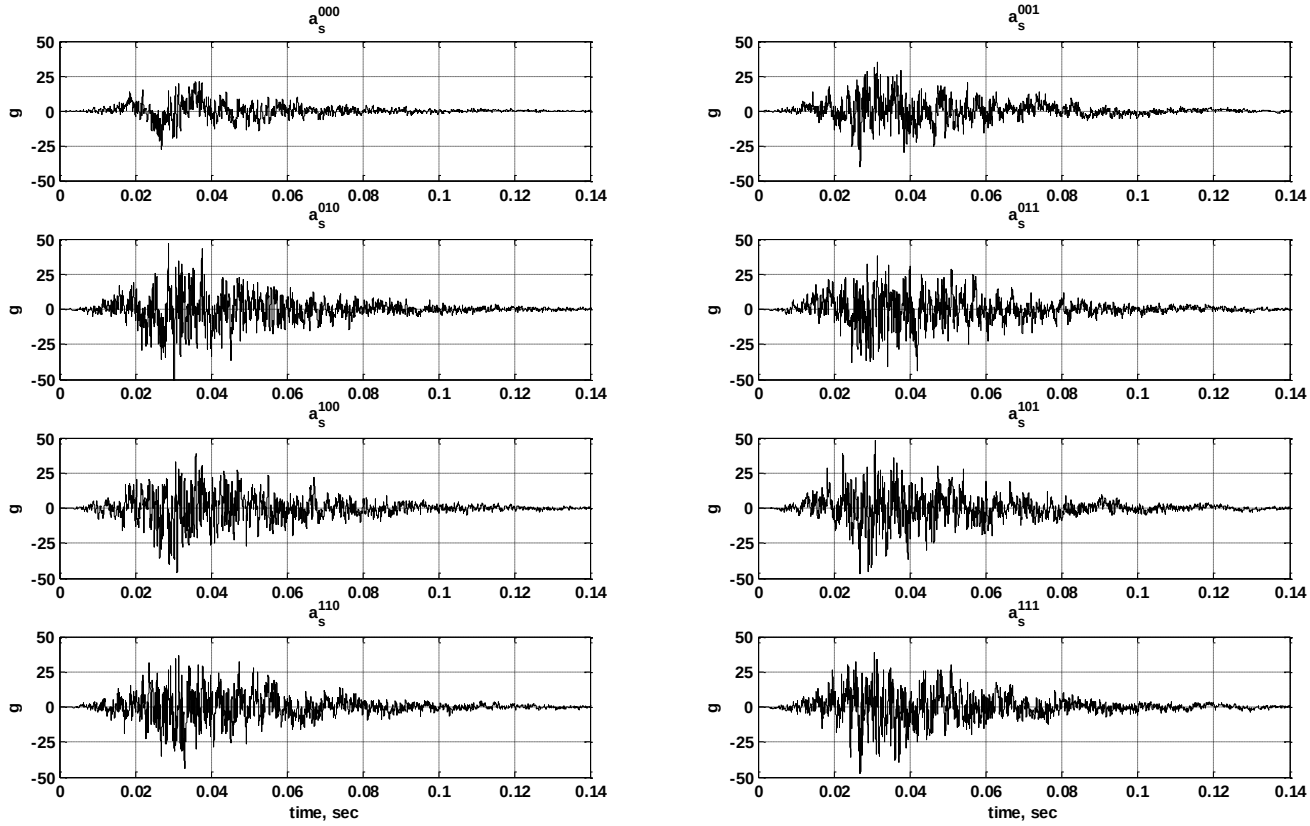

Figure (3-4) Eight a_S Synthesized Accelerations

The significance of the factors $SRS_{\%}$, $EIS_{\%}$ and $T_{E\%}$ was determined from regression analysis based on the response of the general *3DOF* model. The significance of these factors guided the form of the final merit function *M* to synthesize an optimized acceleration a_{S2}. Minitab software (Minitab, Inc., 2014) was used to perform the regression analysis.

The factors, equations (3-1) through (3-3), were the inputs to the regression model and the *3DOF* model responses, equations (3-8) through (3-10), were the outputs. Table (3-2) shows the regression analysis inputs, ($SRS_{\%}$, $EIS_{\%}$, $T_{E\%}$), and the outputs, ($\ddot{u}_{max}^{ave\%}, z_{max}^{ave\%}, En_{max}^{\%}$), for each synthesized acceleration.

Table (3-2) Regression Analysis Input (Factors) and Output (Linear *3DOF* Model Responses)

	Synthesized Accelerations % Errors (Factors)			*3DOF* Linear Model Response % Errors		
Synthesized Accelerations	$SRS_{\%}$	$EIS_{\%}$	$T_{E\%}$	$\ddot{u}_{max}^{ave\%}$	$z_{max}^{ave\%}$	$En_{max}^{\%}$
a_S^{000}	44.02	64.92	-30.83	21.90	17.43	-6.48
a_S^{001}	21.06	39.27	-6.73	36.93	46.97	109.39
a_S^{010}	17.12	11.74	-63.69	10.65	8.17	-12.60
a_S^{011}	12.28	5.80	-63.69	19.33	14.75	1.70
a_S^{100}	5.87	33.59	-21.91	21.80	12.99	-17.92
a_S^{101}	2.91	95.62	-24.57	24.69	22.05	21.55
a_S^{110}	7.83	12.03	-25.67	25.91	11.71	17.03
a_S^{111}	4.97	6.50	-25.20	22.52	12.14	-4.80

A regression analysis was performed for each individual *3DOF* model response. For example the regression analysis for the $z_{max}^{ave\%}$ model response determined the coefficients $C_1 - C_7$ in the following linear equation of the form,

$$z_{\max}^{ave\%} = C_1 + C_2(SRS_{\%}) + C_3(EIS_{\%}) + C_4(T_{E\%}) + C_5(SRS_{\%})(EIS_{\%}) + C_6(SRS_{\%})(T_{E\%}) + C_7(EIS_{\%})(T_{E\%}). \quad (3\text{-}13)$$

The regression analysis solves a set of linear equations determined from the synthesized acceleration results of Table (3-2). A set of responses $z_{max}^{ave\%}$ corresponding to each synthesized acceleration is tabulated in Table (3-2), as are each set of input factors, $SRS_{\%}$, $EIS_{\%}$ and $T_{E\%}$. This result is a set of linear equations, one for each synthesized acceleration. Unknowns $C_1 - C_7$ are determined by solving this system of linear equations.

Beyond determining the coefficients for a linear equation, the significance of each factor is determined by statistical analysis. The significance threshold for each factor was based on $\alpha \leq 0.1$, which corresponds to a 10% probability that the null hypothesis cannot

be rejected in favor of the alternative hypothesis. The null hypothesis, H_0, is that all C_i = 0 in equation (3-13), except C_0. The alternative hypothesis, H_1, is that at least one $C_i \neq 0$, not including C_0. For example, the regression analysis determined the following significant factors and coefficients in equation (3-14) to be,

$$z_{\max}^{ave\%} = -20.96 + 3.92(SRS_{\%}) + 0.250(EIS_{\%}) - 0.805(T_{E\%}) - 0.023(SRS_{\%})(EIS_{\%}) + 0.081(SRS_{\%})(T_{E\%}). \quad (3\text{-}14)$$

In the case of peak *z* average % error model response, the significant factors based on meeting or exceeding $\alpha \leq 0.1$ criteria were $SRS_{\%}$ and $EIS_{\%}$, and the product factors $(SRS_{\%})(EIS_{\%})$ and $(SRS_{\%})(T_{E\%})$. The term $0.805(T_{E\%})$ did not meet the $\alpha \leq 0.1$ criteria, but was retained in equation (3-14) because the individual factor $T_{E\%}$ occurred in the second product factor term $0.081(SRS_{\%})(T_{E\%})$. (Recommended practice by Minitab technical support).

Table (3-3) summarizes the results of three individual regression analyses corresponding to the three responses listed for the linear variant of the general *3DOF* model. Each row of Table (3-3) represents an individual regression analysis. Factors that met the $\alpha \leq 0.1$ criteria are indicated with an "**x**" in the corresponding cell of Table (3-3). Each regression analysis included all eight a_S of Table (3-1). The results indicated for the linear version of *3DOF* model, the $SRS_{\%}$ factor was significant for all linear model responses, the $EIS_{\%}$ factor was significant for relative displacements average % error, and the $T_{E\%}$ factor was significant for peak mass accelerations and peak energy input % errors. In addition to the significance of individual factors, the regression model also indicated that the products of the factors were significant to the $\alpha \leq 0.1$ criteria in four

instances. This finding is an indication that an additional three terms should be included in the merit function *M* to include the products of the factors.

Tables (3-4) and (3-5) are the corresponding results for the two nonlinear varients of the general *3DOF* model.

Table (3-3) General *3DOF* Model – Linear - Significant Factors

Model Response	Model Response					
	$SRS_{\%}$	$EIS_{\%}$	$TE_{\%}$	$(SRS_{\%})(EIS_{\%})$	$(SRS_{\%})(TE_{\%})$	$(EIS_{\%})(TE_{\%})$
(peak mass acceleration % err)$_{ave}$	**x**		**x**		**x**	
(peak displacement % err)$_{ave}$	**x**	**x**		**x**	**x**	
peak energy input % err	**x**		**x**	**x**		

Table (3-4) General *3DOF* Model, Nonlinear Stiffening – Significant Factors

Model Response	Factors					
	$SRS_{\%}$	$EIS_{\%}$	$T_{E\%}$	$(SRS_{\%})(EIS_{\%})$	$(SRS_{\%})(T_{E\%})$	$(EIS_{\%})(T_{E\%})$
(peak mass acceleration % err)$_{ave}$	**x**					
(peak displacement % err)$_{ave}$	**x**	**x**	**x**	**x**	**x**	
peak energy input % err				**x**		

Table (3-5) General *3DOF* Model, Nonlinear Softening – Significant Factors

Model Response	Factors					
	$SRS_{\%}$	$EIS_{\%}$	$T_{E\%}$	$(SRS_{\%})(EIS_{\%})$	$(SRS_{\%})(T_{E\%})$	$(EIS_{\%})(T_{E\%})$
$(\text{peak mass acceleration \% err})_{ave}$						
$(\text{peak displacement \% err})_{ave}$	**x**	**x**	**x**	**x**		
peak energy input % err						

Appendix D contains additional regression analysis results for the linear variant and two nonlinear variants of the general *3DOF* model. Regression models for all factors and all variants of the *3DOF* model are described in equations (D-1) through (D-9) in Appendix D. Additional information is available from the regression analysis for each model response. This includes an R^2 estimates of the degree to which the regression model explains the variability of the *3DOF* model's response. R^2 values for all model variants and factors are in Appendix D.

3.6 Final a_{s2} from Revised Merit Function

As indicated in the regression analysis summary for the three *3DOF* models, Tables (3-3) through (3-5), in addition to the individual factors defined by equations (3-1) through (3-3), the products of these factors was also significant in eight cases. Equation (3-15) is an updated merit function which includes all individual factors, and terms for the product of the factors, given by,

$$M = SRS_{\%} + EIS_{\%} + T_{E\%} + (SRS_{\%})(EIS_{\%}) + (SRS_{\%})(T_{E\%}) + (EIS_{\%})(T_{E\%}) \; . \qquad (3\text{-}15)$$

An updated optimized acceleration, a_{s2}, was synthesized by the process of Figure (3-1) using the revised merit equation (3-15). Figure (3-5) is plot of a_{s2}. Figures (3-6) and (3-7) are plots of the SRS_{S2} and EIS_{S2} from a_{s2}, respectively, superimposed on the corresponding spectra for a_D. The average percent errors $SRS_{\%}$, $EIS_{\%}$ *and* $T_{E\%}$ are 6.1%, 7.8% and -19.7%, respectively, relative to the corresponding values from a_D.

The updated acceleration a_{s2} was applied to a second *3DOF* model based on the US Navy's medium weight shock machine (*MWSM*) and the responses were compared to corresponding responses from the common synthesis methods described in Section 2.3 of Chapter 2. The results of this comparison are described in Chapter 4.

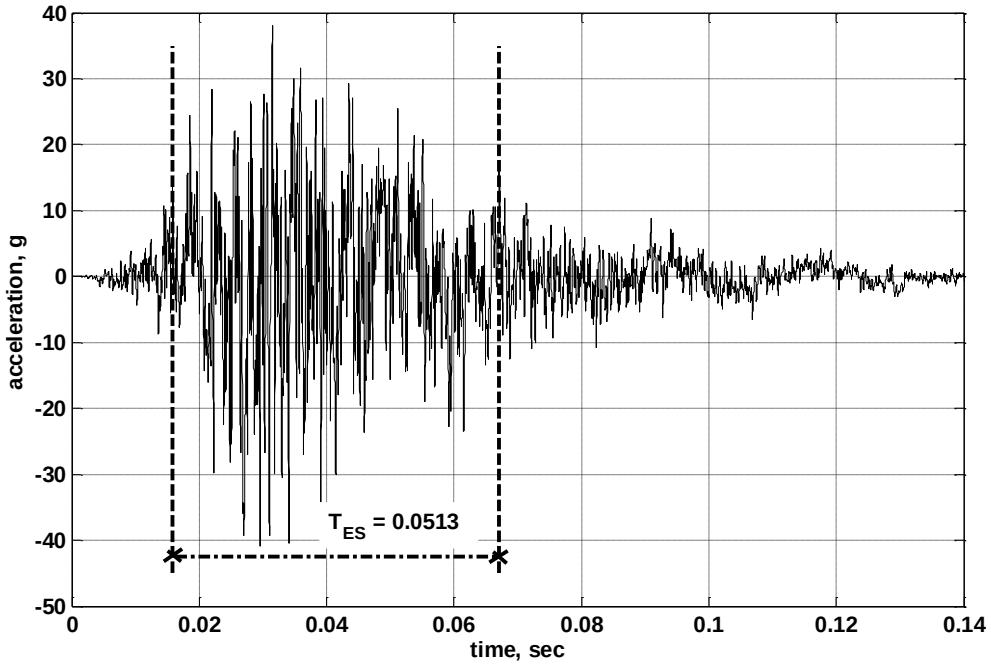

Figure (3-5) Synthesized Acceleration a_{s2}

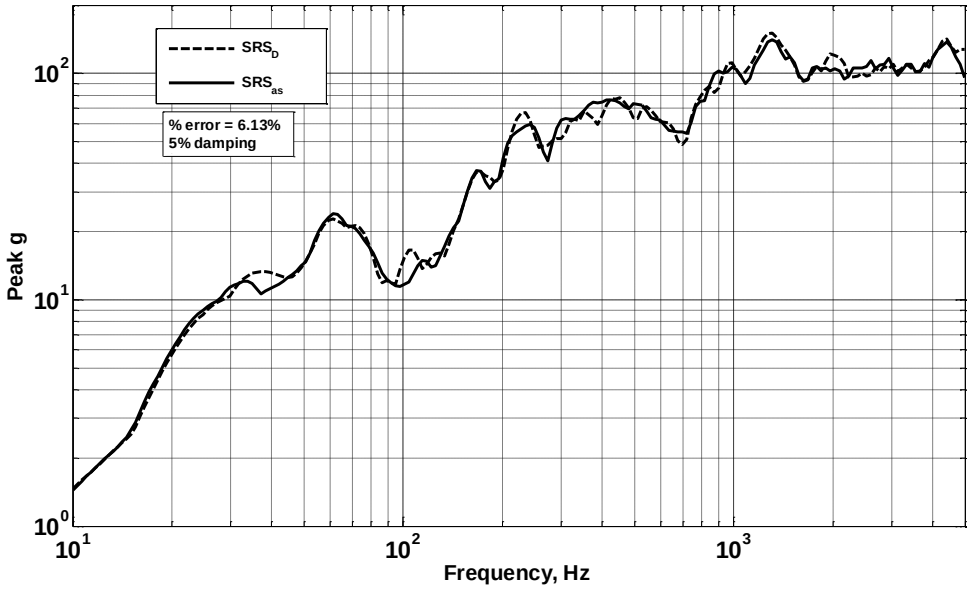

Figure (3-6) SRS_D and SRS_{s2}

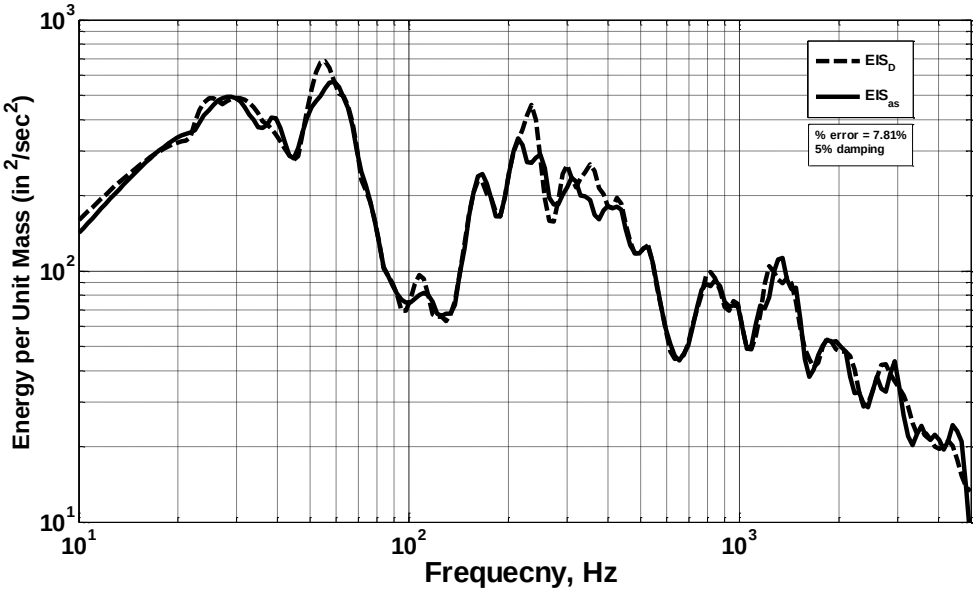

Figure (3-7) EIS_D and EIS_{s2}

4 Multi-degree of Freedom Response to Synthesized Accelerations

4.1 Overview

A design SRS_D and EIS_D were developed from the design acceleration a_D, Figures (2-14) and (2-13), respectively. Five accelerations a_S were synthesized to be compatible with SRS_D, Figure (4-1). Four of the five (half sine, damped sines, wavelets, enveloped sines) were synthesized with current industry practices, which is to achieve the best match between SRS_S and SRS_D, as shown in Figure (2-8). The fifth acceleration, a_{S2}, was synthesized to match not only SRS_D, but also the design energy input spectrum (EIS_D), design duration (T_{ED}) and the design envelope function $E(t)$. Three *3DOF* medium weight shock machine (*MWMS*) models were developed to evaluate the differences between the *3DOF MWSM* model responses from five a_S relative to the corresponding *MWSM* model response to a_D.

4.2 Synthesized Accelerations Evaluated

As described in Chapter 3, a_{s2} was synthesized to minimize the *SRS*, *EIS* and T_E percentage error factors defined by equations (3-1) through (3-3). The minimization was done using the updated merit function of equation (3-15). Four other synthesized accelerations, described in Chapter 2, were synthesized based on common industry practice to only minimize SRS_S percent error defined by equation (3-1). Figure (4-1) contains plots of the design acceleration a_D, the four synthesized accelerations of Figure (2-7), and a_{S2} of Figure (3-5). Note that the time scale of the half sine plot on Figure (4-

1) was expanded by a factor of ten so that the shape of the half sine pulse was visible on the plot. The percentage errors defined by equations (3-1) through (3-3) for all synthesized accelerations are listed in Table (4-1). As expected, a_{S2} resulted in the lowest percentage errors for $EIS_{\%}$ and $T_{E\%}$. With the exception of the half sine, *SRS%* was less than 10% error for all synthesized accelerations. The five synthesized accelerations are compared in Section 4.3, based on the response of *3DOF* models of the US Navy's medium weight shock machine.

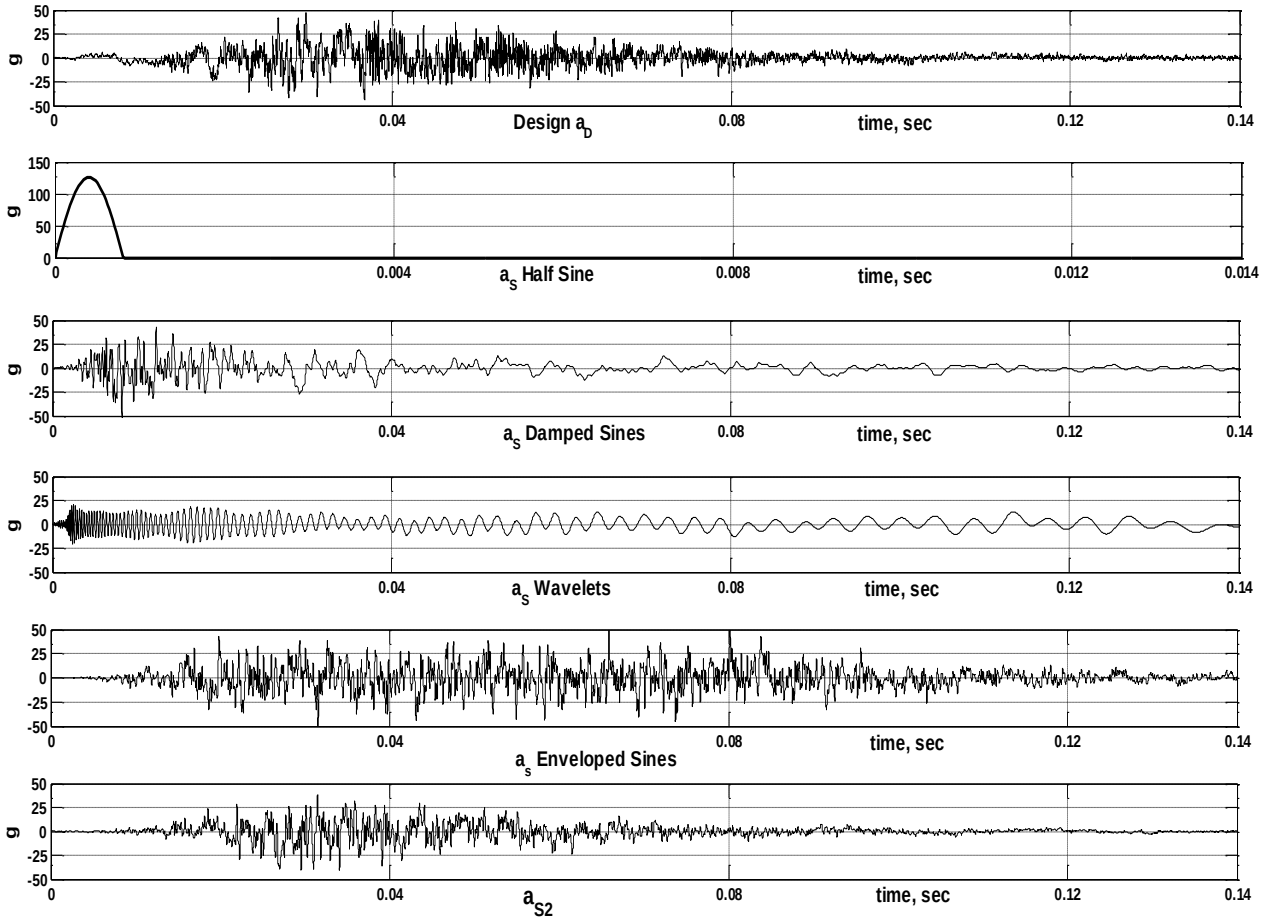

Figure (4-1) Design Acceleration a_D and Synthesized Accelerations

Table (4-1) Percent Errors of Synthesized Accelerations

	Ave *SRS* % Error ($SRS_{\%}$)	Ave *EIS* % Error ($EIS_{\%}$)	T_E % Error ($T_{E\%}$)
Half Sine	83.3%	77.9%	-99.1%
Damped Sines	8.67%	49.9%	-47.3%
Wavelets	6.97%	34.9%	123.9%
Enveloped Sines	4.88%	95.9%	39.4%
a_{s2}	6.1%	7.8%	-19.7%

4.3 *3DOF* Medium Weight Shock Machine Model

To evaluate the accuracy of the synthesized accelerations relative to that of a_D, a second *3DOF* model was developed based on the US Navy's Medium Weight Shock Machine described in MIL-S-901D (Navy, 1989). The *MWSM* model is based on shock test machines developed after World War II to shock harden naval shipboard equipment to survive near-miss underwater explosions. The *MWSM* was chosen to provide a representative and realistic vehicle to compare the five synthesized accelerations based on the *MWSM* model's response. Figure (4-2) is an illustration of the *MWSM*, and Figure (4-3) shows the corresponding *3DOF* model of the machine. The *MWSM* consists of a 3,000 pound hammer that strikes the underside of a 4,400 pound anvil table with a prescribed impact velocity based on the height that the hammer is raised above horizontal when it is released. The equipment to be tested is supported by steel car building channel sections mounted to the anvil table. The number of channels is prescribed by MIL-S-901D based on the weight of the equipment being tested and the span of the equipment

mounting attachment locations. The intent is to achieve a system frequency equivalent to the frequency of the deck of the ship where the equipment is to be mounted.

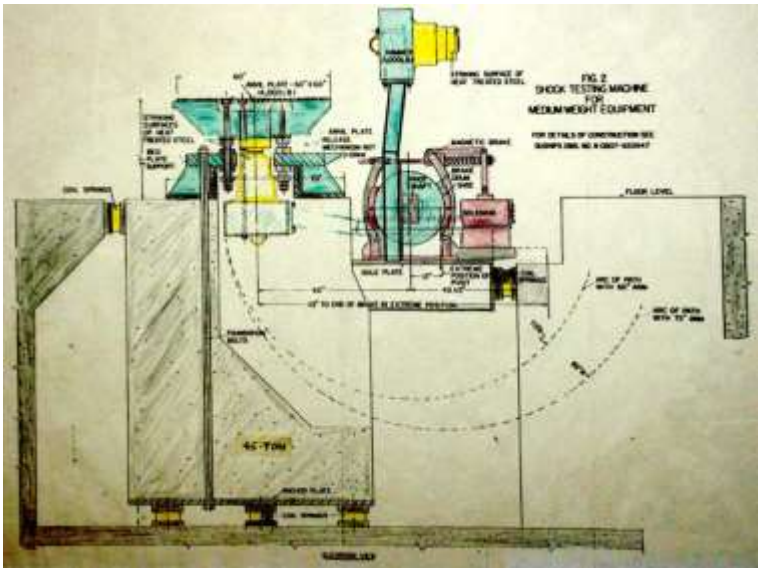

Figure (4-2) Illustration of Medium Weight Shock Machine

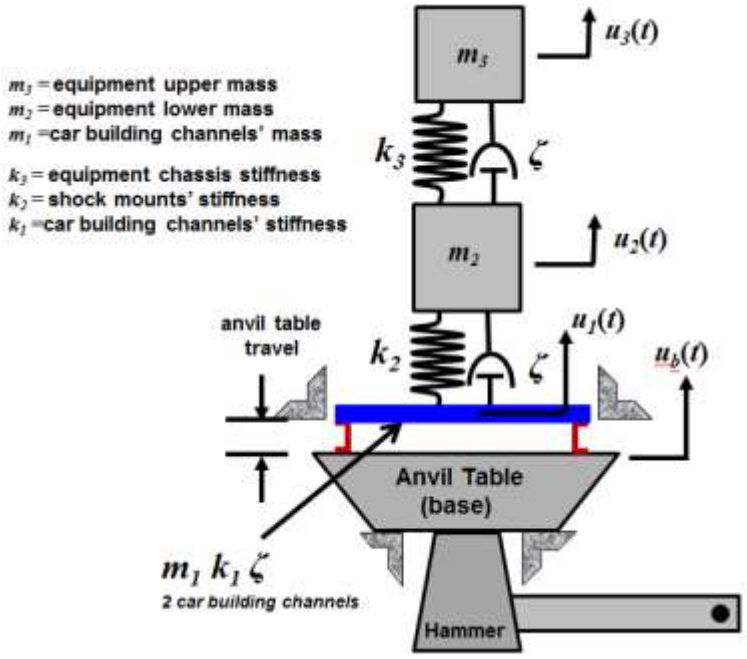

Figure (4-3) *3DOF* Model of Medium Weight Shock Machine

As shown in Figure (4-3), spring stiffness k_1 is the combined stiffness of the mounting channels. Spring k_2 represents the combined stiffness of four commercial

shock absorbers, and spring k_3 represents the stiffness of the chassis of the equipment being tested. In this model stiffness k_2 is based on a commercial shock isolator described in Appendix C. Springs k_1 and k_3 are linear for all variants of the *MWSM* model. As with the general *3DOF* model described in Chapter 3, the *MWSM* model has three variants; linear, nonlinear-stiffening and nonlinear-softening based on the force-displacement relationship of k_2. The *MWSM* model damping was set to 5% of critical based on historical data taken at the Naval Research Lab (Clements, 1972).

4.4 *MWSM* Model Response to Synthesized Accelerations

MWSM model percentage error responses from the synthesized accelerations relative to those of a_D are plotted in Figures (4-4), (4-5) and (4-6) for the linear, nonlinear-stiffening and nonlinear-softening model variants, respectively. These percentage errors correspond to those defined by equations (3-8), (3-9) and (3-10) for average peak mass accelerations, average peak displacements and peak energy input to the model, respectively.

For the linear *MWSM* model, the errors from a_{S2} were lower than the corresponding errors from the other synthesized accelerations for all model responses, Figure (4-4). Model response errors from the half-sine had the greatest magnitude, which is not unexpected due to the significant difference in the half-sine transient pulse compared to that of a_D. Percentage errors from the other three synthesized accelerations (damped sines, wavelets, and enveloped sines, respectively) were relatively low for peak accelerations and displacements, although still greater than those corresponding to a_{S2}. The most significant difference in model response was that of the peak input energy

percent error. The average magnitude of $En^{\%}_{max}$ from a_{S2} was 8.4% compared to an average magnitude error of 51% for the other four synthesized accelerations.

The same trend was observed from the two nonlinear variants of the *MWSM* model responses. The half-sine again had significantly larger errors for peak accelerations, peak displacements and energy input. The other synthesized accelerations, including a_{S2}, had comparable percentage errors for peak accelerations and displacements. However, a_{S2} again had consistently lower energy input percent errors, $En^{\%}_{max}$, in all cases. The merit function to synthesize a_{S2}, equation (3-15), included the energy input spectrum error term $EIS_{\%}$. This translated to the lowest model input energy percent error, $En^{\%}_{max}$, from a_{S2} relative to the other synthesized accelerations, which were synthesized to match SRS_D only.

Peak mass acceleration and the peak relative displacement responses occur at specific locations in the system at a discrete point in time during the transient. A peak mass acceleration will affect the inertial force on an individual component at a specific location in the system. A peak relative displacement will affect a connecting spring element in the system that transmits a dynamic force between two mass components. Spring elements occur at specific locations and the spring forces occur at discrete instances in time. Peak energy input is a measure to the total energy absorbed by the entire structural dynamic system. As such, energy input is an appropriate measure of total damage potential to the structural system. As noted by Edwards (2007):

> "The energy quantities can be calculated for *MDOF* structures by integrating the energy equations over the entire structure. The results represent the total input, absorbed, dissipated and kinetic energy of the *MDOF* structure. On the other

hand, the time derivatives of position, acceleration and velocity have no general significance in *MDOF* structures. These quantities indicate the motion at a discrete location and cannot represent the state of the structure as a whole. This characteristic gives the energy another advantage in the description and specification of shock environments."

For all variants of the *MWSM* model (linear, nonlinear) the peak energy input percent error was significantly lower that the corresponding peak energy input errors of the other synthesized waveforms. Since the optimized acceleration a_{s2} resulted in a more accurate estimation of the total energy input to the three variants of the *MWSM* model compared to the other synthesized accelerations, which did not consider input energy in the synthesis process, it provided an improved estimate of the damage potential to the structural dynamic system.

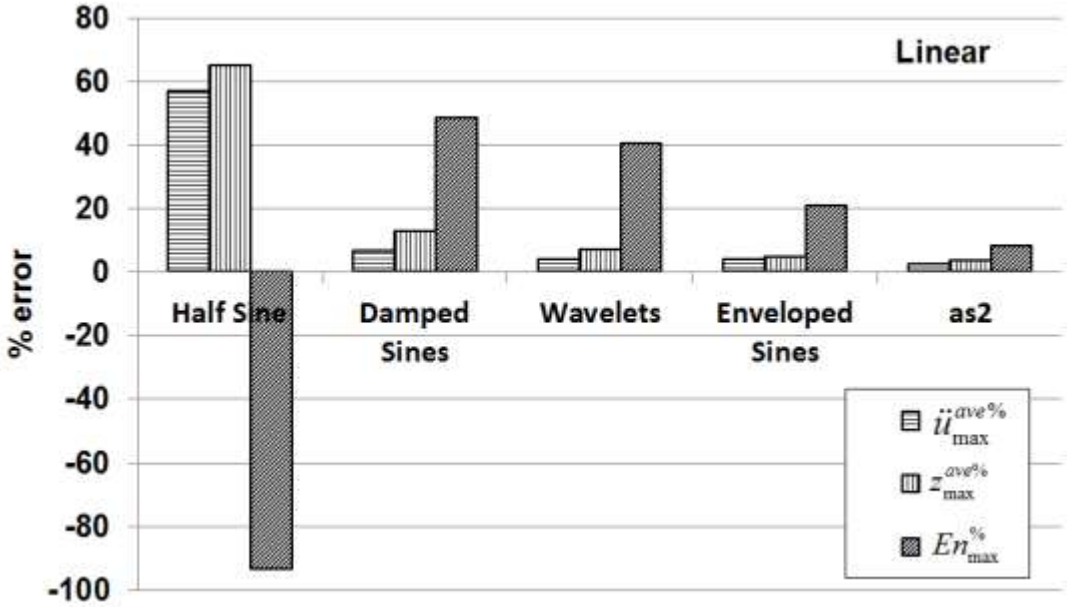

Figure (4-4) Synthesized Accelerations Response % Error – *MWSM* Linear Model

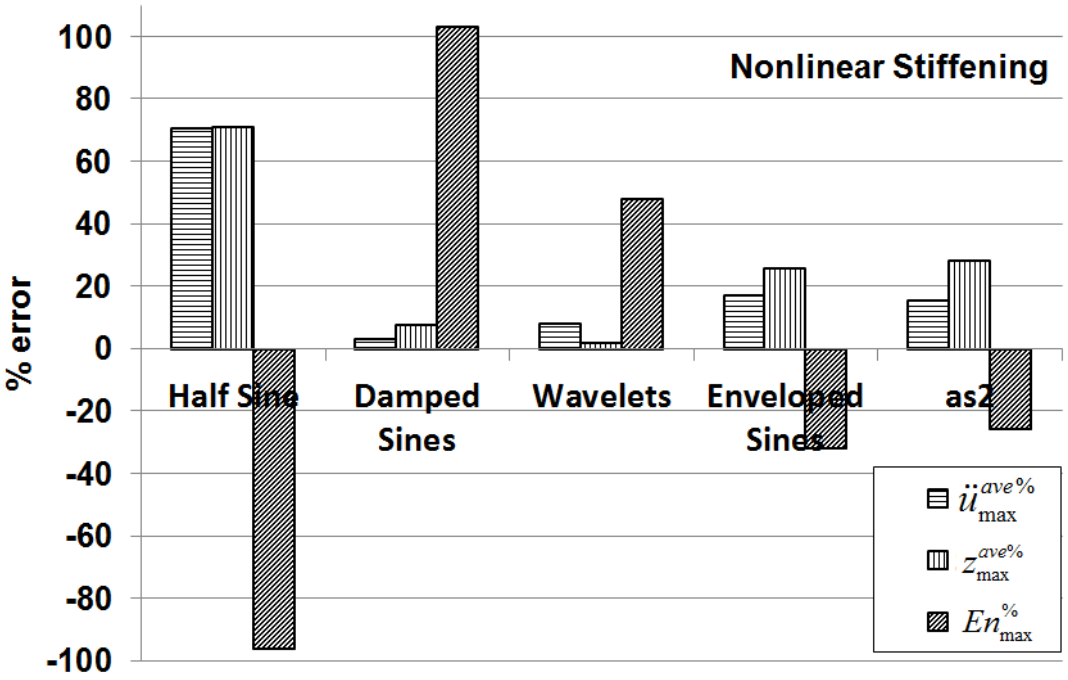

Figure (4-5) Synthesized Accelerations Response % Error – *MWMS* NL Stiffening Model

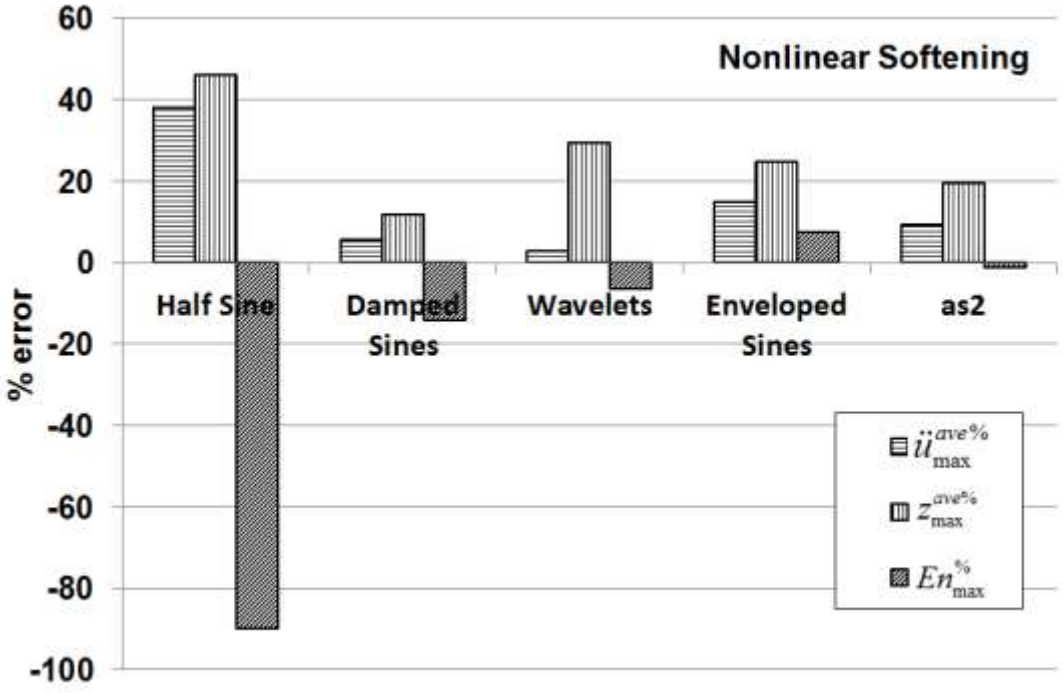

Figure (4-6) Synthesized Accelerations Response % Error - *MWSM* NL-Softening Model

5 Conclusions and Recommendations

The *SRS* has been in existence for eight decades and has achieved worldwide acceptance since inception, especially subsequent to the advent of digital computing. Defense, aerospace and commercial nuclear power communities all have structural dynamic environment design requirements based on a design SRS_D. The *SRS* provides a compact *SDOF* frequency response based measure of a transient acceleration, and with mode superposition can be leveraged to estimate the maximum response of a linear *MDOF* system. The *SRS* is used to characterize the shock environment for both structural dynamic analysis and testing.

However, despite the popularity of the *SRS*, significant limitations exist. The *SRS* is a linear transform and cannot be used directly for structural dynamic analyses of nonlinear *MDOF* structures or structural testing. The controller of an electro-dynamic test machine cannot drive the armature of the shaker table directly from an *SRS* signal. For both nonlinear analysis and testing, an *SRS* compatible transient acceleration signal is required. These limitations motivated researchers to solve the inverse problem; namely to synthesize a transient acceleration signal that is compatible with a prescribed design SRS_D. However, the *SRS* forward linear transform process retains no phasing or temporal information from the transient acceleration time signal. While a shock acceleration time history will transform to a unique *SRS*, the inverse is not true. There are theoretically an infinite number of shock accelerations a_S which can be synthesized to be compatible with a prescribed *SRS*. As such, *SRS* compatible synthesized accelerations can be significantly dissimilar in overall envelope shapes, temporal durations, peak amplitudes and phasing of

the sinusoids relative to the original acceleration. "Manufactured" signals have been published that exhibit curious temporal shapes which have little relation to physical data, but nonetheless are compatible with the prescribed *SRS*.

It is not difficult to synthesize an SRS_D compatible base acceleration with good accuracy. Numerous methods have been published to do this including classical acceleration pulses, the summation of sinusoids (damped sines, wavelets, enveloped sines) and less common techniques such as a trained neural network, maximum entropy principal and others. While somewhat limited, prior research has indicated that a base acceleration synthesized to be compatible with only a prescribed SRS_D, with no other constraints, does not in general yield accurate *MDOF* peak mass accelerations and/or displacements when compared to known model responses. The research herein has confirmed this finding. That said, peak mass acceleration and peak mass displacements at discrete locations in a structure have no general significant for the damage potential of the structure as a whole. A more appropriate global *MDOF* response, which includes energy input to the structure, is a better measure of system damage potential from an SRS_D compatible synthesized acceleration. For these reasons, the constraints to synthesize a base acceleration, and the corresponding response of an *MDOF* structure, have been reevaluated to include additional information. Based on regression analysis, individual percent error factors of the synthesized acceleration ($SRS_{\%}$, $EIS_{\%}$ and $T_{E\%}$) were all determined to be significant to the $\alpha \leq 0.1$ criteria based on the response of general *3DOF* models. The products of the factors were also determined to be significant to the $\alpha \leq 0.1$ criteria. A synthesized acceleration optimized to minimize a merit function comprised of

these six factors, equation (3-15), resulted in the most accurate energy input to all variants (linear and nonlinear) of a *3DOF MWSM* model.

The research herein motivates expanding the a_S synthesis process beyond current procedures. In addition to synthesis of a_S to be compatible with a prescribed SRS_D, other parameters can be included in the process to improve the quality of a_S. These parameters include temporal information (envelope, duration) and the energy input spectrum, *EIS*. Based on linear and nonlinear *3DOF* model response accuracy, the proposed approach resulted in peak system accelerations and displacements that were at parity with, if not better than, current practices. The proposed approach consistently achieved the most accurate energy input for all variants of a *3DOF* model.

6 Bibliography

Alexander, J. E. (1995). A Nonlinear DDAM Procedure. *SAVIAC Proceedings of the 66th Shock and Vibration Symposium, 1,* pp. pp 251-262. Biloxi, MS.

Alexander, J. E. (1998). Structural Analysis of a Nonlinear System Given a Shock Response Spectrum Input. *SAVIAC Proceedings of the 69th Shock and Vibration Symposium, Unlimited Volume.* Minneapolis, MN.

Alexander, J. E. (2009). Shock Response Spectrum - A Primer. *Sound and Vibration, Vol 43 / No 6*(June), pp 6-15.

Alexander, J. E. (2011). Application of Energy Methods in Mechanical Shock to Study Base Excited Nonlinear System Response. *Conference Proceedings of the Society for Experimental Mechanics. Vol 5*, pp. pp 157-175. Rotating Machinery, Structural Health Monitoring, Shock and Vibration.

Barry Controls. (n.d.). *SLM Mount Series*. Retrieved August 15, 2015, from http://www.barrycontrols.com/userfiles/file/product_catalog/machinery/bcdi_prod_machinery_catalog.pdf

Bathe, K., & Gracewski, S. (1981). On Nonlinear Dynamic Analysis Using Substructuring and Mode Superposition. *Computers & Structures, 13*, 699-707.

Biot, M. (1932). *Transient Oscillations in Elastic Systems.* California Institute of Technology.

Brake, M. R. (2011). An Inverse Shock Response Spectrum. *Mechanical Systems and Signal Processing, 25,* 2654-2672.

Bureau of Ships. (1961). *Shock Design of Shipboard Equipment, Dynamic Design-Analysis Method.* Navy Department, Bureau of Ships, Washington D.C.

Chang, C. J., & Mohraz, B. (1990). Modal Analysis of Nonlinear Systems with Classical and Non-Classical Damping. *Computers & Structures, 36*, 1067-1080.

Clements, E. W. (1972). *Shipboard Shock and Navy Devices for its Simulation, NRL Report 7396.* Naval Research Laboratory, Washington, DC.

Clough, H. L., & Penzien, J. (1975). In *Dynamics of Structures.* New York: McGraw Hill.

Dassault Systemes Simulia Corp. (2008). Abaqus (Version 6.8). Providence, RI.

Department of Defense. (2008). *MIL-STD-810G, Environmental Engineering Considerations and Laboratory Tests.* Military Standard.

Department of the Navy, Naval Sea Systems Command. (1972). *Design Data Sheet 072-1, Shock Design Values.*

Edwards, T. S. (2007). Using Work and Energy to Characterize Mechanical Shock. *Institute of Environmental Sciences and Technology, Annual Technical Meeting of the IEST, Conference Proceedings, ISBN: 978-1-60423-442-8, Vol 1*, pp. pp 280-298.

Edwards, T. S. (2009). Power Delivered to Mechanical Systems by Random Vibration. *Shock and Vibration, Vol 16, no. 3*, pp 261-271.

Gaberson, H. A. (1995). Reasons for Presenting Shock Spectra with Velocity as the Ordinate. *Proceedings of the 66th Shock and Vibration Symposium.* SAVIAC.

Gasparini, D., & Vanmarcke, E. H. (Jan 1976). *Simulated Earthquake Motions Compatible with Prescribed Response Spectra.* Pub. No. R76-4, Evaluation of Seismic Safety of Buildings, Report No. 2, MIT, Department of Civil Engineering.

Ghaboussi, J., & Lin, C. C. (1998). New Method of Generating Spectrum Compatible Accelerograms Using Neural Networks. *Earthquake Engineering and Structural Dynamics, 27*, 377-396.

Ghosh, A. K. (1991). On the Generation of Ground Motion Accelerogram Compatible with a Specified Response Spectrum and a Fourier Amplitude Spectrum. *SMiRT 11 Transactions, 11*, 7-12.

Gupta, I. D., & Trifunac, M. D. (1998). Defining Equivalent Stationary PSDF to Account for Nonstationarity of Earthquake Ground Motion. *Soil Dynamics and Earthquake Engineering, 17*, 89-99.

Hartwig, T. (2013). *Evaluation of Transportation Vibration Associated with Relocation of Work in Process as Part of KCRIMS.* Honeywell, Federal Manufacturing & Technology, Kansas City, MO.

Housner, G. W. (1947). Characteristics of Strong Motion Earthquakes. *Bulletin of the Seismological Society of America, Vol 37, No 1*, pp 19-31.

Housner, G. W. (1955, July). Properties of Strong Ground Motion Earthquakes. *Bulletin of the Seismological Society of America, Vol 45, No 3*, pp 197-218.

Housner, G. W. (1959). Behavior of Structures During Earthquakes. *Journal of the Engineering Mechanics Division (ASCE)*, (pp. 109-129).

Housner, G. W., & Jennings, P. C. (1964). Generation of Artificial Earthquakes. *Journal of the Engineering Mechanics Division. Vol 90*, pp. pp 113-150. Proceedings of the ASCE.

Hudson, D. E. (1956). Response Spectrum Techniques in Engineering Seismology. *Proceedings of the World Conference on Earthquake Engineering.* Berkeley, CA.

International Test and Evaluation Steering Committee. (2000). *FR/GE/UK/US, International Test Operations Procedure (ITOP) 4-2-828, Ballistic Shock Testing.*

Irvine, T. (2015, June 24). *SHOCK AND VIBRATION RESPONSE SPECTRA COURSE Unit 29. Shock Response Spectrum Synthesis via Wavelets.* Retrieved 2015, from http://www.vibrationdata.com/Course_Units/UNIT29.pdf.

Iwasa, T., Shi, Q., & Saitoh, M. (2008). Shock Response Spectrum Based on Maximum Total Energy of Single Degree of Freedom Model. *AIAA 2008-1742, 49th Structural Dynamics and Materials Conference.* Schaumburg, IL.: AIAA/ASME/ASCE/ASC Structures.

Iyengar, R. N., & Iyengar, K. T. (1969, June). Nonstationary Random ProcessModel for Warthquake Accelerograms. *Bulletin of the Seismological Society of America, 59 (3)*, pp. 1163-1188.

Iyengar, R. N., & Rao, P. N. (1979). Generation of Spectrum Compatible Accelerograms. *Earthquake Engineering and Structural Dynamics, 7*, 253-263.

Jennings, P. C., Housner, G. W., & Tsai, N. C. (1968). *Simulated Earthquake Motions.* California Institute of Technology , Earthquake Engineering Research Laboratory, Pasadena.

Kost, G., Tellkamp, T., Gantayat, A., & Weber, F. (1978). Automated Generation of Spectrum-Compatible Artificial Time Histories. *Nuclear Engineering and Design, 45*, 243-249.

Kukreti, A. R., & Issa, H. I. (1984). Dynamic Analysis of Nonlinear Structures by Pseudo-Normal Mode Superposition Method. *Computers & Structures, 19*, 653-663.

Lee, S. C., & Han, S. W. (2010). Neural Network Based Models for Generating Artificial Earthquakes and Response Spectra. *Computers and Structures, 80*, 1627-1638.

Levy, S., & Wilkinson, J. P. (1976). Generation of Artificial Time-Hiostories, Rich in All Frequencies, From Given Response Spectra. *Nuclear Engineering and Design, 38*, 241-251.

Lin, Y., & Sun, T. (1993). Mode Superposition Analysis of Viscously Damped Nonlinear Structural Systems Using an Incremental Algorithm. *Journal of Vibration and Acoustics, Transactions of the ASME, 115*, 397-402.

Manfredi, G. (2001). Evaluation of Seismic Energy Demand. *Earthquake Engineering and Structural Dynamics, Vol 30*, pp 485-499.

(2008). *MIL-STD-810G, Method 516.6, Shock.* Department of Defense, Test Method Standard - Environmental Engineering Considerations and Labortaory Tests.

Ministry of Defense. (2006). *Environmental Handbood for Defence Materiel, Part 3, Envirohmental Test Methods, DEF STAN 00-35 Part 3 Issue 4.* MOD.

Minitab, Inc. (2014, April). Minitab (version 16). State College, PA.

NASA. (1999). *Pyroshock Test Criteria, NASA Technical Standard, NASA-STD-7003.* NASA.

NASA. (2001). *Dynamic Environmental Criteria, NASA-HDBK-7005.* NASA Technical Handbook.

Navy, U. S. (1989). *MIL-S-901D* .

Nelson, D. B. (1989). Parameter Specification for Shaker Shock Waveform Synthesis - Damped Sines and Wavelets. *60th Shock and Vibration Symposium. III*, pp. 151-193. Portsmouth: Shock and Vibration Information Analysis Center (SAVIAC).

Newmark, N. M., Blume, J. A., & Kapur, K. K. (1973). Design Response Spectra for Nuclear Power Plants. *American Society of Civil Engineers (ASCE) Structural Engineering Meeting* (pp. 287-303). San Francisco: ASCE.

O'Hara, G. J., & Belsheim, R. O. (Feb, 1963). *Interim Design Values for Shock Design of Shipboard Equipment, NRL Memorandum Report 1396.* U. S. Naval Research Laboratory.

Ordaz, M., Huerta, B., & Reinoso, E. (2003). Exact Computation of Input-Energy Spectra from Fourier Amplitude Spectra. *Earthquake Engineering and Structural Dynamics, 32*, 597-605.

Preumont, A. (1980). A Method for the Generation of Artificial Earthquake Accelerograms. *Nuclear Engineering and Design, 59*, 357-368.

Preumont, A. (1984). The Generation of Spectrum Compatible Accelerograms for the Desigh of Nuclear Power Plants. *Earthquake Engineering and Structural Dynamics, 12*, 481-497.

Rizzo, P. C., Shaw, D. E., & Jarecki, S. J. (1973). Development of Real/Synthesized Time Histories to Match Smooth Design Spectra. Berlin: International Conference on Structural Mechanics in Reactor Technology.

Saragoni, G. R., & Hart, G. C. (1974). Simulation of Artificial Earthquakes. *Earthquake Engineering and Structural Dynamics, 2*, 249-267.

Scanlan, R. H., & Sachs, K. (1974). Earthquake Time Histories and Response Spectra. *Journal of the Engineering Mechanics Division. 100*, pp. 635-655. American Society of Civil Engineering.

Shah, V. N., Bohm, G. J., & Nahavandi, A. N. (1979). Modal Superposition Method for Computationally Economical Nonlinear Structural analysis. *101*, pp. 134-141. Montreal: Transactions of the ASME.

Shinozuka, M. (1973). Digital Simulation of Ground Accelerations. *5th World Conference of Earthquake Engineering*, (pp. 2829-2838). Rome.

Smallwood, D. O. (1986). *Shock Testing on Shakers by Using Digital Control.* Institute of Environmental Sciences. Mount Prospect: Institute of Environmental Sciences.

Smallwood, D. O., & Nord, A. R. (1974). Matching Shock Spectra with Sums of Decaying Sinusoids Compensated for Shaker Velocity and Displacement Limitations. *Shock and Vibration Bulletin, 44*, 43-56.

Soize, C. (2010). Information Theory for Generation of Accelerograms Associated with Shock Response Spectra. *Computer-Aided Civil and Infrastructure Engineering, 25*, 334-347.

The Mathworks, Inc. (2014, August). Matlab (Version R2014a). Natick, MA.

Trifunac, M. D. (2008). Early History of the Response Spectrum Method. *Soil Dynamics and Earthquake Engineering, 28*, 676-685.

U. S. Nuclear Regulatory Commission, Office of Nuclear Regulatory Research. (2014). *Regulatory Guide 1.60, Revision 2.* NRC.

Uang, C. M., & Berto, V. V. (1990). Evaluation of Seismic Energy in Structures. *Earthquake Engineering and Structural Dynamics, Vol 19*, pp 77-90.

Villaverde, R. (1988). Modal Superposition Method for Seismic Design of Non-Linear Multistorey Structures. *Earthquake Engineering and Structural Dynamics, 16*, pp 691-704.

Villaverde, R. (1996). Simplified Response-Spectrum Seismic Analysis of Nonlinear Structures. *Journal of Engineering Mechanics*, pp 282-285.

Zahrah, T. F., & Hall, W. J. (1984). Earthquake Energy Absorption in SDOF Structures. *Journal of Structural Engineering, 110*, 1757-1772.

Zhang, C., Chen, C., & Li, M. (2007). Earthquake Accelerogram Simulation with Statistical Law of Evolutionary Power Spectrum. *ACTA Seismologica Sinica, 20*, pp 435-446.

A *SRS* and Mode Superposition

A significant *SRS* application is to provide an estimate of the maximum response of a base excited linear *MDOF* system with the mode superposition procedure. Mode superposition is a well-established process used frequently to determine the maximum response of a linear *MDOF* model from an *SRS*. The mode superposition process is incorporated in all major commercial finite element structural codes. Early use of the *SRS* in combination with mode superposition dates back to the 1950's. Housner (1959) proposed the velocity shock response spectrum (SRS_{vel}) to estimate the maximum response of a linear *MDOF* structure by summation of maximum modal responses. Mode superposition is used widely in structural dynamic analysis for prescribed *SRS* requirements.

Mode superposition is facilitated by modal decomposition of the linear system matrix equations of motion (*EOM*), from which system Eigen values (natural frequencies) and Eigen vectors (mode shapes) are extracted. The linear *MDOF* equation of motion (A-1) is expressed in relative (z) coordinates, which are defined as the absolute coordinate displacement of each mass, u, relative to the based coordinate displacement, u_b. For each j^{th} mass, the relative coordinate displacement is $z_j = (u_j - u_b)$.

$$[M]\{\ddot{z}(t)\}+[C]\{\dot{z}(t)\}+[K]\{z(t)\}=-[M]\{1\}\ddot{u}_b(t) \tag{A-1}$$

Eigen values and Eigen vectors are determined from the undamped, free vibration form of equation (A-1), given by equation (A-2).

$$[M]\{\ddot{z}(t)\}+[K]\{z(t)\}=\{0\} \tag{A-2}$$

For each n^{th} mode of vibration of the system, it is assumed that the system relative motion $\{z(t)\}_n$ is described by a mode shape vector $\{\varphi\}_n$ and simple harmonic motion of circular frequency ω_n.

$$\{z(t)\}_n = \{\phi\}_n \sin \omega_n t \tag{A-3}$$

Substitution of equation (A-3) into equation (A-2) results in the general form of the Eigen value problem. Eigen values and Eigen vectors correspond to the *MDOF* system natural frequencies ω_n^2 and mode shapes $\{\varphi\}_n$, respectively, for all natural modes of vibration of the system. An n x n Eigen vector matrix [Φ] is formed with Eigen vectors $\{\varphi\}_n$ as the columns.

$$\omega_n^2[M]\{\phi\}_n = [K]\{\phi\}_n \tag{A-4}$$

$$[\Phi]=[\{\phi\}_1\{\phi\}_2\{\phi\}_3\cdots\{\phi\}_n] \tag{A-5}$$

Using the Eigen vector matrix [Φ], the matrix *EOM* is transformed from a physical basis $\{z\}$ to a modal basis $\{x\}$, using the transform,

$$\{z(t)\} = [\Phi]\{x(t)\} \tag{A-6}$$

Due to the orthogonality of normal modes, the transformation of the *MDOF* system of equations decouple into a series of *n SDOF* modal equations corresponding to each n^{th} natural frequency and n^{th} model shape of the physical system. P_n is the participation factor for the n^{th} mode of the system.

$$\ddot{x}_n(t) + 2\zeta_n\omega_n\dot{x}_n(t) + \omega_n^2 x_i(t) = -\mathrm{P}_n\ddot{u}_b(t) \tag{A-7}$$

$$P_n = \frac{\{\phi\}_n^T[M]\{1\}}{\{\phi\}_n^T[M]\{\phi\}_n} \tag{A-8}$$

Since the *SRS*, by definition, is the peak acceleration response of an *SDOF* oscillator, the *SRS* gives the maximum response of each $SDOF_n$ modal equation. Mode superposition is the summation of the maximum modal contributions and inverse transformed back to the physical basis, equation (A-9).

$$\{\ddot{u}(t)\} = \{\phi\}_1\mathrm{P}_1\ddot{x}_1(t) + \{\phi\}_2\mathrm{P}_2\ddot{x}_2(t) + \{\phi\}_3\mathrm{P}_3\ddot{x}_3(t) + \cdot\cdot\{\phi\}_{n\max}\mathrm{P}_{n\max}\ddot{x}_{n\max}(t) \tag{A-9}$$

$$\{\ddot{u}\}_{\max} \le \left|\{\phi\}_1\mathrm{P}_1\left|\ddot{x}_1(t)\right|_{\max}\right| + \left|\{\phi\}_2\mathrm{P}_2\left|\ddot{x}_2(t)\right|_{\max}\right| + \cdots + \left|\{\phi\}_{n\max}\mathrm{P}_{n\max}\left|\ddot{x}_{n\max}(t)\right|_{\max}\right| \tag{A-10}$$

If SRS_n is substituted for $\left|\ddot{x}_n(t)\right|_{\max}$, an estimate of the maximum response of the *MDOF* system results, given by equation (A-13). However, due to the differences in timing of the modal maxima, all $\left|\ddot{x}_n(t)\right|_{\max}$ will not occur at the same time. As such, an absolute sum is overly conservative. Equation (A-13) combines the modal maxima with a root-sum-squared summation, providing an improved estimate of the maximum *MDOF* response.

$$SRS_n \equiv \left|\ddot{x}_n(t)\right|_{\max} \tag{A-11}$$

$$\{\ddot{u}\}_{\max} \le \sum_{n=1}^{n\max}\{\phi\}_n\mathrm{P}_n SRS_n \tag{A-12}$$

$$\{\ddot{u}\}_{\max} \cong \sum_{n=1}^{n\max}\sqrt{\left(\{\phi\}_n\mathrm{P}_n SRS_n\right)^2} \tag{A-13}$$

Mode superposition given by (A-13) is not exact, but does provide a reasonable estimate of the maximum *MDOF* response. An overview of the *SRS* is given by Alexander (2009),

including *SRS* historical development, typical shock events characterized by the *SRS*, the application of the *SRS* in combination with mode superposition.

Mode superposition given by equation (A-9) requires linear equations of motion. Linear equations are necessary to perform a modal analysis to extract the system natural frequencies and mode shapes. If the equations of motion are nonlinear, the natural frequencies and mode shapes are not stationary. In these cases, liner mode superposition is not possible, which obviates the ability to use a design SRS_D directly to estimate the maximum system response with equation (A-13). For mechanical structural dynamic systems, [M] is typically a constant as the masses do not change during the transient. However it is possible for the damping matrix [C] and/or stiffness matrix [K] to be a function of the *MDOF* response, either of which leads to nonlinear equations of motion. The most common form of nonlinearity is that of a non-stationary stiffness matrix where the stiffness is a function of displacement. Examples include commercial shock isolators which can have either stiffening or softening force-displacement relationships. A nonlinear-elastic characteristic stiffness is the one examined for the research herein. If the strain in the material exceeds the proportional limit, the stiffness matrix is also non-stationary.

Numerous authors, motivated by the efficiency of the mode superposition procedure, have studied the treatment of nonlinear equations of motion with a pseudo-force technique to retain the ability to perform a mode superposition solution (Shah, Bohm, & Nahavandi, 1979) (Bathe & Gracewski, 1981) (Kukreti & Issa, 1984) (Chang & Mohraz, 1990) (Lin & Sun, 1993) (Alexander J. E., 1995). One advantage of mode superposition is that the higher frequency modes contribute very little to the total physical system response, and as such can be dropped without introduction of appreciable error. This technique, called modal truncation, can reduce the size of the problem significantly to facilitate faster computer solution time. For the nonlinear problem, one approach is to partition [C] and/or [K] into linear and nonlinear components, and transfer the nonlinear terms to the right hand side of equation (A-1) as pseudo-forces.

$$[K(z)] = [K_L] + [K_{NL}(z)] \tag{A-14}$$

$$[C(\dot{z})] = [C_L] + [C_{NL}(\dot{z})] \tag{A-15}$$

Partitioning the equation in this way results in equation (A-16). The left hand side of equation (A-16) is a linear equation of motion.

$$[M]\{\ddot{z}\} + [C_L]\{\dot{z}\} + [K_L]\{z\} = -[M]\{1\}\ddot{u}_b - [C_{NL}]\{\dot{z}\} - [K_{NL}]\{z\} \tag{A-16}$$

A linear equation of motion (left hand side of equation (A-16)) allows an Eigen value extraction and transformation to modal coordinates, similar to equation (A-9). This

procedure, however, still requires a transient analysis for updating $[C_{NL}]$ and $[K_{NL}]$ as the system responses change.

Villaverde (1988) (1996) took another approach to nonlinear mode superposition. The motivation was again that mode superposition is a quick, efficient procedure as opposed to a time intensive nonlinear transient analysis with numerical integration. Villaverde acknowledged that, while the approach gave approximate results, it had adequate accuracy for preliminary design. Unlike the prior nonlinear mode superposition approach described, Villaverde was able to avoid a transient analysis by development of a nonlinear *SRS*, determined from a known transient design earthquake acceleration time-history. The nonlinear *SRS* was determined from peak response values of nonlinear *SDOF* oscillators. The nonlinearity of the oscillators examined was elastic-perfectly plastic spring properties. Villaverde was one of the few authors who compared the results of the approximate procedure with the exact transient results based on the response of *MDOF* models. Comparison of Villarvede's nonlinear *SRS* mode superposition procedure approximate results to the exact result from the known earthquake acceleration time-history transient analysis demonstrated average errors ranging from 8% to 40% based on peak displacements for both *3DOF* and *10DOF* examples.

B General *3DOF* Model

A general *3DOF* model, Figure (B-1), was developed to evaluate eight synthesized acceleration a_S. The eight a_S are plotted in Figure (3-4) of Chapter 3. Response of the general *3DOF* model was used to study eight a_S, based on the corresponding *3DOF* model response from the design acceleration a_D. Three variants of the model were developed, based on the force-displacement relationships of the springs k_1, k_2 and k_3. Mass and stiffness values of the linear model were prescribed to result in natural frequencies in frequency bandwidth of SRS_D and EIS_D, shown in Figure (2-14) of Chapter 2. Damping of the *3DOF* model was set to 5% of critical damping ($\zeta = 0.05$) using mass and stiffness proportional Raleigh damping.

Mass and stiffness values for the linear model are tabulated in Table (B-1). The spring force-displacement relationship for the linear model springs is shown graphically in Figure (B-2). Coordinates for masses m_1, m_2 and m_3 are u_1, u_2 and u_3, respectively. The base coordinate is u_b. Natural frequencies of the linear model are listed in Table (B-2).

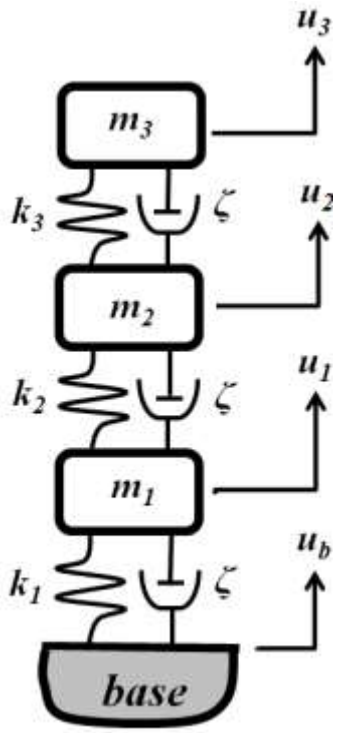

Figure (B-1) General *3DOF* Model

Table (B-1) Properties of Linear General *3DOF* Model

Mass lb_f-sec^2/in		Stiffness lb_f/in	
m_1	5.252E-3	k_1	28,000
m_2	6.734E-3	k_2	27,000
m_3	6.216E-3	k_3	26,000

Table (B-2) Natural Frequencies of Linear General *3DOF* Model

Natural Frequencies	
f_1	145.4 *Hz*
f_2	393.4 *Hz*
f_3	567.0 *Hz*

Two nonlinear elastic variants of the *3DOF* model were developed based on the force-displacement behavior of each spring as the displacement increases beyond the linear spring extension or contraction limit Δ, Table (B-3). One nonlinear variant had stiffening springs, Figure (B-3) and the other nonlinear model variant had softening springs, Figure (B-4). For the stiffening model, the stiff portion of the force-displacement curve beyond the linear limit was set to 200% of the linear stiffness. For the softening model, the softening portion of the force-displacement stiffness was set to 50% of the linear stiffness.

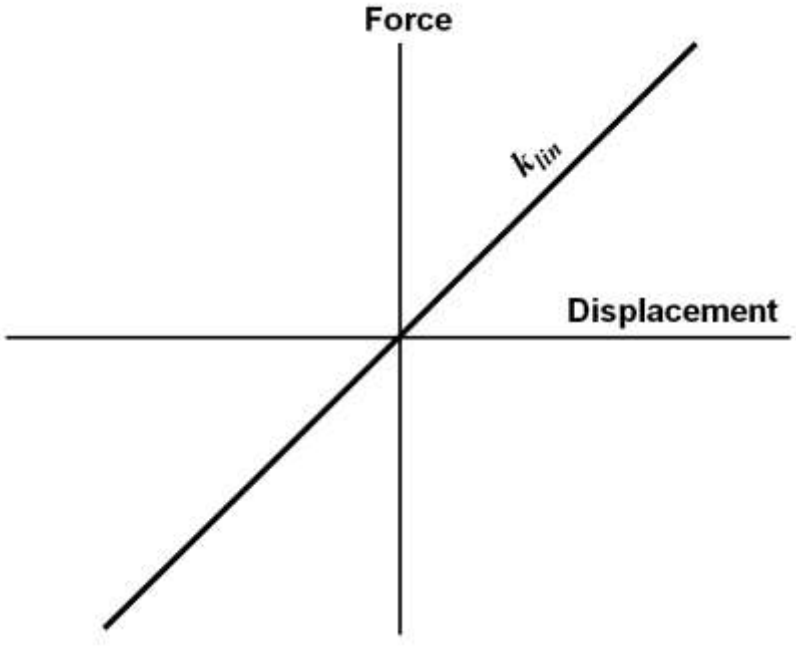

Figure (B-2) Force – Displacement Relationship Linear Spring

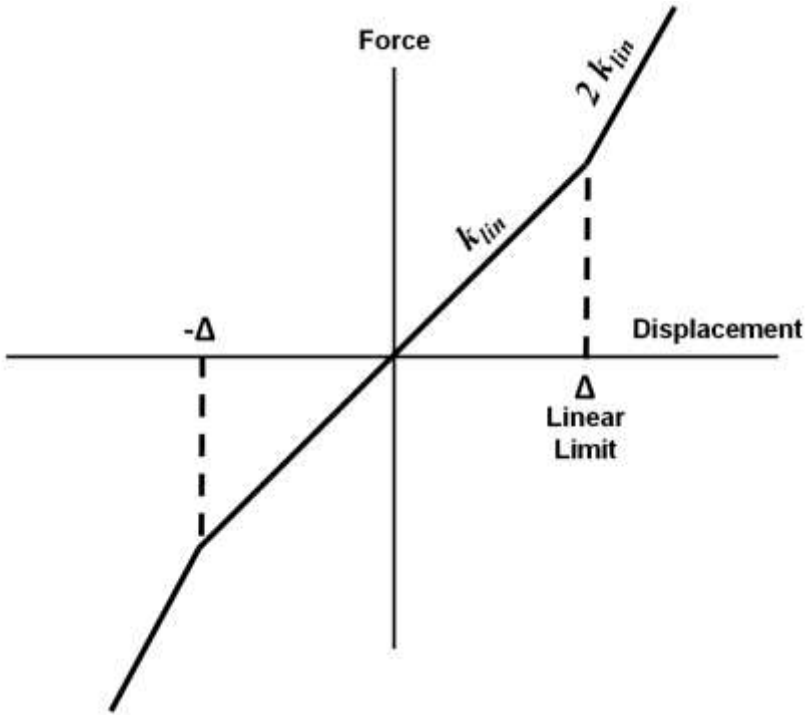

Figure (B-3) Force – Displacement Relationship Nonlinear Elastic Stiffening Spring

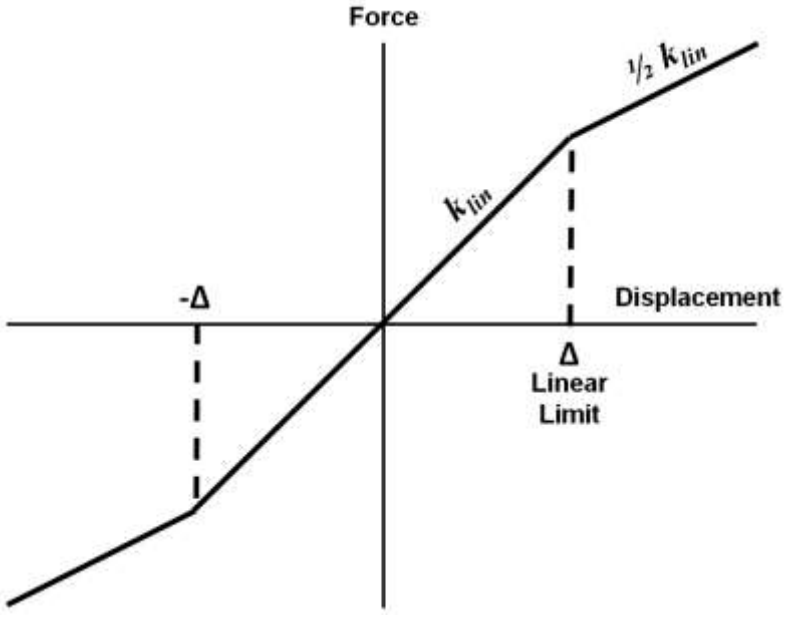

Figure (B-4) Force – Displacement Relationship Nonlinear Elastic Softening Spring

Table (B-3) Linear Limits for Springs 1, 2 and 3

Linear Limits for Springs k_1, k_2, k_3 , in	
Δ_1	0.0019273
Δ_2	0.001387
Δ_3	0.000833

C Medium Weight Shock Machine *3DOF* Model

Medium Weight Shock Machine testing is required by the US Navy for shock qualification of shipboard equipment in the 500-6,000 pound weight range. The purpose of the machine is to simulate the shock environment resulting in near miss underwater explosions in close proximity to the ship. The *MWSM* model is described briefly in Section 4.3 of Chapter 4. The details of the *MWSM 3DOF* model are included in this appendix.

The equipment to be shock tested is mounted on the anvil table shown in Figure (C-1). The equipment is mounted to the anvil table with a prescribed number of car building channels, based on the weight of the equipment and the distance between the attachment locations. The number of car building channels is prescribed based on MIL-S-901D (Navy, 1989) to represent the deck frequency of the ship where the equipment is mounted. The machine consists of a 3,000 pound hammer that strikes the underside of the 4,400 pound anvil table. Hammer impact velocity is based on the hammer height above horizontal when released.

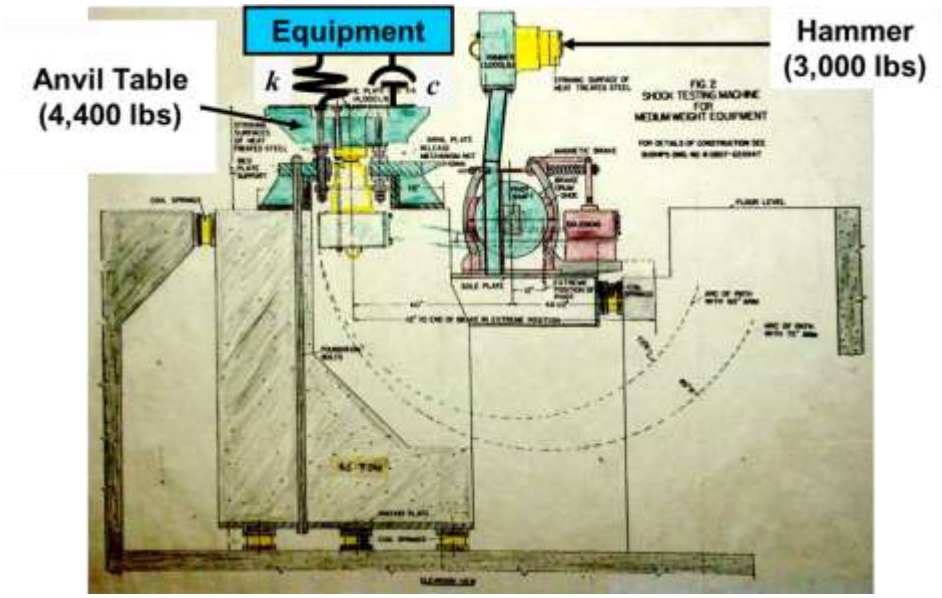

Figure (C-1) Schematic of MIL-S-901D Medium Weigh Shock Machine

Figure (C-2) is schematic of the *MWSM 3DOF* model where the equipment to be tested is represented as two lumped masses m_2 and m_3. The stiffness k_1 represents the combined stiffness of all car building channels. Damping of the *MWSM 3DOF* model was set to 5% of critical damping ($\zeta = 0.05$) based test data taken by the Naval Research

Laboratory (Clements, 1972). The equipment masses m_2 and m_3 are connected with a chassis spring of stiffness k_3. Spring stiffness k_2 connects the lower base of the equipment to the car building channels, and represents the combined stiffness of four commercial shock absorbers (Barry Controls) selected based on the shock acceleration magnitude and the weight of the equipment. Mass m_1 corresponds to 50% of the mass of the two car building channels and k_1 is the combined stiffness of the car building channels. Two car building channels are specified by MIL-S-901D based on the weight of the equipment (500 pounds) in this model and the distanced between the attachments connecting the equipment to the anvil table. Coordinates for masses m_1, m_2 and m_3 are u_1, u_2 and u_3, respectively. The anvil table base coordinate is u_b.

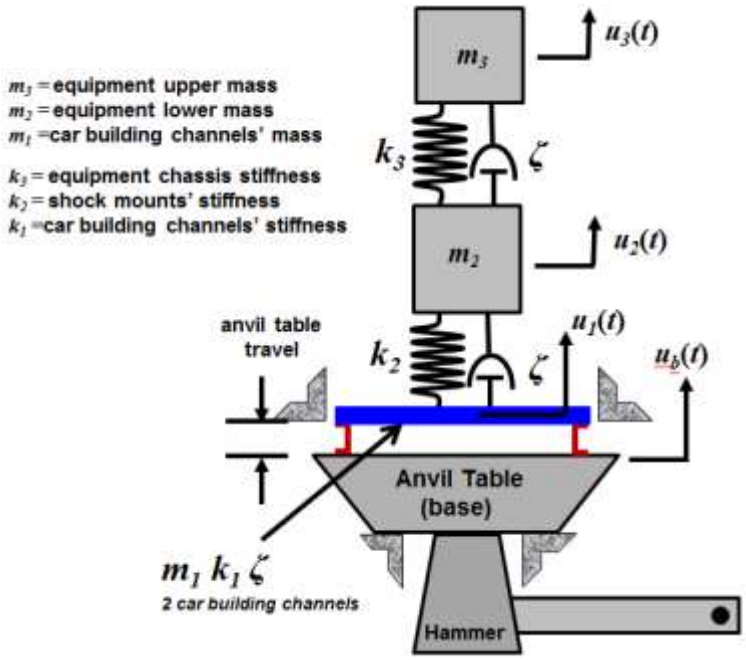

Figure (C-2) *3DOF* Model of the Medium Weight Shock Machine

The *3DOF MWMS* model was used to evaluate the accuracy of the five synthesized accelerations, shown in Figure (4-1) of Chapter 4, based on the response of the model from each. As with the general *3DOF* model, three variants of the *3DOF MWSM* model were created to determine the response from each of the five synthesized acceleration; one linear and two nonlinear. The linear model mass and spring stiffness values are listed in Table (C-1). The shock absorber stiffness, k_2, is based generally on the Barry Controls SLM-96 commercial shock isolator **(Barry Controls)**, Figure (C-3). The shock isolator is a nonlinear elastic stiffening isolator as shown by the force-displacement curve of Figure (C-4). The linear stiffness of one shock isolator is approximately 6,430 lb/in. The total stiffness k_2 is based on four shock isolators; one on each corner of the equipment being tested.

Table (C-1) *MWSM* Linear Model Parameters

Mass lb_f-sec^2/in		Stiffness lb_f/in	
m_1	0.331	k_1	258,610
m_2	0.777	k_2	25,720
m_3	0.518	k_3	100,000

Figure (C-3) Barry Controls SLM Series Shock Isolator

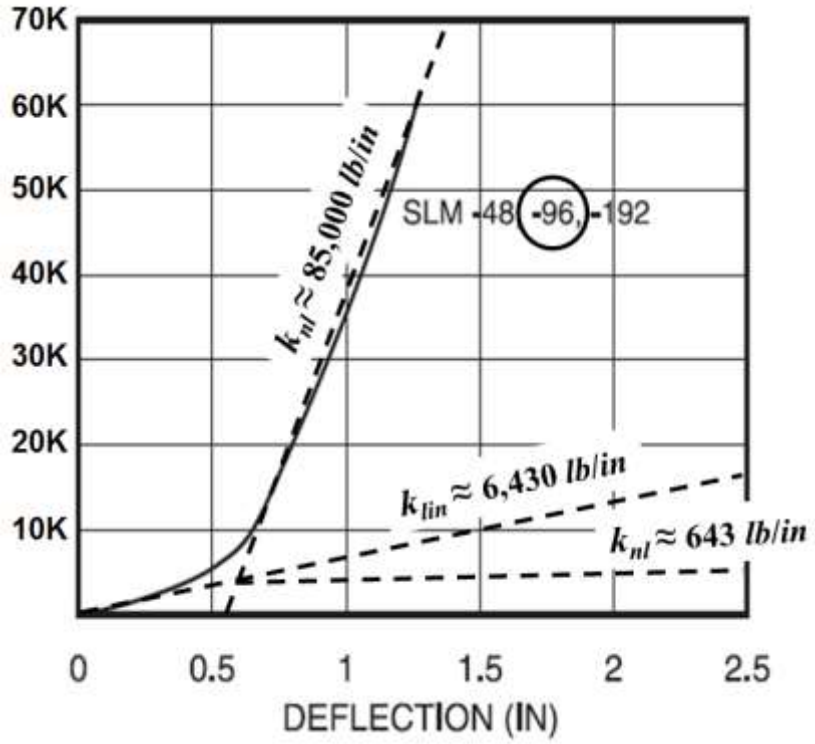

Figure (C-4) Force-Deflection Relationship of Barry Controls SLM-96 Shock Isolator

A nonlinear stiffening *MWMS* model was developed based on stiffening behavior of the SLM-96 isolator, Figure (C-4), as displacement increases beyond the linear limit. The stiff portion of the force-displacement curve is approximately 85,000 lb/in, Figure (C-4). The nonlinear stiffening spring constant of k_2 was set to four times that value to represent four shock isolators.

A third *MWSM* model variant was developed based on a nonlinear elastic softening shock isolator for stiffness k_2. In this case, when the deflection of spring k_2 exceeded the linear limit, the softening portions of the force-displacement curve was set to 10% of the linear stiffness value. The nonlinear k_2 stiffness values for both nonlinear *MWMS* models are listed in Table (C-2).

Table (C-2) *MWSM* Nonlinear Spring 2 Stiffness Values

Stiffness NL- stiffening model, lb_f/in		Stiffness NL- softening model, lb_f/in	
k_2	25,7203	k_2	25,7201
k_2 stiff	340,000	k_2 soft	2,572

D Regression Analysis

A summary of the regression analysis is discussed in Section 3.5 of Chapter 3. Additional details of the regression analysis are in this appendix. The response of the three variants of the general *3DOF* model, described in Appendix B, is the basis for each regression analysis. Nine individual regression analyses were performed to determine the significance of the factors $SRS_{\%}$, $EIS_{\%}$ and $T_{E\%}$. These analyses include three variants of the general *3DOF* model. An individual regression analysis includes the six factors and one of the models responses of Table (D-1). For the nine total model responses of Tables (D-1), (D-2) and (D-3) nine individual regression analyses were performed. The three general *3DOF* model variants were:

- linear
- nonlinear-stiffening
- nonlinear-softening

Three responses used as the basis for the regression analysis for each model were:

- average peak mass acceleration % error
- average peak displacement % error
- peak energy input % error

For each individual regression analysis, the general *3DOF* model was subjected to the eight synthesized accelerations listed in Table (3-1), and also plotted in Figure (3-4) of Chapter 3. The factors evaluated were the percentage errors of the *SRS*, *EIS* and T_E, from each synthesized acceleration relative to the corresponding values from the design acceleration a_D. The regression analysis results for each variant of the general *3DOF* model are described individually in the following sections.

Significant factors for the general *3DOF* models are indicated in Tables (D-1) through (D-3). A significant factor for a model response is indicated by an "x" in the cell corresponding to the factor and model response. The significance of the product of the factors, or cross-terms, was also evaluated by the regression analysis.

The criteria for significance of a factor was set to an alpha value of less than or equal to 0.10 ($\alpha \leq 0.10$). Alpha is frequently referred to as the level of significance. Alpha is defined as the maximum level of risk for rejecting a true null hypothesis and is expresses as a probability ranging between 0 and 1.

The regression analysis calculates a p-value for each factor. The p-value represents the probability of incorrectly rejecting the null hypothesis. If the p-value is less than or equal to the defined alpha value ($\alpha \leq 0.10$ in this case), the null hypothesis (H_0) can be rejected in favor of the alternative hypothesis (H_1) (Minitab, Inc., 2014). In

this case, the null hypothesis H_0 is that a factor is not statistically significant for a response of the *3DOF* model and the alternative hypothesis H_1 is that the factor is statistically significant for the response of the model.

R^2 values are listed for each regression equation. R^2 indicates how well the model (regression equation) fits the data. It is a value between 0 and 100%. Specifically, the R^2 values indicated herein are "adjusted R^2" which will increase only if a new term improves the model more than would be expected by chance. Without adjustment, R^2 will always increase when a new term is added. Without this adjustment, a model with more terms may appear to be a better fit even when it could be due to chance.

D1 General *3DOF* Model – Linear

The regression model determined the significance of individual factors for each of the three responses evaluated for the linear version of the general *3DOF* model. Table (D-1) indicates the significant factors for the linear variant of the general *3DOF* model. It is noted that individual factors can be significant, but also that the product of the factors can also be significant.

Table (D-1) General *3DOF* Model, Linear – Significant Factors

Model Response	Factors					
	$SRS_{\%}$	$EIS_{\%}$	$T_{E\%}$	$(SRS_{\%})(EIS_{\%})$	$(SRS_{\%})(T_{E\%})$	$(EIS_{\%})(T_{E\%})$
(peak mass acceleration % err)$_{ave}$	**x**		**x**		**x**	
(peak displacement % err)$_{ave}$	**x**	**x**		**x**	**x**	
peak energy input % err	**x**		**x**	**x**		

The regression model determines a predictive equation for each model response, given by equations (D-1) through (D-3) for the linear *3DOF* model.

$$\ddot{u}_{\max}^{ave\%} = 9.716 + 1.455(SRS_{\%}) + 0.0211(EIS_{\%}) - 0.488(T_{E\%}) + 0.0504(SRS_{\%})(EIS_{\%}) \quad \text{(D-1)}$$

$$z_{\max}^{ave\%} = -20.96 + 3.92(SRS_{\%}) + 0.250(EIS_{\%}) - 0.805(T_{E\%}) - 0.023(SRS_{\%})(EIS_{\%}) + 0.081(SRS_{\%})(T_{E\%}) \quad \text{(D-2)}$$

$$En_{\max}^{\%} = -7.14 + 10.05(SRS_{\%}) + 0.919(EIS_{\%}) + 2.11(T_{E\%}) - 0.152(SRS_{\%})(EIS_{\%}) \quad \text{(D-3)}$$

Figures (D-1) through (D-3) are plots of the results from the three predictive equations and the exact results from the *3DOF* transient analyses. The plots provide a basis of comparison of the degree to which the regression equations match the corresponding response from the transient model. The agreement between the regression equations and transient analysis results from the linear *3DOF* linear model is evident in the plots of Figures (D-1) through (D-3). R^2 values for regression equations (D-1) through (D-3) are 95.5%, 94.0% and 62.0%, respectively.

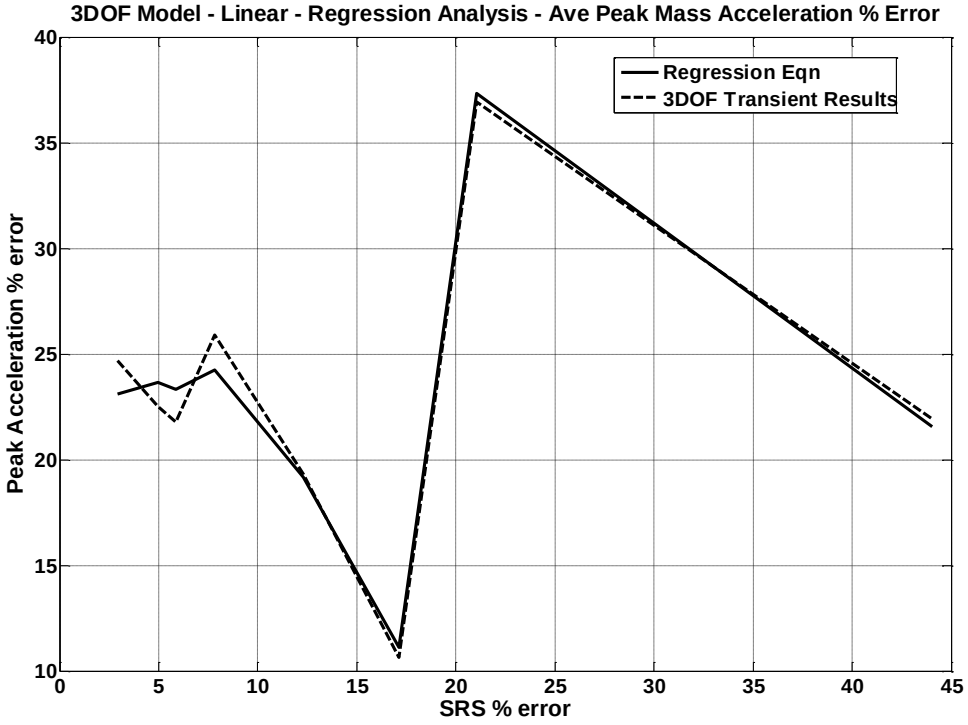

Figure (D-1) General *3DOF* Model – Linear; Ave Peak Acceleration %Error; Regression Equation & *3DOF* Transient

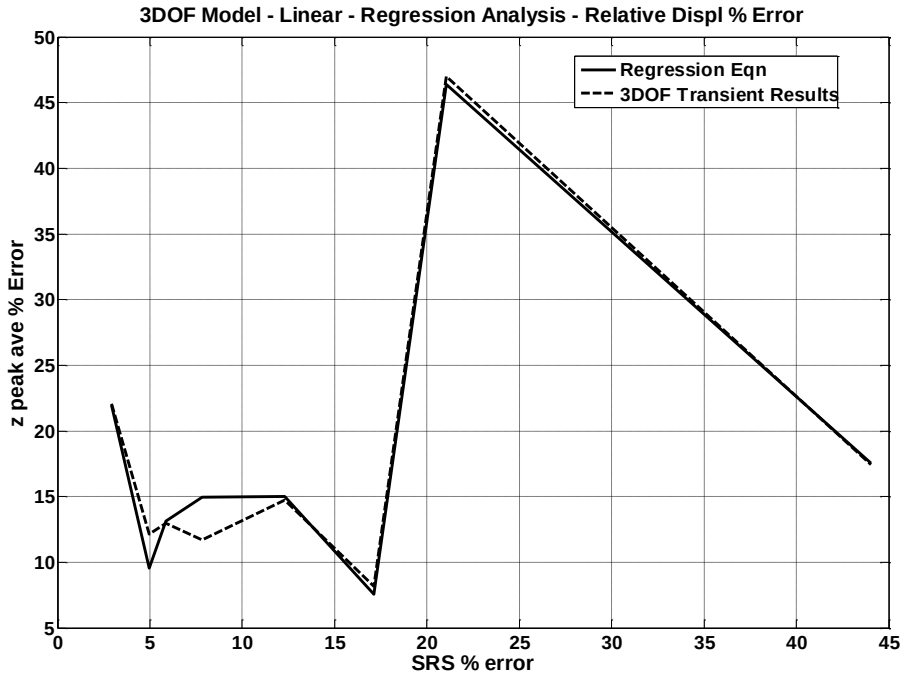

Figure (D-2) General *3DOF* Model – Linear; Ave z-Displacement %Error; Regression Equation & *3DOF* Transient

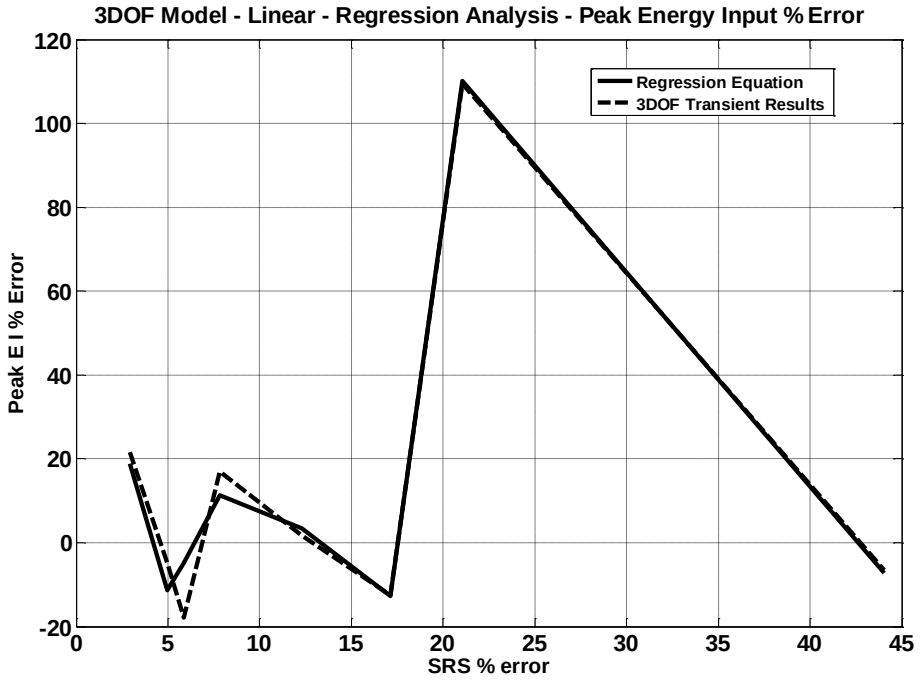

Figure (D-3) General *3DOF* Model – Linear; Peak Energy Input %Error; Regression Equation & *3DOF* Transient

D2 General *3DOF* Model – Nonlinear Stiffening

Table (D-2) indicates the significant factors from the regression analysis for the stiffening variant of the general *3DOF* model.

Table (D-2) General *3DOF* Model, Nonlinear Stiffening – Significant Factors

Model Response	Factors					
	$SRS_{\%}$	$EIS_{\%}$	$T_{E\%}$	$(SRS_{\%})(EIS_{\%})$	$(SRS_{\%})(T_{E\%})$	$(EIS_{\%})(T_{E\%})$
(peak mass acceleration % err)$_{ave}$	**x**					
(peak displacement % err)$_{ave}$	**x**	**x**	**x**	**x**	**x**	
peak energy input % err				**x**		

The predictive equations for the stiffening *3DOF* model are equations (D-4) through (D-6). R^2 values are 39.4%, 99.97% and 57.1%, respectively.

$$\ddot{u}_{\max}^{ave\%} = 10.10 + 0.571(SRS_{\%}) \tag{D-4}$$

$$z_{\max}^{ave\,\%} = -14.91 + 0.16\,(SRS_{\%}) - 0.097\,(EIS_{\%}) - 0.916\,(T_{E\%}) - 0.0260\,(SRS_{\%})(EIS_{\%}) + 0.0429\,(SRS_{\%})(T_{E\%}) \tag{D-5}$$

$$En_{\max}^{\%} = -28.83 + 3.819(SRS_{\%}) + 0.515(EIS_{\%}) - 0.0818(SRS_{\%})(EIS_{\%}) \tag{D-6}$$

D3 General *3DOF* Model – Nonlinear Softening

Table (D-3) indicates the significant factors from the regression analysis for the stiffening variant of the general *3DOF* model.

Table (D-3) General *3DOF* Model, Nonlinear Softening – Significant Factors

Model Response	Factors					
	$SRS_{\%}$	$EIS_{\%}$	$T_{E\%}$	$(SRS_{\%})(EIS_{\%})$	$(SRS_{\%})(T_{E\%})$	$(EIS_{\%})(T_{E\%})$
(peak mass acceleration % err)$_{ave}$						
(peak displacement % err)$_{ave}$	**x**	**x**	**x**	**x**		
peak energy input % err						

The predictive equations for the softening *3DOF* model are equations (D-7) through (D-9). R^2 values are 60.8%, 87.2% and 19.0%, respectively.

$$\ddot{u}_{\max}^{ave\%} = 17.47 - 0.879(SRS_{\%}) - 0.163(EIS_{\%}) + 0.0236(SRS_{\%})(EIS_{\%}) \quad \text{(D-7)}$$

$$z_{\max}^{ave\ \%} = -2.643 + 5.017\,(SRS_{\%}) + 0.533\,(EIS_{\%}) + 0.623\,(T_{E\%}) - 0.0260\,(SRS_{\%})(EIS_{\%}) - 0.0779\,(SRS_{\%})(EIS_{\%}) \quad \text{(D-8)}$$

$$En_{\max}^{\%} = 25.26 - 1.002(SRS_{\%}) \quad \text{(D-9)}$$

Note:

For equation (D-7), $SRS_{\%}$ p-value = 0.311, $EIS_{\%}$ p-value = 0.275 and $(SRS_{\%})(EIS_{\%})$ p-value = 0.116, none of which met $\alpha \leq 0.10$ criteria.

For equation (D-9), the $SRS_{\%}$ p-value = 0.155, which did not meet $\alpha \leq 0.10$ criteria